

Magnetic reconnection

Masaaki Yamada, Russell Kulsrud, and Hantao Ji

Center for Magnetic Self-Organization in Laboratory and Astrophysical Plasmas, Princeton Plasma Physics Laboratory, Princeton University, Princeton, New Jersey 08543, USA

(Published 5 March 2010)

The fundamental physics of magnetic reconnection in laboratory and space plasmas is reviewed by discussing results from theory, numerical simulations, observations from space satellites, and recent results from laboratory plasma experiments. After a brief review of the well-known early work, representative recent experimental and theoretical works are discussed and the essence of significant modern findings are interpreted. In the area of local reconnection physics, many findings have been made with regard to two-fluid physics and are related to the cause of fast reconnection. Profiles of the neutral sheet, Hall currents, and the effects of guide field, collisions, and microturbulence are discussed to understand the fundamental processes in a local reconnection layer in both space and laboratory plasmas. While the understanding of the global reconnection dynamics is less developed, notable findings have been made on this issue through detailed documentation of magnetic self-organization phenomena in fusion plasmas. Application of magnetic reconnection physics to astrophysical plasmas is also discussed.

DOI: [10.1103/RevModPhys.82.603](https://doi.org/10.1103/RevModPhys.82.603)

PACS number(s): 52.35.Vd, 94.30.cp, 96.60.Iv

CONTENTS

| | | | |
|--|-----|--|-----|
| I. Introduction | 604 | magnetic reconnection | 626 |
| II. Magnetic Reconnection Observed in Space and Laboratory Plasmas | 607 | 1. MHD analysis with effective resistivity | 626 |
| A. Magnetic reconnection in solar flares | 607 | 2. Effects of guide field | 627 |
| B. Magnetic reconnection in the magnetosphere | 608 | B. Plasma heating and acceleration | 628 |
| C. Magnetic reconnection in self-organization of fusion plasmas | 609 | 1. Plasma heating during plasma merging | 628 |
| 1. Magnetic reconnection in tokamaks | 610 | 2. Strong ion heating during reconnection in RFP | 629 |
| 2. Magnetic relaxation in reversed field pinches | 610 | C. Observation of accelerated plasmas in the exhaust of reconnection site in space | 629 |
| D. A dedicated laboratory experiment on reconnection | 611 | VI. Two-fluid Physics of the Reconnection Layer | 630 |
| III. Theoretical Background of Reconnection Study | 612 | A. Numerical simulation of two-fluid reconnection | 630 |
| A. Early history of magnetic reconnection theory | 612 | B. Analytical theory for two-fluid reconnection | 632 |
| B. MHD models for magnetic reconnection | 615 | C. Experimental observations of two-fluid effects in the reconnection layer | 634 |
| C. Recent progress in MHD theory | 618 | 1. Measurements of profile of reconnection layer | 634 |
| IV. Recent Major Facilities and Means for Reconnection Study | 619 | 2. Verification of Hall effects in the reconnection layer | 635 |
| A. Dedicated laboratory experiments on reconnection | 619 | a. Observation of Hall effects in space | 635 |
| 1. Early reconnection experiments | 619 | b. Observation of Hall effects in laboratory experiments | 636 |
| 2. Plasma merging experiments | 620 | 3. Identification of the electron diffusion layer | 637 |
| a. Todai spheromak-3/4 facility | 620 | 4. Scaling of the reconnection rate with collisionality | 637 |
| b. Swarthmore Spheromak Experiment facility | 621 | 5. Effects of guide field | 638 |
| 3. Controlled driven reconnection experiments | 622 | 6. Observation of two-fluid effects in the magnetotail | 639 |
| a. MRX facility | 622 | VII. Kinetic Effects of Magnetic Reconnection | 639 |
| b. Versatile Toroidal Facility | 622 | A. Kinetic equilibrium | 640 |
| B. Satellites for study of magnetic reconnections | 623 | 1. Harris solutions and its generalizations | 640 |
| 1. Solar satellites | 623 | 2. Experimental observations of the Harris sheet | 641 |
| 2. Space satellites | 624 | B. Kinetic effects within the reconnection plane | 641 |
| C. Numerical modeling of magnetic reconnection | 625 | 1. Kinetic effects without guide field | 641 |
| 1. Fluid models | 625 | 2. Kinetic effects with guide field | 643 |
| 2. Particle models | 625 | C. Mechanisms for anomalous resistivity | 643 |
| V. MHD Analysis of Recent Experimental Results and Observations | 626 | VIII. Magnetic Self-Organization and Reconnection | 646 |
| A. Experimental observations and MHD analysis of | | | |

| | |
|--|-----|
| A. Sawtooth reconnection in tokamaks | 646 |
| 1. Electron temperature evolution | 646 |
| 2. q profile evolution | 647 |
| 3. Physical processes during sawtooth reconnection | 647 |
| B. Magnetic reconnection in reversed field pinch and spheromak plasmas | 648 |
| C. Effects of global boundaries on reconnection | 650 |
| 1. The formation of a current layer | 650 |
| 2. Effects of boundary conditions | 652 |
| D. Magnetic reconnection in astrophysical plasmas | 653 |
| 1. Magnetic reconnection in interstellar medium | 653 |
| 2. Magnetic reconnection in accretion disks | 654 |
| 3. Magnetic reconnection in magnetospheres of compact objects | 654 |
| IX. Summary, Discussions, and Major Outstanding Issues | 655 |
| A. Local physics issues for the reconnection layer | 656 |
| B. Global physics issues for reconnection | 657 |
| C. Final remark | 658 |
| Acknowledgments | 658 |
| Appendix: The Nature of Reconnection | 658 |
| References | 660 |

I. INTRODUCTION

Magnetic fields are observed at all scales in the Universe, in the Earth's dipole field, in the magnetosphere, in the solar corona, and on a larger scale from the interstellar medium to galaxy clusters. How are magnetic fields generated in the Universe? How are they involved in determining the characteristics of plasmas? Understanding magnetic reconnection, a topological rearrangement of magnetic field lines, provides a key to these questions. In magnetized astrophysical and laboratory plasmas, magnetic reconnection rearranges the magnetic field-line configurations restructuring macroscopic quantities of plasmas such as flow and thermal energy.

Magnetic reconnection is seen in the evolution of solar flares, coronal mass ejection, and interaction of solar winds with the Earth's magnetosphere and is considered to occur in the formation of stars (Parker, 1979; Kulsrud, 1998; Biskamp, 2000; Priest and Forbes, 2000). It occurs as the self-organization process in current carrying fusion plasmas, typically observed in major and minor disruptions of tokamak discharges, and in relaxation processes in reversed field pinch (RFP) and spheromak plasmas (Taylor, 1986; Yamada, 1999b). Magnetic reconnection involves a topology change of a set of field lines, which leads to a new equilibrium configuration of lower magnetic energy. During this process magnetic energy is converted to kinetic energy through acceleration or heating of charged particles.

Solar flares exhibit the clearest visual examples of magnetic reconnection and have been investigated for more than a half century. Through soft-x-ray pictures, which are considered to represent magnetic field-line configurations, we can visualize examples of global topology change of plasma configurations (Masuda *et al.*,

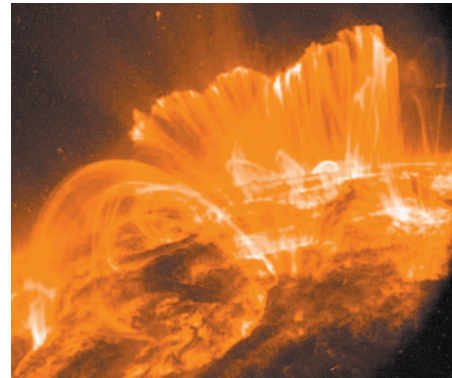


FIG. 1. (Color) Solar flare image at 171 Å from TRACE satellite on 9 November 2000. From apod.nasa.gov

1994; Tsuneta, 1996; Gabriel *et al.*, 1997; Golub *et al.*, 1999; Lin *et al.*, 2003). As shown in transition region and coronal explorer (TRACE) satellite data (Golub *et al.*, 1999) (Fig. 1), the topologies of soft-x-ray images are seen to change within a time scale of minutes or hours in the solar atmosphere, in which the magnetic diffusion time for a typical flare is estimated to be as long as 10^6 years. These observations suggest the presence of fast global magnetic reconnection phenomena, implying anomalously efficient dissipation of magnetic energy. Giovanelli (1946) noted that the abundant magnetic field energy in the chromosphere could be converted to electron kinetic energy. Satellite measurements later showed that his concept can be applied to solar corona reconnection.

How do magnetic field lines move around in plasmas and how do they reorganize? Ideal magnetohydrodynamics (MHD), developed in the early 1950s, describes the dynamics of highly conductive plasmas, where the electric field parallel to the magnetic field line E_{\parallel} vanishes (Parker, 1957; Sweet, 1958; Vasyliunas, 1975; Dungey, 1995). In this model, magnetic field lines always move with the plasma and remain intact (i.e., can never break or tear apart). If magnetic field lines approach each other in the plasma as shown in Fig. 2, associated field gradients become locally strong at the encountering point.

This interaction of field lines leads to a singular current-density sheet where E_{\parallel} becomes sufficiently large ($E_{\parallel} = \mathbf{E} \cdot \mathbf{B}/B \neq 0$) to induce non-ideal-MHD plasma behavior and to cause the magnetic field lines to lose their identity. Dungey (1953) showed that such a current sheet can indeed be formed by the collapse of the magnetic field near an X -type neutral point as shown in Fig. 3 and suggested that lines of force can be broken and rejoined in the current sheet. This sheet is called a neutral sheet or diffusion region. When the field lines are reconnected, the topology of magnetic configuration changes and $\mathbf{j} \times \mathbf{B}$ forces result in the conversion of magnetic energy to kinetic energy.

Examining this situation more precisely, one can represent any magnetic field by a set of lines that densely fills the system. The lines are tangent to the magnetic

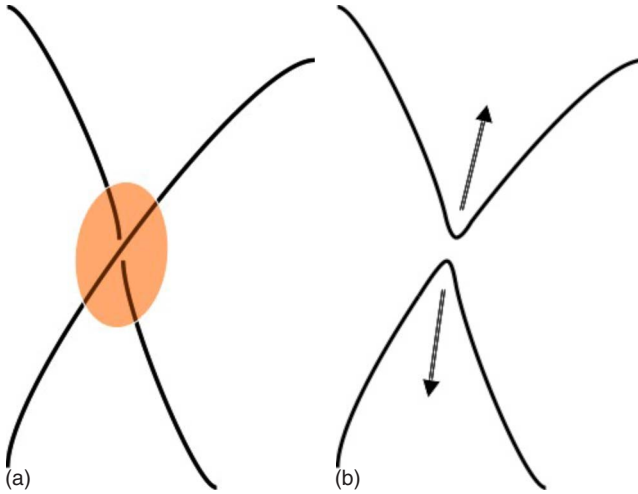


FIG. 2. (Color online) Schematic view of magnetic reconnection.

field and their density equals the field strength. If the system is time dependent, the profiles of the lines are different at every instant. In general, there is no way to tell from one moment to the next which line any initial line turns into; i.e., the lines do not have a physical identity. If the plasma moving with the field lines is infinitely conducting, a physical identity can be assigned to the lines. If the lines are carried with the velocity of the plasma, they will continue to represent the magnetic field at any later time. This allows one to clearly picture the magnetic field.

The field thus consists of strings embedded in the plasma which are neither created or destroyed. The magnetic force is represented by imagining the strings to have longitudinal tension and transverse pressure. If the strings are sharply bent, the curvature force replicates the magnetic tension force. If the lines are closer together and bunched in a region, there is a transverse force due to their pressure that replicates the magnetic pressure force. Any plasma on a given line stays on that line as it moves and cannot move to another line. This is basically the flux freezing process associated with ideal MHD.

An important example of this is shown in Fig. 4, illustrating the solar-wind interaction with the Earth's magnetosphere. The plasma on the incoming solar wind is embedded on solar-wind lines that are different from the

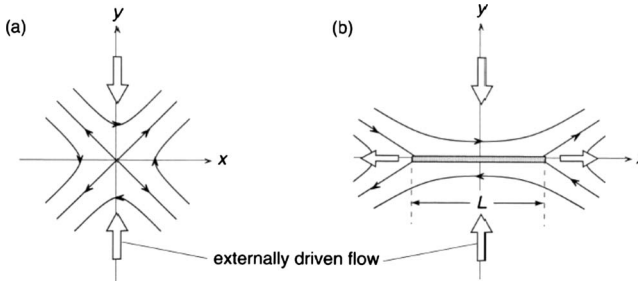


FIG. 3. Formation of current sheet by externally driven flow. From [Forbes, 2007](#).

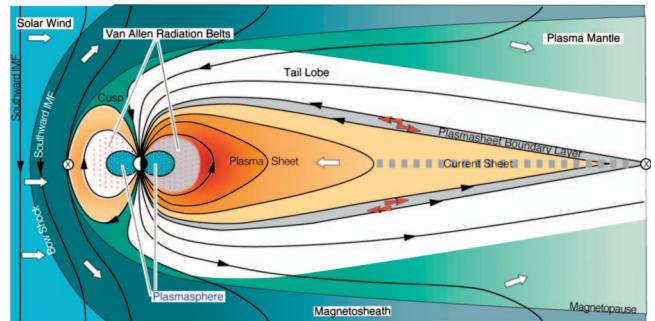


FIG. 4. (Color) Cross section of the simplest model of the magnetosphere in the day and night meridian. From <http://space.rice.edu>

magnetospheric lines. In this picture there is no way for the solar-wind plasma and energetic particles to penetrate into the Earth's magnetosphere. The solar wind is accordingly forced to move around the magnetosphere.

This is where magnetic reconnection comes into play. The plasma is not truly infinitely conducting although in space and astrophysical plasmas the conductivity is very high. Because of the possibility of magnetic reconnection, some of the solar-wind lines can break near the surface separating them and they can reattach to lines in the magnetosphere, which also break. As a result some of the solar-wind lines end up attached to the magnetosphere, allowing the solar-wind plasma to penetrate the magnetosphere. Solar cosmic rays can also get in and are directly observed.

How such physical processes occur and how fast line breaking takes place are the subjects of research of the last 50 years. As a result of experimental, numerical, and theoretical research much progress has been made in understanding reconnection. Early work based on elementary MHD physics demonstrated the possibility of reconnection but predicted reconnection rates that are too slow to explain the observations. As a result of the application of more sophisticated physics, much insight has been gained, and the reasons why reconnection is so much faster than first supposed are beginning to emerge. It is essentially a converse of the remarkable property of flux freezing described previously.

During the past decades, progress in understanding the physics of magnetic reconnection has been made on the three fronts: space and astrophysical observations, theory and numerical simulations, and laboratory experiments. Space and astrophysical observations have provided evidence that magnetic reconnection plays an important role in natural plasmas and generated strong motivations for fundamental research. Theory and numerical simulations provide insights to help break down the complex reconnection phenomena into a set of simpler processes and to gain improved physics understanding of each process. Magnetic fusion experiments provide examples of magnetic reconnection through self-organization of their configurations. Laboratory experiments dedicated to the study of the fundamental reconnection physics measure the key plasma param-

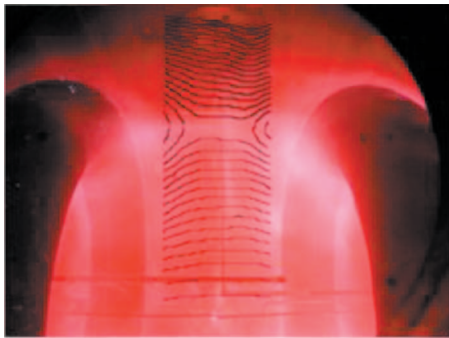


FIG. 5. (Color) Photograph (time integrated) of controlled driven reconnection discharges (in hydrogen) in the MRX, superimposed with flux contours calculated from measurements by magnetic probes (see <http://mrx.pppl.gov/>). Oppositely directed field lines are seen to meet and reconnect in the reconnection region. From Yamada, 1999b.

eters simultaneously at large number of points in the reconnection region (Yamada, 2001). By contrast, a space satellite provides data only at a few selected points. Dedicated laboratory experiments quantitatively cross-check theoretically proposed physics mechanisms and models and provide a bridge between space observations and theoretical ideas (Sweet, 1958). Recent significant progresses in data acquisition technologies has allowed detailed magnetic field structures of reconnection regions to be measured by space satellites and in laboratory experiments. Figure 5 presents contours of constant flux which was deduced from experimentally measured data using magnetic probes located at multiple (30) locations in the reconnection region of the magnetic reconnection experiment (MRX) (Yamada *et al.*, 1997a; Yamada, 1999a).

The primary objectives of this review are to highlight the recent progress in understanding magnetic reconnection and to illuminate key physics mechanisms for fast reconnection. One of the most important questions has been why reconnection occurs much faster than predicted by classical MHD theory. During the past ten years, notable progress in understanding the physics of this fast reconnection has been made through numerical simulations, observations from satellites, and dedicated laboratory plasma experiments. Extensive theoretical and experimental work has established that two-fluid effects, resulting from the fundamentally different behavior of ions and electrons, are important within the critical layer where reconnection occurs. The two-fluid effects are considered to influence the rate at which reconnection occurs in the magnetosphere, stellar flares, and laboratory plasmas. Dedicated laboratory experiments and magnetospheric satellite measurements show strikingly similar data in the profiles of magnetic field and electrostatic and magnetic fluctuations. Recent improvements in the understanding of reconnection on the investigations of magnetic self-organization in laboratory and space-terrestrial plasmas will also be covered.

Beginning with a discussion of the seminal ideas of Sweet and Parker, Petschek, and Dungey, this review of

magnetic reconnection research will survey findings from significant studies that have continued up to the present time. While theory led the early research progress in this area, more recent research has been dominated by experiments and numerical simulations. Since the early work is fairly well known, we place more emphasis on recent experimental, numerical, and theoretical work and focus on modern findings of most significance. There are a number of different views as to which physical processes are most important for reconnection. In particular, the relative importance of two-fluid Hall processes versus fluctuation-induced anomalous-resistive processes is debated. Our goal is to provide a balanced presentation of these views.

We address the following major questions which have been studied intensively:

- (1) What are the mechanisms of magnetic reconnection in the collisionless plasma? How does the two-fluid physics influence the speed and dynamics of local reconnection? What determines the structure of reconnection layers?
- (2) Why is the reconnection rate so fast in collisionless plasmas? What is a scaling for reconnection rate on collisionality?
- (3) How do fluctuations and turbulence affect the reconnection dynamics? Which fluctuations are most relevant, how are they excited, and how do they determine the reconnection rate and influence the conversion of magnetic energy?
- (4) How is the local physics that has been studied in great detail connected to the global environment around the reconnection layer?

A number of physics topics that are vigorously debated at present and not yet resolved at the moment are the following: (1) How is magnetic energy converted to the kinetic energy of electrons and ions? In what channel does the energy flow take place? (2) How is the reconnection layer generated by a global boundary? (3) Why does reconnection occur impulsively in most cases? Keeping these questions in mind we review most of the significant modern experimental discoveries in magnetic reconnection research and discuss many of the theoretical investigations to which they have led.

In this review we make an effort to cover both the major experimental results and space observations that have provided useful information on the physics of magnetic reconnection over the past few decades. This review is different from recent reviews which have emphasized theoretical aspects of reconnection or results from numerical simulations. To cover wide physics aspects of magnetic reconnection, see Biskamp (2000), Priest and Forbes (2000), and Birn and Priest (2007).

Our perspective is that magnetic reconnection is influenced and determined by both local plasma dynamics in the reconnection region and global boundary conditions. One major question is how large-scale systems generate local reconnection structures through formation of current sheets—either spontaneously or via imposed

boundary conditions. We devote the bulk of our effort to addressing local reconnection layer physics in Secs. V–VII. Although reconnection often involves changes in global topology, its properties are less understood. Section VIII is devoted to global issues of magnetic reconnection.

II. MAGNETIC RECONNECTION OBSERVED IN SPACE AND LABORATORY PLASMAS

A. Magnetic reconnection in solar flares

Since the inception of the concept, magnetic reconnection has been considered to play a major role in the evolution of solar coronae as well as in CMEs (Parker, 1979; Tsuneta, 1996; Priest and Forbes, 2000). Solar flares have been central objects for studying physical mechanisms of magnetic reconnection. The topologies of soft-x-ray pictures are seen to change within a time scale of minutes or hours, much shorter than the Sweet-Parker time (Parker, 1957). The study of the dynamics of solar flares has been intensified through the detailed pictures of solar coronal activities recently taken by modern satellites from Skylab in the 1970s, through Yohkoh, and in present times through Solar and Heliospheric Observatory (SOHO), TRACE, Ramaty high energy solar spectroscopic imager (RHESSI), and Hinode. These satellites have revealed the solar atmosphere with unprecedented spatial and temporal resolution covering wavelengths from ultraviolet through soft and hard x rays to gamma rays. With many large coronal loops seen actively interacting with themselves (Fig. 1), their topology is observed to change rapidly on a very short time scale of a few minutes during an eruptive phase.

During magnetic reconnection, conversion of magnetic energy should occur in the solar corona, where a much higher plasma temperature than that of the photosphere is routinely observed. Finding the true cause of heating of the corona to more than 10^6 deg (100 eV) is a major goal of solar plasma physics (Birn and Priest, 2007). While there are other possibilities such as wave heating, reconnection is the most likely candidate for the coronal heating mechanism since the magnetic field represents the dominant energy source in the corona. Sources of the magnetic field at the photosphere are dynamic and highly fragmentary. The magnetic flux at the surface in the quiet Sun is replaced every 14 h (Hagenaar, 2001). Close *et al.* (2004) investigated the statistical properties of magnetic field lines of the lower corona (under 2500 km) by constructing magnetic field lines from magnetograms of the SOHO data, tracking them, and recalculating their connectivity. They discovered that the time for all field lines to change their connection is only 1.5 h. This suggests that very fast reconnection is taking place at numerous places. In the past decade, many mechanisms have been proposed. Priest *et al.* (2002) proposed a *tectonics* model in which a hierarchy of multiple current sheets is formed at the coronal separatrix surfaces of their model, in analogy with dynamics of the Earth's geophysical plate tectonics.

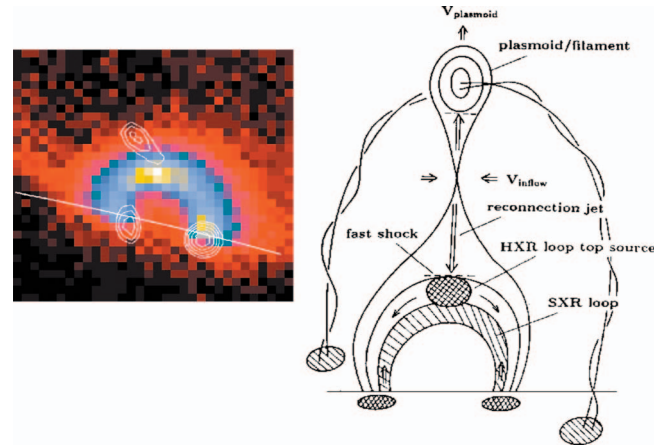


FIG. 6. (Color) Hard-x-ray image from the top of an arcade adapted from Masuda *et al.*, 1994 and a CME model from Shibata *et al.*, 1995.

There are different types of eruptions in the solar atmosphere such as coronal mass ejections, prominence eruptions, and eruptive flares, and they are considered to be related. Coronal mass ejections (CMEs) are large-scale ejections of mass and magnetic flux from the corona into interplanetary space. They are thought to be produced by a loss of equilibrium in coronal magnetic plasma structures, which induces abrupt changes in magnetic topology. A typical CME carries roughly 10^{15} Wb of flux and 10^{13} kg of plasma into space (Priest and Forbes, 2000). During the active period of the Sun, one CME is seen per day. The intermittent emergence of new flux from the convection zone and reshuffling of the footpoints of closed coronal field lines causes coronal field stress to accumulate. When the stress exceeds a certain threshold, the stability of the magnetic field configuration breaks and erupts. This model is called a storage model. However, this plausible explanation is difficult to verify by observation due to limited measurements of magnetic field topology.

Many theories and numerical simulations have been attempted in order to determine the detailed mechanisms of the CME. The Carmichael-Sturrock-Hirayama-Kopp-Pneuman (CSHKP) model (Carmichael, 1964; Sturrock, 1966; Hirayama, 1974; Kopp and Pneuman, 1976) has been regarded as a standard model, while some modification has been made later as shown in Fig. 6. Initially, coronal arcades of magnetic field lines are in equilibrium supporting a high-density filament called a prominence which resides on top of the arcade lines. When the prominence magnetic field and its overlaying coronal arcade break, a CME occurs.

An intriguing illustration of magnetic reconnection occurs in the wake of a coronal mass ejection. As the mass is ejected from the solar surface it pulls out field lines of a magnetic loop. As the ejected mass moves away from the Sun, the opposing magnetic field lines of the loop are drawn out (see Fig. 6), and these field lines begin to reconnect at an *X* point. The reconnection sends particles down the field lines and when the par-

ticles hit the surface they emit radiation that appears as a pair of ribbons. As more lines reconnect the X point rises and the ribbons separate correspondingly. The correlation of this rise and the separation of the ribbons illustrates the reconnection event [see Pneuman (1984) for a detailed description and Harvey and Recely (1984) for a specific event].

Some theoretical work has focused on two-dimensional (2D) models of the evolution of force-free magnetic arcades, in which field-line footpoints are advected by flows in the solar photosphere. A 2D flux-rope model has been proposed by Forbes and Priest (1995) to describe the eruptive processes of solar flares by a sequence of ideal MHD equilibria. They demonstrated that the equilibrium of a flux rope jumps from one state to the other through the formation of a current sheet or reconnection layer in the solar atmosphere. Recent work addresses three-dimensional (3D) effects.

Recent satellites have provided a wealth of observational evidence of magnetic reconnection. Cusp-shaped flare loops consistent with the classical CSHKP models were observed and a plasmoid ejection model was proposed (Shibata *et al.*, 1995). The profiles of hard-x-ray emissions show evidence of particle acceleration at the top of soft-x-ray flares, concomitantly with the appearance of impulsive flares or CMEs. Masuda *et al.* (1994) postulated that magnetic reconnection occurs as predicted by the classical CSHKP model for long-duration-event flares and that high speed jets produced by reconnection intersect with the top of the reconnected flare loop to produce a hot region represented by strong hard-x-ray emission. Based on this observation, a standard model was proposed modifying the earlier flare models as shown in Fig. 6. Yokoyama *et al.* (2001) measured the reconnection speed based on evolution of the soft-x-ray pictures from Yohkoh and concluded that the reconnection speed is in the relatively wide range of $(0.001\text{--}0.05)V_A$.

The features of energetic particles in solar flares are studied using the hard-x-ray and γ -ray imaging systems of the Reuven RHESSI (Lin *et al.*, 2003). Emissions from energetic ions up to GeV energies and electrons up to 100 MeV energies are observed during large solar flares (Lin, 2006). Comparative studies of these images with TRACE images show that the locations of these emissions overlap with the arcade footpoints on the photosphere, suggesting that these emissions are due to collisions of energetic particles with the solar surface. These results are consistent with the physical picture shown in Fig. 6. The observed energy spectra are often of a power-law form, and the estimated total energy from these particles can be as large as 50% of the total released energy of solar flares. These results suggest that there exist efficient mechanisms for accelerating non-thermal particles to high energies during magnetic reconnection. This poses a significant challenge to our understanding of magnetic reconnection physics as theoretical investigations on particle acceleration have just begun. One particular idea recently proposed is based on Fermi acceleration from contracting magnetic

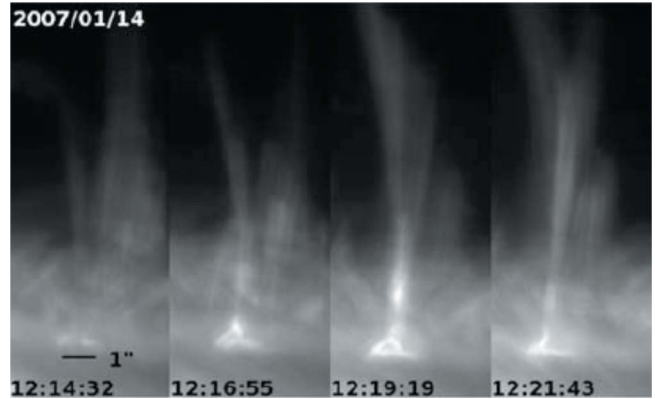


FIG. 7. (Color online) Time evolution of typical Ca jets observed in Ca II H broadband filter of Hinode-SOT. Times are shown in UT. From Shibata *et al.*, 2007.

islands with magnetic reconnection (Drake *et al.*, 2006). Some signatures of magnetic island correlating with energetic electrons have been observed in magnetospheric plasmas (Chen *et al.*, 2008).

A recent solar satellite was launched from Japan in 2006 to study the properties of the solar atmosphere. Its data are revealing much about evolution of the chromospheric and coronal plasmas, as well as how plasma waves might transport energy to the corona. De Pontieu *et al.* (2007) found evidence of Alfvén waves propagating with the speed of 10–25 km/s and argued that the waves are energetic enough to accelerate the solar wind and possibly heat the quiet corona. Shibata *et al.* (2007) reported the ubiquitous presence of chromospheric jets at inverted Y-shaped exhausts outside sunspots in active regions (Fig. 7). They are typically 2000–5000 km long and 150–300 km wide, and their velocity is 10–20 km/s. They suggested that magnetic reconnection similar to that seen in the corona occurs at a much smaller spatial scale throughout the chromosphere and that the heating of the solar chromosphere and corona may be related to small-scale reconnection. With these two different views from the same satellites, future investigations may answer one of the most important questions: how is the solar corona heated to a temperature more than the two orders of magnitude higher than that of the photosphere?

B. Magnetic reconnection in the magnetosphere

The solar wind travels inside the solar system, carrying magnetic fields with it. When the solar wind interacts with a planetary magnetic field or with other solar wind with different velocity vector components, magnetic boundary layers develop. These boundaries, current sheets are seen and magnetic reconnection is thought to occur. When the field lines meet nearly antiparallel in these boundaries, a current sheet develops with the magnetic field becoming zero (neutralized) at the sheet center. It is sometimes called a neutral sheet. Current sheets are seen on both the dayside (magnetopause) and the nightside of the Earth's magnetosphere (magnetotail) as

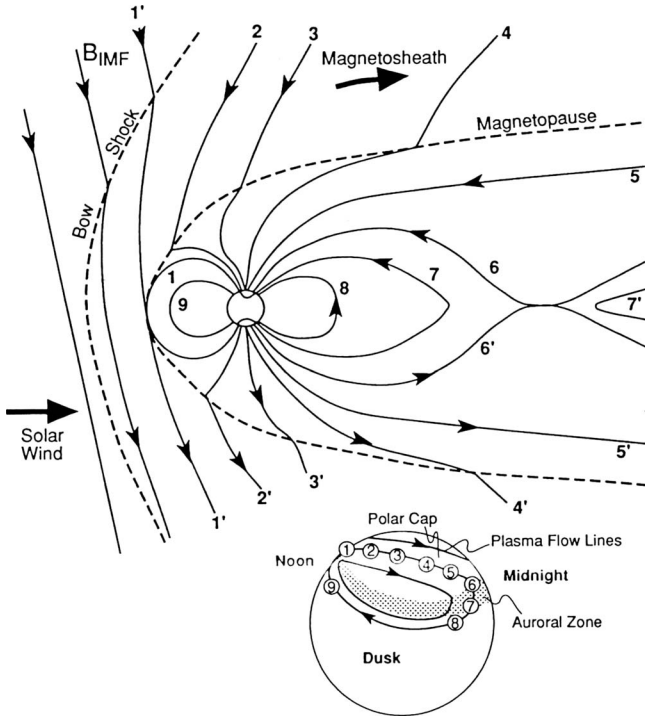


FIG. 8. Schematics of magnetic reconnection and generated flow of plasmas in the magnetosphere. IMF field line (1') reconnects the Earth dipole field line (1) at the magnetopause. Field lines 6 and 6' reconnect at the second X line in the tail. From [Hughes, 1995](#).

shown in Fig. 8 ([Vasyliunas, 1975; Dungey, 1995; Kivelson and Russell, 1995](#)) at places where interactions occur between the magnetic fields of the solar wind and the Earth's dipole field. Such current sheets are expected around all other magnetized planets.

Satellite observations show that the thickness of the current sheath thickness is of the order of the ion skin depth or the ion gyroradius. The ion skin depth is typically 100–200 km in the magnetosphere while it is larger by one order of magnitude (1000–2000 km) in the magnetotail. In this situation, the reconnection dynamics cannot be described by conventional MHD theory of reconnection. This is because ions and electrons behave differently in the reconnection region requiring two-fluid and kinetic physics. Also, the reconnection could be a very turbulent process in both time (intermittent) and space (patchy) since the relative drift of electrons with ions can excite electrostatic or electromagnetic fluctuations. A number of researchers have observed electric and magnetic turbulences in the magnetopause as well as in the magnetotail.

The magnetopause is the boundary that separates the geomagnetic field and plasma of terrestrial origin from the solar-wind plasma ([Hughes, 1995](#)). Figure 8 shows the magnetosphere on both the dayside and nightside. On the dayside magnetopause, pressure balance is maintained between the incoming solar wind and the Earth's magnetic field. Ampere's law applied across the boundary shows that currents have to flow in the boundary sheet as in the figure. On the nightside of the magneto-

sphere there is a magnetotail in which the lines of force stretch behind the Earth in a direction away from the Sun. As seen in Fig. 8, a current sheet is formed between the tail lobes, which is occupied by the magnetic field lines that connect to the two polar regions of the Earth. The energy and plasma in these magnetotails are intermittently released into the inner magnetosphere during the magnetic substorms. It is generally believed that, during a substorm, solar-wind plasma and energy are injected into the magnetosphere and then released from it through magnetic reconnection processes ([Hughes, 1995](#)).

When the magnetic field on either side of the dayside magnetopause has different tangential components, a current sheet develops and dissipates, as the magnetic fields reconnect. If a southward interplanetary magnetic field (IMF) and the northward Earth dipole field meet at the magnetopause, reconnection occurs efficiently. The reconnected field lines, still tied to the polar cap on one end, are embedded in the solar wind on the other side and are blown away to the nightside of the Earth. Dungey showed that this motion of the reconnected magnetic field lines would induce the observed pattern of plasma flow in the upper atmosphere of the polar cap, as shown in Fig. 8 as lines 1–5. The plasma on the flux tube driven away by the solar-wind flow would sense an electric field of $E = v_{SW} \times B_{SW}$ in the dawn-dusk direction. This electric field shows up in the polar cap and drives electron flow through the ionosphere from the noon to midnight direction.

If this process was to continue indefinitely, the entire geomagnetic fields would become connected to the open field lines of IMF. Actually, another reconnection at another x line happens and the half of the reconnected flux returns to closed magnetospheric lines in the lobes which is connected to the Earth while the other half is blown downstream with the solar wind. The newly connected closed dipole (dipolarized) field line contracts toward the Earth increasing the kinetic pressure of the dipolarized plasma. The stressed dipole field lines flow toroidally around the Earth from the night to dayside. The convective flow circuit is closed as shown in Fig. 8 as lines 6–9. This figure illustrates the plasma flow lines caused by the sequences of reconnection processes as lines 1–9. The entire process described here as a steady process actually happens intermittently in bursts, which are called substorms. This Dungey picture describes the fundamental role of magnetic reconnection in substorms.

C. Magnetic reconnection in self-organization of fusion plasmas

A large amount of experimental evidence for magnetic reconnection is found in fusion research devices by measurements of field-line rearrangement. Most fusion laboratory experiments are carried out in toroidal (donut-shaped) plasma systems that satisfy the conditions for a MHD treatment of the plasma. Experimental examples of magnetic reconnection are “sawtoothing”

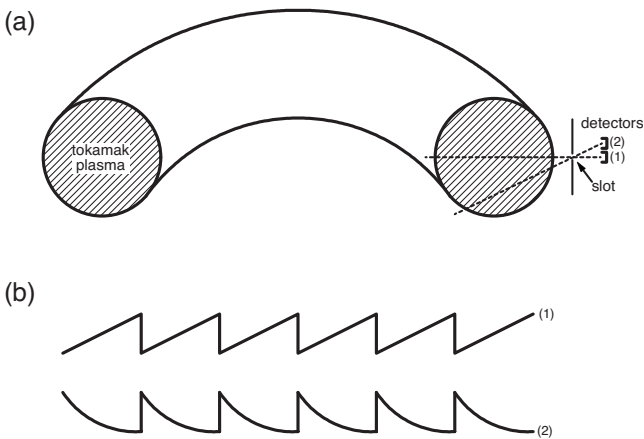


FIG. 9. Observation of sawtooth oscillation by soft-x-ray diagnostics. (a) Schematic setup to measure the minor cross section of tokamak with two (inner and outer) chords. (b) Soft-x-ray signals along the inner (1) and outer (2) cords.

tokamak fusion plasmas with the Lundquist numbers exceeding 10^7 , magnetic self-organization in spheromaks, and RFP plasmas. Many experiments have been carried out to investigate magnetic reconnection phenomena in these devices to gain better control of their confinement features. Generally, it is found that magnetic reconnection is determined both by 3D global boundary conditions and by local plasma parameters in the reconnection layer.

In toroidal fusion devices, toroidal currents are induced to heat the plasma and produce poloidal magnetic fields that effectively confine the high pressure plasma by a compressing pinch force. Tokamaks, RFPs, and spheromak configurations belong to this category. While these configurations generate self-pinching poloidal fields (PFs), toroidal fields (TFs) are supplied differently. In tokamaks a strong toroidal field is supplied externally. The toroidal field of a RFP is created by the combined effects of internal currents and an externally applied poloidal current. A spheromak does not have any externally applied toroidal field, and its toroidal field being entirely created by an internal plasma current. There is a remarkable feature common to the RFP and spheromak configurations. This is that their plasmas constantly tend to relax to a quiescent state through global magnetic self-organization in which magnetic reconnection plays a key role.

1. Magnetic reconnection in tokamaks

Sawtooth relaxation oscillations were discovered by von Goeler *et al.* (1974) in a tokamak discharges. They are a typical example of global magnetic reconnection in a plasma. The sawtooth oscillation (Kadomtsev, 1975; Wesson, 1987) is observed as a periodic repetition of peaking and sudden flattening of the electron temperature (T_e) profile in the minor cross section as shown in Fig. 9. The conventional diagnostics for this phenomena are soft-x-ray diodes measuring bremsstrahlung emission along different chords across the plasma. The ob-

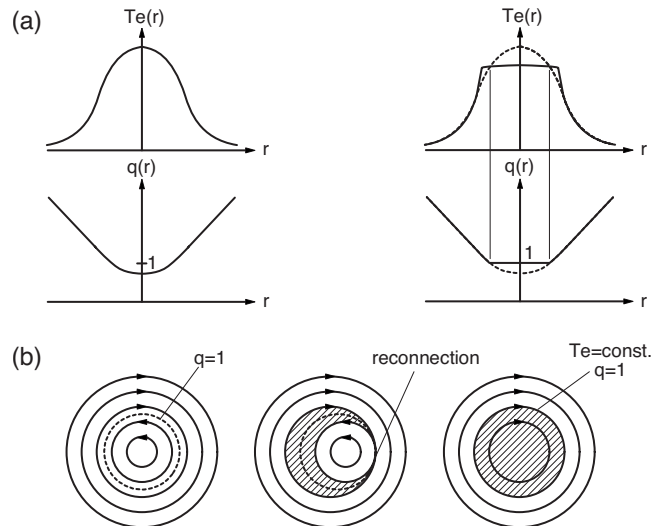


FIG. 10. Sawtooth relaxation and reconnection. (a) Schematic view of changes of T_e and q profiles across poloidal plane during sawtooth crash in a tokamak plasma. (b) Description of Kadomtsev model (Kadomtsev, 1975) in a poloidal plane; $m=1$, $n=1$ MHD instability develops near the $q=1$ flux surface leading to magnetic reconnection.

served signals usually have the shape of sawtooth, hence the name. Recently, the electron cyclotron emission (ECE) diagnostics have accurately measured the evolution of the temperature profiles.

An axisymmetric tokamak plasma consists of nested toroidal flux surfaces on each of which T_e is assumed constant. The MHD stability of a tokamak plasma is determined by the safety factor q , which is 2π times the inverse of the rotational transform of toroidal magnetic field lines (Wesson, 1987). A peaked T_e profile generally leads to a more highly peaked current profile because of a higher Spitzer conductivity at the center of plasma. The resultant strong peaking makes the plasma unstable to a helical MHD kink mode, which develops near a resonant flux surface. The resulting helically deformed plasma induces magnetic reconnection near the $q=1$ surface, as shown in Fig. 10. This reconnection produces a topological rearrangement of the magnetic field lines relaxing the plasma into a lower energy state. Kadomtsev (1975) proposed that the reconnection event (crash) should lead to a uniform current-density configuration with $q=1$ and a flat electron temperature (T_e) profile. The same cyclic evolutions are repeated afterward.

During a sawtooth crash in the Tokamak Fusion Test Reactor (TFTR) tokamak plasma, magnetic reconnection was observed to cause only a partial mixing of field lines. This was evidenced by the small changes in the q profile which were documented by Levinton *et al.* (1993), Yamada *et al.* (1994), and Nagayama *et al.* (1996). This change of q value represents magnetic reconnection. Recent progress in the study of tokamak sawtooth reconnection will be discussed in Sec. VIII.

2. Magnetic relaxation in reversed field pinches

The RFP is an axisymmetric toroidal pinch in which plasma is pinched and confined by a poloidal magnetic

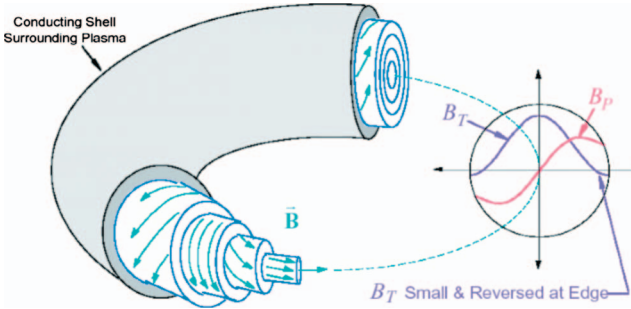


FIG. 11. (Color) Schematic of a RFP plasma configuration showing magnetic field lines strongly sheared. B_T is the toroidal field and B_P is the poloidal field. Reconnection can occur at multiple surfaces, such as those indicated in the cutaway view of the toroidal plasma. The radial dependence of the poloidal and toroidal magnetic fields is plotted. From Sarff *et al.*, 2005.

field created by toroidal plasma current and by a toroidal field created internally and externally. As postulated by Taylor (1974), the RFP configuration is generated by a process of self-organization of plasma in which plasma settles into a state of minimum energy for a given helicity.

In an RFP discharge, magnetic reconnection occurs during this self-organization process of a toroidally confined plasma and can be both continuous and impulsive. The magnetic energy is stored in a force-free magnetic equilibrium configuration via a slow adjustment to an external driving force. Then, through a sawtooth event, the magnetic field suddenly reconnects and the plasma reorganizes itself to a new MHD equilibrium state. In this device, local reconnection on different surfaces leads to a global relaxation whose macroscopic properties are studied. The RFP magnetic field is sheared (Fig. 11), its pitch changing its direction from a toroidal direction at the center to a nearly poloidal direction at the edge. Because of the shearing of the field lines, reconnection occurs at multiple radii, each radial location corresponding to a rational surface at which the safety factor $q = m/n$ (m and n are poloidal and toroidal mode numbers, respectively). Often the multiple reconnections occur suddenly and simultaneously, leading to a sudden global rearrangement of the entire magnetic field. During these reconnections it is found that global helicity tends to be conserved while the total magnetic energy is dissipated (Ji *et al.*, 1995).

In a representative RFP device, the Madison Symmetric Torus (MST), simultaneous reconnection at different radii corresponding to different n with $m=1$, is observed. When the current-density profile becomes highly peaked, tearing modes develop reconnecting magnetic field lines, and plasma reorganizes itself rapidly to a new MHD equilibrium state. In this self-organization of magnetic field lines, a conversion of magnetic flux and energy from poloidal to toroidal occurs. Figure 12 shows the time evolution of toroidal and poloidal magnetic fluxes, together with that of magnetic helicity K (discussed in Sec. VIII) and magnetic energy W indicating

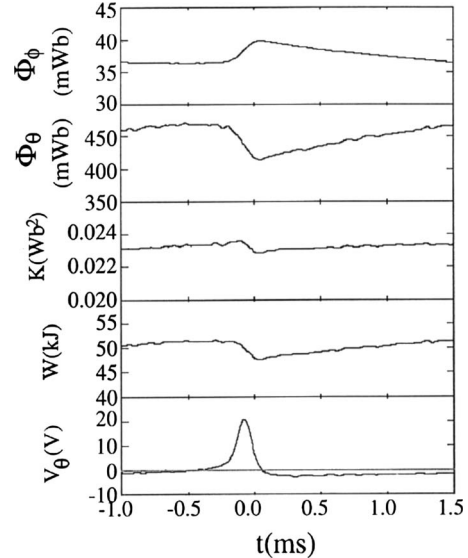


FIG. 12. A magnetic reconnection event in MST plasma. Shown from the top are time evolutions of toroidal, poloidal magnetic flux, magnetic helicity K (explained in Sec. VIII), magnetic energy W , and one-turn poloidal voltage. Adapted from Ji *et al.*, 1995.

abrupt conversion of poloidal magnetic flux to toroidal flux making the total magnetic energy smaller (Ji *et al.*, 1995). The ion temperature increases significantly at the expense of magnetic energy. Multiple reconnection events are often observed and the reconnection is impulsive in time. Recent theoretical and experimental results showed that the different reconnections are coupled. Essentially all effects of magnetic self-organization in MST (dynamo, ion heating, and momentum transport) are strongly amplified when multiple coupled reconnections occur. One of the most important questions for global reconnection is why reconnection occurs impulsively. The study of magnetic reconnection in RFP is discussed in Sec. VIII.

D. A dedicated laboratory experiment on reconnection

Recently, more than a half dozen dedicated laboratory devices have been built to study the basic mechanisms of magnetic reconnection. The MRX device is a typical example of such a device. Reconnection in the MRX is driven by utilizing a flexible toroidal plasma configuration (Yamada *et al.*, 1997a). The MRX device creates an environment in which the MHD criteria are satisfied on the global scale with a large Lundquist number and a size much larger than the ion gyroradius. One advantage of the modern experiments is that the current sheets are made to be toroidally continuous and free from constraints caused by the termination of end plates or electrodes.

In the MRX, reconnection is driven in a controlled manner with toroidal-shaped flux cores that contain coil windings in both the toroidal and poloidal directions. By pulsing currents in these coils, two annular plasmas are inductively created around each flux core (Yamada *et al.*,

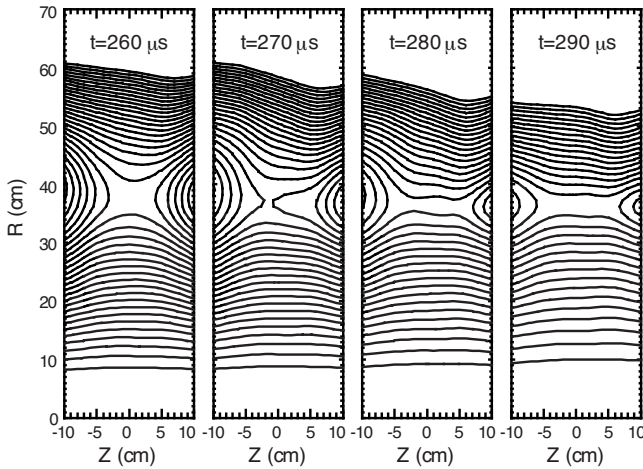


FIG. 13. Demonstration of magnetic reconnection seen through measured field lines in the MRX. In the low beta plasma outside of the neutral sheet, poloidal flux counters represent magnetic field lines and are seen to break and reconnect. From [Yamada et al., 1997a](#).

1981, 1997a). After the plasmas are created, the coil currents are programmed to produce a narrow neutral sheet or current layer and to drive magnetic reconnection in it. The dynamics of local reconnection layer shown in Fig. 13 is then studied in it. When the experiments are carried out in a collision-dominated plasmas with no guide magnetic field (antiparallel reconnection), a typical 2D Sweet-Parker diffusion region profile (a rectangular box shape), with two Y-shaped ends, is observed. The time evolution of the magnetic field lines is measured and displayed as a movie.¹ This movie shows the time evolution of the measured flux contours of the reconnecting field. By monitoring these contours, the reconnection rate as a function of plasma parameters is studied ([Ji et al., 1998, 1999](#)).

During the past decade, extensive studies have been carried out in many other laboratories which are dedicated to the study of magnetic reconnection. The results of the MRX and the other dedicated laboratory devices are later described in more detail.

III. THEORETICAL BACKGROUND OF RECONNECTION STUDY

A. Early history of magnetic reconnection theory

The idea of magnetic reconnection first originated in the attempts to understand the heating of the solar corona and the origin of the enormous energy observed in solar flares. It was early recognized ([Giovannelli, 1946; Hoyle, 1949; Dungey, 1953](#)) that solar flares occur in the neighborhood of sunspots where the magnetic field is observed to have magnitudes of several kilogauss. Such fields contain large quantities of energy, and if a mechanism could be found to convert this energy into heat,

radiation, and kinetic energy, it would provide an origin for the energy emitted by a solar flare.

However, a simple estimate of the resistive decay time of the magnetic field shows that direct conversion of magnetic energy by Ohmic dissipation would take many years. Instead, attention was concentrated on the origin of the energetic particles associated with the flares. [Giovannelli \(1946\)](#) showed that the changing field strengths in the sunspot fields would produce large voltages that were capable of accelerating charged particles to high energies. It was suspected that such voltages in the presence of the magnetic fields would lead to mass motions when the electric field was applied across the magnetic field and would be shorted out when it was parallel to the field. Thus, attention was directed to neutral point regions where the magnetic field was zero.

The destruction of the field by MHD forces was emphasized by [Dungey \(1953\)](#) who pointed out that near neutral points the magnetic field would be flattened into current layers and changed by magnetic reconnection, leading to release of energy.

[Sweet \(1958\)](#) pointed out at the sixth International Astronomical Union (IAU) Conference in 1956 that the electric current density j could be concentrated in thin layers [the current sheets of [Dungey \(1953\)](#)], where its magnitude is enhanced such that Ohmic dissipation, proportional to j^2 , could release magnetic energy at an increased rate. In actual fact, it is not Ohmic dissipation that leads to the conversion of magnetic energy to other forms. The true energy conversion mechanism is Ohmic dissipation acting differentially to change the shape of the magnetic lines so that they develop a strong curvature in the current layer. This change itself releases only a small amount of energy. The main conversion is caused by the curved lines unfolding and accelerating the plasma out of the ends of the current layer, simultaneously lowering the magnetic energy, accelerating the plasma, and increasing its kinetic energy. This kinetic energy leads to shocks and viscous dissipation which turns the energy into radiation and accelerates particles. This sequence of events is termed magnetic reconnection although it is only the first stage that involves physical reconnection of the magnetic lines.

At the IAU conference, [Sweet \(1958\)](#) introduced the detailed model for reconnection and conversion of energy as described next. This model was first called the Sweet model for reconnection. The same model was independently discovered and elaborated by [Parker \(1963\)](#) and it eventually became known as the Sweet-Parker model of magnetic reconnection.

As described in the Appendix, magnetic field lines in an infinitely conducting plasma have physical reality. These lines can neither be created, destroyed, nor broken. This is a very good assumption everywhere in space and astrophysics except in narrow current regions where the electrical current density becomes extremely high. However, reconnection can break lines in such a current layer where the infinite conduction approximation no longer holds as shown in the Appendix. Figure 2 shows that the reconnection only involves a small part of the

¹See the MRX website at <http://mrx.pppl.gov/mrxmovies>

reconnecting lines analogous to breaking and reconnecting strings. Once the reconnection is affected, the curvature force associated with the changed configuration of the lines produces a large acceleration, which completes the conversion of magnetic energy to other forms.

In the Earth's magnetosphere there is a second consequence of magnetic reconnection. Once the terrestrial lines cross the magnetospheric surface and connect to the solar-wind lines, energetic particles from the solar-wind part of a line can flow into the magnetospheric part. This global effect results from changing the line over a very small part in the current layer between the solar wind and the magnetosphere.

The introduction of the Sweet-Parker model led to a long period of research into the physics of magnetic reconnection. Although the Sweet-Parker model leads to much faster conversion of magnetic energy than is expected from resistive decay in the absence of current sheets, estimates showed that it is still much too slow to account for the fast conversion observed in solar flares. The history of magnetic reconnection research is of attempts to modify the simple Sweet-Parker model to increase the reconnection rate enough to account for solar flares and magnetospheric reconnection.

One of the first applications of reconnection was made by [Dungey \(1961\)](#) who showed that reconnection of solar-wind magnetic lines could account for the entire gross structure of the magnetosphere as discussed in Sec. II.

The important questions concerning the Dungey model are as follows: Does this reconnection occur and how fast does it happen? As solar-wind lines impinge on the magnetosphere they have a choice: whether to go around it much as water goes around a boat moving through water or to reconnect. The fraction that reconnects and ends up in the Earth's magnetotail is controlled by the reconnection rate. Assuming this is the Sweet-Parker rate, approximately one in one hundred thousand lines reconnects ([Kulsrud et al., 2005](#)) as opposed to the measured value of one in ten ([Hughes, 1995](#)). The predictions of Sweet-Parker strikingly disagree with the observations.

A number of other important applications are discussed in Sec. II.

In most applications, the amount of Sweet-Parker reconnection in the time available is much smaller than that needed to produce the observed amount of reconnected flux. This serious discrepancy was apparently removed by an important modification to the Sweet-Parker model, introduced by [Petschek \(1964\)](#) in 1963.

The Petschek theory introduces slow shocks. If these shocks emerge at a sufficiently small distance from the X point, they produce much faster reconnection rates and can lead to results compatible with observations. The theory was controversial because the origin of the shocks was unclear. Eventually, the Petschek model was considered to be of limited applicability barring a discovery of the shock origin. Its main virtue is, that if it could be made to work, it would explain the desired

faster reconnection rates. Details of the Petschek model are given in Sec. III.B.

Although many other mechanisms have been found to speed up reconnection on the larger scales found in astrophysics, none of them is as powerful as the Petschek mechanism nor produces fast enough reconnection to agree with observations. For this reason the Petschek mechanism is extremely important. A large research effort has been devoted to it and we will spend some time reviewing this work.

The status of the Petschek model was unclear for a long time. Some understanding of the shocks emerged in [Ugai and Tsuda \(1977\)](#). They carried out a detailed numerical simulation in a two-dimensional model for the current layer with appropriate boundary conditions. Their reconnection model had a resistivity that was a specific nonconstant function of space. The resistivity was strongly enhanced in a sizable region about the central X point of the current layer where the field was zero. (The resistivity was larger at the X point than in the exterior region to the current layer by a factor of 100.) Their solution differed from that of Sweet-Parker and possessed Petschek-like shocks. These shocks emerged from the position in the current layer where the resistivity was most rapidly changing.

A similar numerical simulation was carried out by [Sato and Hayashi \(1979\)](#). They allowed the resistivity to be a function of the current density. They triggered the reconnection by imposing a space-dependent inflow into the current layer of flux lines and plasma. Because the resistivity depended on the space-dependent current density, their resistivity was also space dependent as in the Ugai-Tsuda paper. Shocks again were found to emerge at the place where the resistivity was most rapidly changing.

The relation between the resistive scale and the location of the shocks was explored over a wide range of resistivity scales by [Scholer \(1989\)](#). He showed that the shocks always start at the place where the plasma resistivity was most rapidly varying. This is approximately where the resistivity has decreased by a factor of 2 from its maximum value at the current layer center.

[Biskamp \(1986\)](#) was the first to study the Petschek theory with a constant resistivity. His calculation was carried out on a global scale with only a small part of his simulation volume occupied by the reconnecting current layer. (This layer emerged naturally during the simulations.) He made eight simulations and determined the rate of reconnection in each case. Expressing these in terms of magnetic field strengths and scale sizes at the boundary of his computational region, he showed that neither the Petschek nor the Sweet-Parker reconnection rates agreed with the computational results. Expressing the theoretical rates in terms of magnetic field strengths just outside of the current layer and using the length of the current layer as the global length in the two theories, he found that the Sweet-Parker formula for the reconnection rate agreed with all of the eight computational rates. The Petschek formula did not agree with any. He concluded that the Sweet-Parker model was the correct

one. However, he did not emphasize that the resistivity was a constant in space in his calculations, and thus his conclusions did not contradict the earlier results of [Ugai and Tsuda \(1977\)](#) and [Sato and Hayashi \(1979\)](#).

[Uzdensky and Kulsrud \(2000\)](#) carried out a direct boundary-layer theory of the layer assuming constant resistivity and again showed that (1) the Sweet-Parker model was correct and (2) if one tries to artificially impose the Petschek model by introducing subsidiary current layers to represent shocks at some initial time, then at first the reconnection rate is that of Petschek. But the shocks were quickly swept away at the Alfvén speed and the reconnection rate quickly returned to that of Sweet and Parker, in the time for an Alfvén wave to go the global length. The proper scaling of quantities in the boundary layer analysis enabled them to incorporate all possible values for the parameters describing reconnection: the resistivity, the field strength just outside the current, and the current layer length. This boundary layer model is able to take into account any possible magnetic Reynolds number.

The numerical calculations of magnetic reconnection drew attention to the fact that in most astrophysical applications the Sweet-Parker layers were so thin that the ordinary MHD equations were not applicable. Therefore, it is necessary to go beyond ordinary resistive MHD equations which describe a single fluid and to treat the electrons and ions as two separate fluids to properly describe magnetic reconnection. It is necessary to allow the electrons and ions to move separately. This freedom was included in the numerical simulations from 1990 on. At this time computers became powerful enough to carry out a kinetic treatment of electrons with fluid ions or kinetic ions with fluid electrons. With more general physics it was found that, even without Petschek shocks, the reconnection rate could be considerably faster than the Sweet-Parker rate. The faster rate arises because the two-fluid effects allow the current layer to be thicker than the Sweet-Parker layer while allowing the electron current to flow in a thin enough layer to break the field lines. The broader current layer in which the ions flow allows a faster ion outflow and leads to faster reconnection. (The non-MHD current layer thickness is of order the ion skin depth, thicker in many cases than that of the Sweet-Parker model.)

When these faster rates are extrapolated to the larger systems encountered in the Sun and magnetosphere, they still do not adequately explain the observations. To get satisfactorily large reconnection rates, one needs to either somehow generate the Petschek shocks or, alternatively, significantly reduce the length of the reconnecting current layers.

A different approach to speeding up the reconnection rate involves enhancing the plasma resistivity, which naturally increases the reconnection rate. Enhanced resistivity is produced when there are plasma microinstabilities in the current layer and these instabilities occur when the relative flow velocity of the electrons through the ions exceeds the sound velocity. Instabilities with frequencies in the lower hybrid regime are considered im-

portant. A large amount of research has gone into exploring these instabilities and the resistivity that they produce. If the relative drift velocity of the electrons relative to the ions must exceed the ion acoustic speed, then this implies a lower limit to the current density. When combined with the equilibrium of the current layer this implies that its thickness must be equal or less than the ion skin depth and this leads to reconnection rates similar to those predicted by the two-fluid theory.

[Kulsrud \(2001\)](#) and [Uzdensky \(2003\)](#) suggested that if the enhanced resistivity depends strongly on the current density, then a natural mechanism arises to generate the Petschek shocks at a small distance to the X point and a much faster reconnection rate emerges. From the theory of anomalous resistivity generated in current layers it can be shown that such a strong current dependence is related to an equally strong dependence of the growth rate of the instabilities on the current density or equivalently on the relative electron-ion drift velocity.

Another theoretical possibility for fast reconnection was suggested by [Lazarian and Vishniac \(1999\)](#). They made use of the fact that the reconnection rate depends on the global length of the current layer. Since the current layer formation process is not well understood, it has been conventional to take this length to be the global size of the system which is generally large in astrophysical systems. This implies that the reconnection rate is very slow even with non-MHD corrections. Lazarian and Vishniac considered that in an astrophysical turbulence in which the large-scale field reverses, the turbulence can bring oppositely directed lines together over lengths much shorter than the global length. Thus, even the Sweet-Parker rate could be fast. The shorter length implies a smaller amount of magnetic energy being converted in each event but this could be compensated for by having many of these short current layers. If there are enough such layers in the turbulent region, a large amount of magnetic energy conversion occurs in a short time. [Kuritsyn et al. \(2007\)](#) suggested that the length of the current layers that form may involve the internal physics of the current layer itself, reducing the long length of the current layer to a more manageable size and leading to faster reconnection.

A much more complicated picture of reconnection has now emerged which involves non-MHD physics in the layer. A number of experimental devices for studying reconnection have been recently built. An example is the magnetic reconnection experiment at Princeton ([Yamada et al., 1997a, 1997b](#)). One simple result has emerged from the MRX experiment. When this experiment runs in collisional conditions it is found that the reconnection rate is that of Sweet-Parker while when it runs under collisionless conditions the reconnection rate is considerably faster. Many of the above effects have been observed in collisionless conditions. In the past few years, two-fluid effects have been verified. Magnetic fluctuations have been observed in the current layer that appear strong enough to enhance the resistivity and raise the reconnection rate above that of Sweet-Parker. If one employs the *measured* value of the enhanced re-

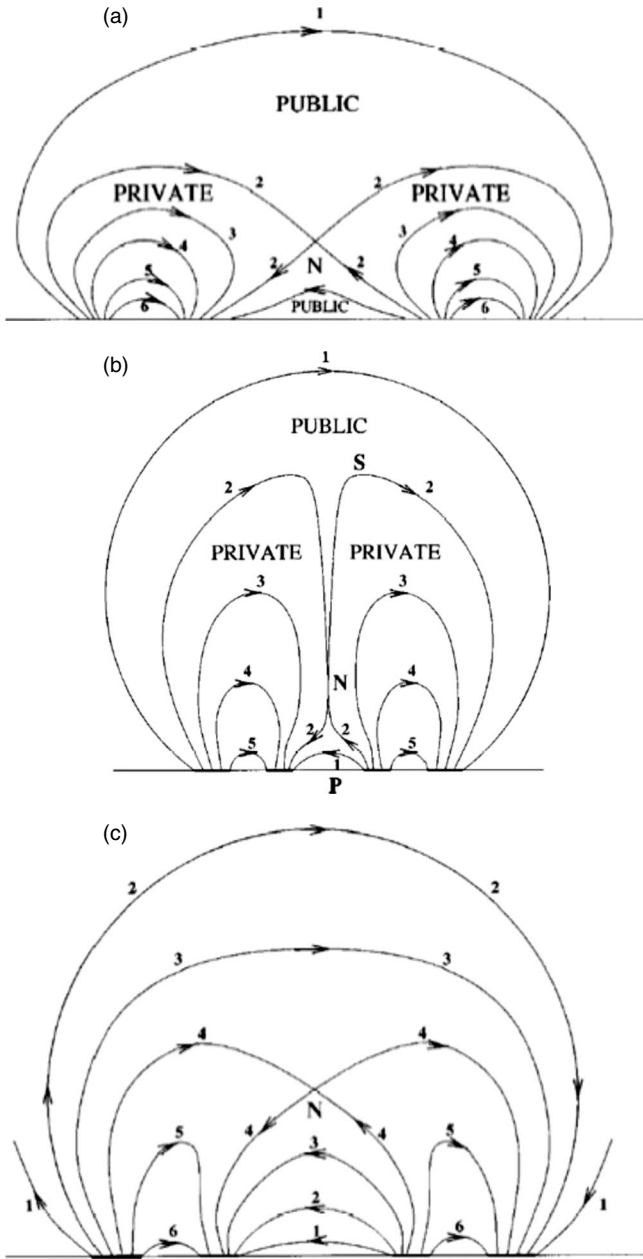


FIG. 14. Evolution of field lines when a pair of sunspots move toward each. From Kulsrud, 1998.

sistivity, the measured outflow velocity, and the compressibility of the plasma in the Sweet-Parker model, then one can duplicate the measured reconnection rate. It is yet to be determined which of the two effects, two fluid or anomalous resistivity, is more responsible for the fast reconnection rate or energy conversion in the MRX.

B. MHD models for magnetic reconnection

In Sweet's model for magnetic reconnection, he considered what would happen if two pairs of sunspots approached each other as in Fig. 14. Each pair has its own magnetic dipole field and as these sunspot pairs approach each other their dipole fields frozen in the solar atmosphere would be crushed together forming a thin

layer. He compared this to the case of a vacuum nonconducting solar atmosphere in which the magnetic field would simply add vectorially and the neutral (N) point of intersection would simply shift from line to line with the consequence that some lines originally connected to a single dipole would end up connecting one sunspot to the other. Comparing this to the highly conducting solar atmosphere case he showed that the line passing through the N point would continue to pass through it. This line divides the private lines connecting to only one dipole and the public interconnecting lines and would continue to divide the same public and private lines.

This line would remain invariant only as long as the solar atmosphere remains sufficiently conducting that the lines remain frozen in the solar plasma. That is to say in Ohm's law,

$$\mathbf{E} + \mathbf{v} \times \mathbf{B}/c = \eta \mathbf{j}, \quad (1)$$

the last term can be neglected (see the Appendix).

No matter how small the resistivity the dipole fields would be crushed so closely together that the region between them would become narrow enough that the current density would be raised to a point where the resistive term is no longer negligible. At this time, the fields would start to interpenetrate, just as in the vacuum solution, and the private lines would cross the N point and become public lines. This resistive penetration would continue until, after a period of time, the field structure approaches the vacuum field structure [Fig. 14 (bottom)] in which many lines would have reconnected.

The lines are labeled by the surface from which they emerge. In the vacuum case of Fig. 14 (bottom), after the sunspots have approached the lines labeled 1–3 in one sunspot split and merge with the corresponding lines from the other spot. These lines have become two public lines one passing below the N point and the other passing above it. For the conducting case [Fig. 14 (middle)] (prior to any reconnection) the same lines at first remain private. Due to the reconnection, first line 2 reconnects to its pair, then line 3, and so forth. The only difference in the last two cases is the time it takes to relax to the final potential field. This time is governed by the physical processes taking place in the narrow current sheet. By the law of induction it is possible to quantify the rate at which the private lines disappear to become public lines. This rate is equal to the electric field E_N at the central N point and normal to the page.

The layer is expanded in Fig. 15. In the absence of resistivity, E_N must be zero since B is zero, and no flux can change. If E_N was not zero, it would drive an infinite current and this current would generate a large magnetic field that would stop the collapse of the layer and push the private flux back. With resistivity the electric field is nonzero and is proportional to ηj . The thinner the layer the larger j is. Thus, the rate of reconnection is inversely proportional to δ , the thickness of this layer. At the N point $E_N = \eta j$ and, since $j \approx B/4\pi\delta$, the rate of reconnection of lines is

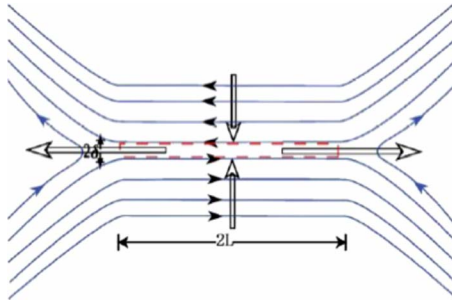


FIG. 15. (Color online) Sweet-Parker model.

$$d\psi/dt = \Lambda B/\delta, \quad (2)$$

where $\Lambda = \eta c/4\pi$ and ψ is the amount of reconnected flux per unit length out of the page.

It would seem that reconnection could go at any speed if δ was sufficiently small. However, this is not the case. As the lines in the current layer reconnect, they pull out of this layer and go to the public region. As the lines pass into the current layer to be reconnected, coronal mass is also carried into the layer, and as the lines leave the layer, mass must also be carried out at a velocity whose magnitude is limited as follows. The excess pressure in the layer is approximately equal to the magnetic pressure $B^2/8\pi$ and this pressure pushes the mass out of the layer. By Bernoulli's law the resulting outward velocity is about v_A , the Alfvén speed, and this limiting speed poses a bottleneck to the reconnection rate. If v_R is the reconnection velocity, then by conservation of mass the amount of mass coming into the layer of length L , $v_R L$, must be equal to the rate of outflow of mass $v_A \delta$ so that the reconnection velocity is

$$v_R = (\delta/L)v_A. \quad (3)$$

This decreases with δ . Equation (2) shows that δ cannot be too large and Eq. (3) shows that it cannot be too small. Taking $d\psi/dt = -v_R B$ we can combine the two equations to obtain both v_R and δ ,

$$v_R = \sqrt{v_A \Lambda / L} = v_A / \sqrt{S}, \quad (4)$$

$$\delta = \sqrt{\Lambda L / v_A} = L / \sqrt{S}.$$

The Lundquist number S is the same as the magnetic Reynold's number $R_M = Lv/\Lambda$ with the velocity taken as the Alfvén velocity.

The time to reconnect all the private lines is of order $t_R = L/v_R \approx \sqrt{S}(L/v_A)$. This time should be compared with the resistive decay time for the region if there was no current layer, $L^2/\Lambda \approx SL/v_A$, a time longer than the time to reconnect by \sqrt{S} . Since the Lundquist number is very large in the corona, often larger than 10^{12} , the reconnection model leads to a large reduction in the time to destroy or rearrange the flux from the sunspots. t_R is still very long compared to the duration of a flare, 10^6 times the dynamic time, $L/v_A \approx 10^9/10^8 \approx 10$ s, so t_R is 10^7 s ≈ 0.3 years. This is much longer than the observed energy release time, which is of order 10^3 s.

Although Sweet's model for reconnection gives a large decrease in the theoretical flare time, it is still much larger than the observed times. This theory was derived analytically by Parker (1957, 1963) and leads to the same result.

Prior to Sweet's work, Parker and co-workers had been considering how fast reconnection might go, but they overlooked the problem associated with mass conservation. Curiously, the priority for this model is somewhat tangled in time. Parker and Krook (1956) attempted to understand how reconnection went somewhat before the 1956 IAU conference, at which Sweet first presented his ideas, and more or less got the correct theory. Parker's modifications and improvements appeared in a paper by Parker (1957) while the IAU conference proceedings were not published until 1958. Since the contributions of the two authors although independent were roughly equal in importance, their reconnection model has consistently been referred to as the Sweet-Parker model. For definiteness we have described reconnection in the context of the two pairs of sunspots, but the ideas of reconnection in a current layer apply more generally to almost any reconnection event in the framework of resistive MHD.

To summarize, the physics leads to such slow reconnection rates: first, a very narrow current layer is needed because the effective resistivity is so small. The thinness of the current layer is limited by the necessity for the plasma on the reconnecting lines to be expelled along this thin current layer. The breaking of the lines occurs over a very small region near the center because reconnection is a topological change. Lines can break and reconnect in a very small region where nonideal (resistive) physics occurs, and once reconnected they rearrange themselves by ideal forces. The reconnected lines inside the layer, although weak, have a large curvature so they can unfold themselves by magnetic tension, as well as the pressure gradient force considered by Sweet and Parker. This tension force is of the same order as the pressure force so that the Sweet-Parker model still gives the correct order of magnitude for the reconnection rate. (It is necessary that although the layer must be very thin only near the N point for the diffusion velocity to be important, it cannot become thicker away from this point because the incoming matter along the entire line also has to be accelerated to the Alfvén velocity. This cannot happen if the layer became thicker because this would decrease the curvature of the lines and reduce their magnetic force. Thus, the layer thickness must have the same thickness along the entire line as at the N point.)

There is an exception to this picture that occurs in reconnection on the dayside of the magnetosphere (Mozer, 2004). Although the solar-wind flow is slowed down by the Earth's bow shock it is not reduced to zero except at the exact subsolar point. On either side of this point the solar wind still has a considerable velocity, and when it reaches the magnetosphere it turns tangent to it. The original solar wind is traveling at about ten times the Alfvén speed. The flow is reduced by a factor of 4 by

the shock, while the Alfvén speed is increased by 2 so that the flow is larger than the downstream Alfvén speed. When it turns to flow along the magnetosphere, the velocity is further reduced but still quite substantial and this flow eases the burden of acceleration of the flow along the magnetopause. This in turn speeds up the reconnection rate at the subsolar point.

The results of the Sweet-Parker model, while remarkable, still are a long way from explaining the speed with which a solar flare releases energy. Aside from Mozer's suggested modification of it, its predicted reconnection rate is also too slow to account for the fraction of the incoming solar-wind lines that reconnect on the Earth's magnetosphere.

The situation for magnetic reconnection at the magnetosphere is clearer than that of a solar flare because the case for a current layer is more compelling. The solar wind possesses a magnetic field, and when it encounters the surface of the magnetosphere one expects that if the solar wind was an ideal plasma, it would be deflected around the Earth leaving a cavity, called the magnetosphere. However, on the surface of the cavity, the magnetopause, the solar-wind field is not aligned with the Earth's magnetic dipole field, and there is automatically a narrow current layer separating them.

As discussed in Sec. II, the reconnected solar-wind lines in the Dungey model of the magnetosphere have a part in the solar wind and a part in the magnetosphere. One end is dragged along with the solar-wind velocity v_S , while the other end is anchored in the electrons in the Earth's ionosphere. This part of the line will be dragged through the ionosphere at a much slower rate. Since the ions in the ionosphere are immobilized by collisions with neutrals, the electron motion produces an electrical current in the ionosphere that is measured from the ground enabling one to actually count the number of reconnected lines flowing across the polar cap of the Earth per unit time. It is found that, on the average, one line in ten of the incoming solar-wind field lines is reconnected [see Hughes (1995)]. The Sweet-Parker theory predicts that the fractional number of reconnection lines is $(v_A/v_S)/\sqrt{S}$, where $S=v_A L/\Lambda$. A simple estimate gives a value of about 10^{-5} [see p. 438 of Kulsrud (2005)].

In the early 1960s one was faced with two serious discrepancies between the direct observations of magnetic reconnection times and the times predicted by the Sweet-Parker theory. The situation was improved by Petschek who proposed that inclusion of slow shocks in the Sweet-Parker outflow region would greatly speed up the mass flow and remove a major hurdle for the Sweet-Parker theory, which a large amount of mass must flow through the very narrow current channel of constant width.

To increase the flow over a wider channel, extra forces are needed. These forces can be provided by slow shocks (see Fig. 16). In the Petschek model, these shocks start at the ends of a short Sweet-Parker layer and fan out with an angle v_R/v_A . As the external plasma crosses the shocks it is accelerated in the downstream direction

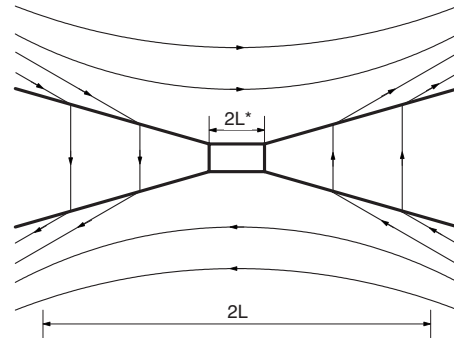


FIG. 16. Petschek model.

up to the Alfvén speed by the intense currents in the shocks. A simple analysis shows that the reconnection is then given by the reconnection rate corresponding to the much shorter length L^* of the Sweet-Parker layer. L^* is the distance from the X point at which the shocks start. (From now on we refer to Sweet's N point by the more conventional X point.)

In the downstream region, the magnetic field in the channel is essentially a B_\perp field perpendicular to the current layer. The shock speed is that of a slow shock supported by this transverse B_\perp field and is $B_\perp/\sqrt{4\pi\rho}$. This velocity is equal to v_R , the transverse velocity of the incoming flow, so that the shock is stationary. Since the shock takes care of the downstream flow, the only question that remains is: what is the distance L^* from the X point at which the shocks begin?

The reconnection velocity is the Sweet-Parker velocity modified by replacing L by L^* , i.e.,

$$v_R = v_A \sqrt{\Lambda/L^*} v_A, \quad (5)$$

faster than the Sweet-Parker velocity by $\sqrt{L/L^*}$.

Petschek's showed that all the MHD relations were satisfied independent of the choice for L^* so it appears that L^* could be arbitrarily small. Petschek found that there is a limit on the shortness of this length, $L^* > L(\ln S)^2/S$, at which length the current in the shocks seriously perturbs the upstream flow.

Petschek proposed this as the correct length leading to

$$v_R(\text{Petschek}) = v_A \pi/8 \ln S. \quad (6)$$

[This result actually differs by a factor of 2 from the original Petschek result. There is a minor error in the Petschek paper and a correction was pointed out by Vasyliunas (1975); see Priest and Forbes (2000).]

Since $\ln S$ is of order 10 or 20, the Petschek model predicts a very fast reconnection velocity, a finite fraction of the Alfvén velocity. But since in the two main applications S is very large, of order $10^{12}-10^{14}$, the length L^* must be extremely short, namely, L/S . In most astrophysical and space applications this is a microscopic length. This extremely short length for the Sweet-Parker layer in the Petschek model was not commented on at the time his model was proposed.

It was recognized that the Petschek formula involved the magnetic field strength B_i just outside of the layer. Because of the perturbations produced by the shock currents, this could be considerably larger or smaller than the global field strength B_e . Petschek chose his limit on L^* qualitatively so that the upstream magnetic field was not seriously perturbed. The relation between B_i and B_e in the Petschek model was made quantitative by [Priest and Forbes \(1986\)](#), who showed that, for various solutions of the external field, B_i could be considerably stronger than B_e . For some global flows their theory predicts that the reconnection rate can reach the Alfvén speed based on the global field B_e .

The validity of the Petschek model was not challenged until the Biskamp simulation mentioned in Sec. [III.A.](#) [Biskamp \(1986\)](#) showed that, for constant resistivity, the Sweet-Parker model was the correct one. In these simulations Biskamp did find shocks but they only emerged at a distance L^* comparable to the global scale L , much larger than that would have been predicted by Petschek. The scaled boundary layer numerical simulation of [Uzdensky and Kulsrud \(2000\)](#) confirmed these results.

C. Recent progress in MHD theory

Although Petschek claimed that there was no problem matching the velocity in the shocked region to a very short Sweet-Parker region, say of length L^* , Biskamp expressed some skepticism as to this smooth matching. [Kulsrud \(1998, 2001\)](#) attempted to qualitatively understand how the transverse magnetic field that supports the shocks could form from the external reconnecting field. It should arise by the rotation of the latter field lines. A crude estimate showed that rotation was too slow to balance the loss of the B_y field that is carried downstream at the Alfvén velocity. There seemed to be a problem with connecting the magnetic field that supports the shock to the magnetic field in the Sweet-Parker layer.

The difficulty was quantitatively clarified by [Malyshkin et al. \(2005\)](#) who showed that, in the purported connection, the second derivative of Ohm's law evaluated at the X point was violated. His clarification for the case where there is no guide field in the y direction is as follows.

Throughout this review, unless otherwise stated the so-called magnetopause coordinates are used, in which the incoming reconnection flow is in the x direction, the reconnecting field is in the z direction, and the current is in the y direction.

Malyshkin chose the X point as the coordinate origin and assumed complete symmetry about this point. He evaluated all quantities and their derivatives in the MHD equations at the origin.

The continuity equation is

$$\nu \equiv \partial v_z / \partial z = - \partial v_x / \partial x \approx -v_R/\delta \quad (7)$$

and Ampere's law is

$$j_y = -\frac{1}{4\pi} \frac{\partial B_z}{\partial x} \approx -\frac{B_0}{4\pi\delta}. \quad (8)$$

Eliminating δ between these two equations we have

$$\nu \approx v_R 4\pi j_y / B_0. \quad (9)$$

Now the equation of motion along the x axis is

$$\rho v_z \partial v_z / \partial z = -j_y B_x. \quad (10)$$

Differentiating this with respect to z at the origin, we find

$$\rho \nu^2 = -j_y \partial B_x / \partial z = -j_z \beta, \quad (11)$$

where $\beta = \partial B_x / \partial z$.

Ohm's law is

$$E_y + (v_z B_x - v_x B_z) / c = \eta j_y \quad (12)$$

and differentiation of this twice with respect to z at the origin gives

$$\nu \beta = \eta c \partial^2 j_y / \partial z^2 = \eta c j''_y, \quad (13)$$

where the primes refer to z derivatives. This equation is his key result.

Substitution for ν and β from the Sweet-Parker model, $\nu \approx v_R / \delta$ and $\beta = B_x / L \approx \delta B_0 / L^2$, shows that Eq. (13) is approximately satisfied. The z scale size of j_y is taken to be the global length L so that $j''_y \approx -j_y / L^2$. This estimate follows if we assume the variation of the B_0 , equal to B_z along $x = \delta$, is given by external equilibrium conditions on the global scale L .

Comparing the Petschek model with the Sweet-Parker model we see that Petschek's ν is larger by L/L^* , and his $\beta \approx B_x / L^*$ is larger by $(L/L^*)^{3/2}$ so $\nu \beta$ is larger by $(L/L^*)^{5/2}$. On the other hand, the scale length for j_y is also L since it is controlled, through B_0 , by the global external conditions. In his theory $j_y \approx B/\delta$ and δ is proportional to $1/\sqrt{L^*}$ so $j''_y \approx j_y / L^2$ is only larger by $(L/L^*)^{1/2}$. Thus, unless $L^* \approx L$, the Petschek model contradicts Eq. (13).

In this way we see that one can trace the difficulty in the Petschek theory to the neglect of the second derivative of Ohm's law which actually determines the position of the shocks. In fact, one can see that β is the rate of build up of B_x and this rate is constrained by the other equations and, in particular, by the rate of variation of j . Physically, β is roughly the rate of “turning” of the reconnecting line from the z direction to the x direction to give the shock supporting transverse field.

Malyshkin extended this argument to include the case where the resistivity varies finitely over a short distance L_η compared to L . He confirmed the result found in the MHD simulations with variable resistivity that shocks must start at the scale size of the resistivity. He also considered the Sato-Hayashi case where the resistivity depends on the current density and confirmed a qualitative model proposed by [Kulsrud \(2001\)](#) and [Uzdensky \(2003\)](#). They showed that if the resistivity dependence on current density is very sensitive (i.e., a large gradient

$d\eta/dj$) then reconnection can be increased by a large amount since this allows a very small scale for the resistivity in a natural way.

Malyshkin's results confirmed the doubts concerning the Petschek model for constant resistivity MHD. He showed that shocks appear when the resistivity is not constant and that they start at the resistivity scale length.

IV. RECENT MAJOR FACILITIES AND MEANS FOR RECONNECTION STUDY

A uniqueness of the recent reconnection research is that major progress in the scientific areas has been made by utilizing multiple research tools: computer simulation codes, space satellites, and laboratory experiments which are dedicated for the study of magnetic reconnection. Data from satellites have been effectively utilized to investigate reconnection phenomena in both solar and magnetosphere plasmas. Recent experiments have been carried out in plasma systems which satisfy the global conditions for MHD treatment of the plasma with $V_A/c \ll 1$, $S \gg 1$, and $\rho_i/a \ll 1$, providing realistic examples of magnetic reconnection. In this section, we highlight early electron current sheet experiments, merging spheromaks, and modern laboratory experiments, major satellites for reconnection research, and the current status of numerical simulation codes.

A. Dedicated laboratory experiments on reconnection

1. Early reconnection experiments

Before 1980, most laboratory experiments dedicated to magnetic reconnection research were carried out in short pulse "pinch" plasmas or fast high-density pulsed plasma discharges of a few microseconds duration (Bratenahl and Yeates, 1970; Syrovatskii *et al.*, 1973; Baum and Bratenahl, 1974; Frank, 1974; Ohyabu *et al.*, 1974; Syrovatskii, 1981). Although diagnostics with high spatial and temporal resolution were not available, interesting findings were made. The reconnection rate was measured to be larger than the classical value in the experiment by Bratenahl and Yeates (1970) and it was attributed to possible microinstabilities driven by electrons' drift against ions in the neutral sheet, although a quantitative analysis was not made. These experiments were carried out in the collision-dominated MHD regime, and the low Lundquist numbers ($S=1-10$) attained in these experiments made it difficult to quantitatively compare the results with MHD theories based on large S . Despite these difficulties, the current-density profiles of the neutral sheet were measured by magnetic probes, and density profiles were measured on the Alfvén transit time ($<1 \mu\text{s}$) by Frank *et al.* (Frank, 1974; Syrovatskii, 1981). Figure 17(a) presents their experimental setup where formation of a flat current sheet was induced in a Z pinch discharge along the axis (z axis) of a straight cylinder. Figure 17(b) shows the time evolution of reconnecting magnetic field profiles in the y axis (not a conventional coordinate system), perpendicular to the

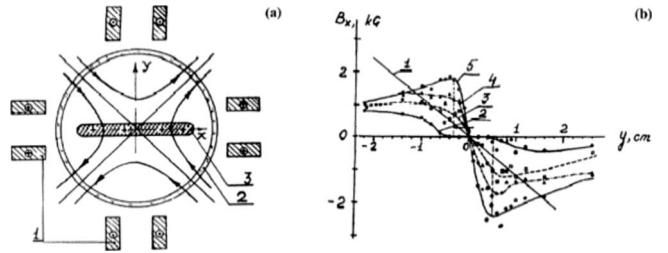


FIG. 17. EMHD reconnection experiments in a linear plasma device: coil and current sheet geometry (left) and measured magnetic field profiles at different times (right). From Frank, 1974.

sheet. After the magnetosonic waves converged, a current sheet stretched in the x axis began to form in the vicinity of the neutral line along the y axis. The final thickness of the sheet appeared to be determined by pressure balance of the reconnecting magnetic field and the plasma kinetic pressure (Syrovatskii, 1981).

In a linear plasma experiment (Stenzel and Gekelman, 1981; Gekelman *et al.*, 1982), magnetic reconnection was studied using parallel conductor plate currents with a strong guide field ($B_G \gg B_{\text{reconn}}$). A reconnection region was created by driving currents in the two parallel sheet conductors shown in Fig. 18(a), and a detailed local study of magnetic reconnection was performed using internal probes based on multiple reproducible plasma discharges.

The experiments were carried out in a cylindrical vacuum chamber (1.5 m diameter, 2 m length) in which a low pressure ($p \sim 10^{-4}$ torr, argon) discharge was produced with a 1 m diameter oxide-coated cathode. The plasma parameters were $n_e \sim 10^{12} \text{ cm}^{-3}$ and $T_e \sim 10 \text{ eV}$, the electron-ion collision mean free path was $\sim 2 \text{ cm}$, the axial magnetic field was 12–100 G, and $\beta_\perp \sim 1$ for a plasma current of about 1.5 kA.

The electrons were magnetized ($\rho_e \ll L$) while ions were unmagnetized even outside the reconnection region ($\rho_i \gg L$), a regime often called an electron MHD (EMHD) regime. The plasma was largely resistive and the Lundquist number was small ($1 < S < 10$). Although it was reported that a Petschek slow MHD shock was observed (Stenzel and Gekelman, 1979), it could not be theoretically supported since the experiment was performed in EMHD regime.

This experiment was noteworthy in studying EMHD dynamics and wave-related mechanisms in the reconnection region and identifying local microscopic physics associated with current sheet formation with a guide field. Profiles of the electron pressure $n_e T_e$, magnetic force density $j \times B$, and ion velocity vectors were measured in the diffusion region. A neutral current sheet was seen to develop in less than two Alfvén transit times ($\tau_A \sim 20 \mu\text{s}$). The neutral sheet became narrower as it was measured further from the cathode. Figure 18(b) shows field lines through contours of vector potential A_y at $y = 137 \text{ cm}$ from the cathode and at $t = 50 \mu\text{s}$; here y is the axial distance from the cathode and $t = 0$ is the start time

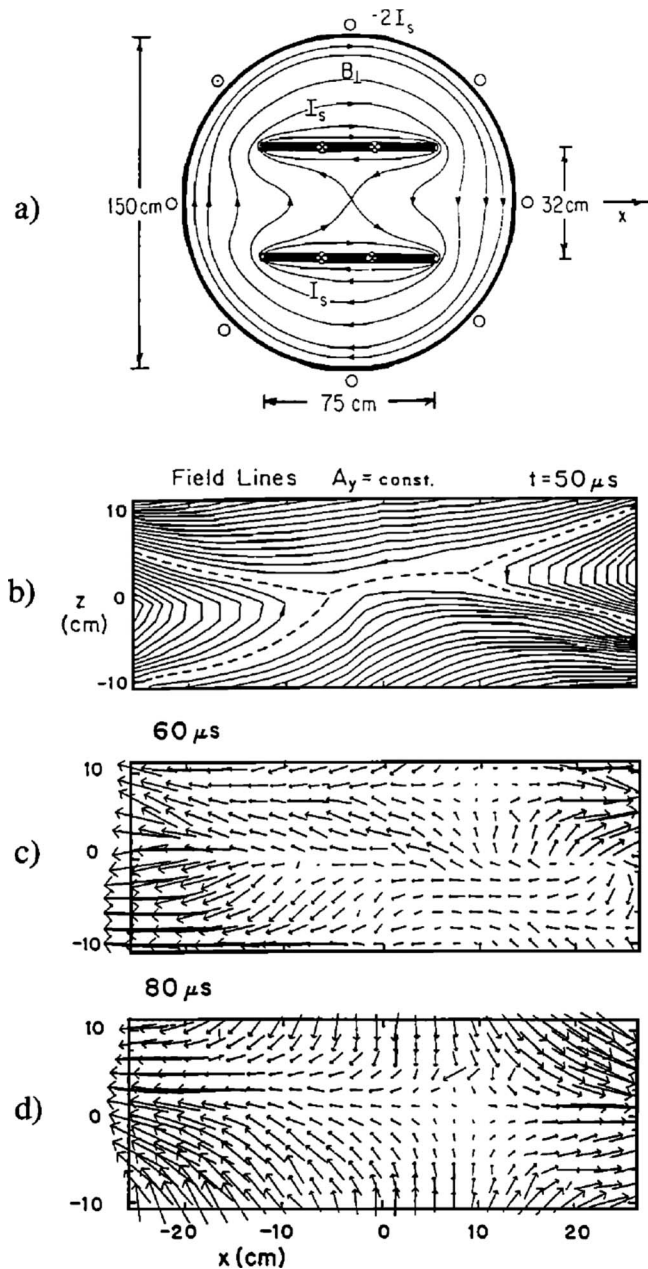


FIG. 18. LPD experiment: (a) Cross-sectional view of experimental setup without plasma, (b) magnetic flux contours, and (c) and (d) ion velocity vectors. The magnetotail coordinate system (y is in the out-of-plane direction) is employed in this experiment. Adapted from Stenzel and Gekelman, 1981 and Gekelman *et al.*, 1982.

of the discharge. After a few Alfvén times, a classic plasma flow pattern was observed with ions jetting from the neutral sheet with velocities close to the Alfvén speed. The 2D features of particle acceleration were measured (Gekelman *et al.*, 1982). Figures 18(c) and 18(d) show typical 2D ion flows drifting radially from diffusion region to outside at $t=60$ and $80 \mu\text{s}$. The local force on the plasma $\mathbf{j} \times \mathbf{B} - \nabla p$ was compared with the measured particle acceleration using differential particle detectors. The ion acceleration was seen to be strongly modified by scattering off wave turbulence and the ob-

served fluctuations were identified as oblique whistler waves. But it was not clear whether the whistler waves were solely responsible for the observed large ion scattering rate. It was concluded later that the observed anomalous scattering rate and high resistivity were in large part due to ion acoustic turbulence although higher frequency whistler waves were present. The role of whistler waves for the observed anomalous resistivity was not conclusively determined.

The physical effects of the strong guide field used in the experiment were not discussed explicitly in their analysis of their data, while it was expected to play a significant role in the force balance. After they modified the shape of the end anode, they found evolution of the neutral current sheet depended on the strength of the axial magnetic field. As the axial field was raised from 20 to 100 G, the classic double-Y-shaped neutral-sheet topology changed to the O-shaped magnetic island. This result was later reproduced in the MHD regime on the MRX (Yamada *et al.*, 1997a, 1997b). The stability of the current sheet was also investigated. When the current density in the center of the sheet exceeded a critical value, spontaneous local current disruptions were observed with the center of the sheet moving out to the sides. This experiment was extended to a 3D study (Gekelman and Pfister, 1988), in which tearing of the current sheet was observed.

Their experiment was valuable in measuring the local structure of the non-MHD feature of a reconnection region for the first time and in finding the relationship between the reconnection rate and wave turbulence. One of the most important questions on reconnection, how the diffusive neutral sheet is formed in a plasma relevant to space and astrophysics, was not answered because the MHD conditions for the global plasma were not satisfied due to the boundary condition in which the reconnection layer is too close to the wall ($\rho_i \gg L$). We note that the short ion mean free path (compared to L) may explain the fluidlike behavior of the ions as shown in Fig. 18. The role of line tying in their linear plasma is not clear. In the subsequent sections reconnection experiments in MHD regimes where the Lundquist numbers exceeds 100 with both electrons and ions being magnetized ($\rho_e \ll \rho_i \ll L$) are discussed.

2. Plasma merging experiments

Local and global MHD issues for magnetic reconnection have been extensively investigated in 3D geometry in the colliding spheromak experiments. The studies showed that a double spheromak geometry is a well suited configuration for basic studies of magnetic reconnection.

a. Todai spheromak-3/4 facility

In the Todai Spheromak-3 (TS-3) experiments (Yamada *et al.*, 1990, 1991; Ono *et al.*, 1993), two spheromak-type plasmatoroids merged together, contacting and connecting along a toroidally symmetric line. A spheromak is a spherical or toroidal shaped plasma in

which force-free currents ($j \times B = 0$) set up an equilibrium configuration depending on whether there is a current (flux) hole at the major axis (Taylor, 1986). The two toroidal spheromaks, carrying equal toroidal current with the same or the opposite toroidal field, are forced to merge by controlled external coil currents. These are called cohelicity merging or counterhelicity merging, respectively. Figure 19(a) shows an experimental schematic for the TS-3 merging experiment. To document the internal magnetic structure of the reconnection on a single shot, a two-dimensional magnetic probe array is placed on an R - Z plane or toroidal cutoff plane. Plasma parameters are $B \sim 0.5\text{--}1\text{ kG}$, $T_e \sim 10\text{ eV}$, and $n_e \sim (2\text{--}5) \times 10^{14}\text{ cm}^{-3}$. The time evolution of the poloidal flux contours showed that merging of spheromaks of opposite helicity occurs faster than merging of the same helicity [Fig. 19(b)]. It was argued that for the merging of plasmas of two antiparallel toroidal fields, the central toroidal field is quickly reduced to zero and the attracting force becomes dominant accelerating reconnection. The toroidal current-density contours were deduced for the same sequence of shots (Yamada *et al.*, 1991; Ono *et al.*, 1993), verifying an important 2D feature of magnetic reconnection.

A strong dependence of the reconnection speed on the global forcing was observed, i.e., the merging velocity of the two plasmas. It is observed that the reconnection rate γ , defined by a flux transfer rate $(1/\Psi)\delta\Psi/\delta t$, increases nearly proportionally to the initial colliding velocity v_i . This result cannot be explained by the classical 2D MHD theories of Sweet and Parker and/or Petschek which are based on the local dynamics. The experiment suggests the importance of an external driving force in determining the reconnection rate and supports an important aspect of a driven-reconnection model.

A violent plasma acceleration in the toroidal direction was observed by Ono *et al.* (1996) as the field lines contracted after the merging of two toroidal plasmas of the opposite helicities. As reconnection proceeded, evidence of the toroidal slingshot effect (Yamada *et al.*, 1991) was observed. An energy transfer from magnetic to plasma thermal energy was expected in this dynamic reconnection process of toroidal field annihilation. A strong ion heating was measured during the counterhelicity merging with details in Sec. V.B.

b. Swarthmore Spheromak Experiment facility

The Swarthmore Spheromak Experiment (SSX) (Brown, 1999) (Fig. 20) facility studies magnetic reconnection also through the merging of spheromaks. Reconnection physics, particularly its global characteristics, has been studied in a number of geometries with diameters varying from 0.17 to 0.50 m (Brown, 1999; Cothran *et al.*, 2003; Brown *et al.*, 2006). Different types of flux-conserving conductors consisting of two identical copper containers have been used. Merging of a pair of counterhelicity spheromaks generates turbulent 3D magnetic reconnection dynamics at the midplane.

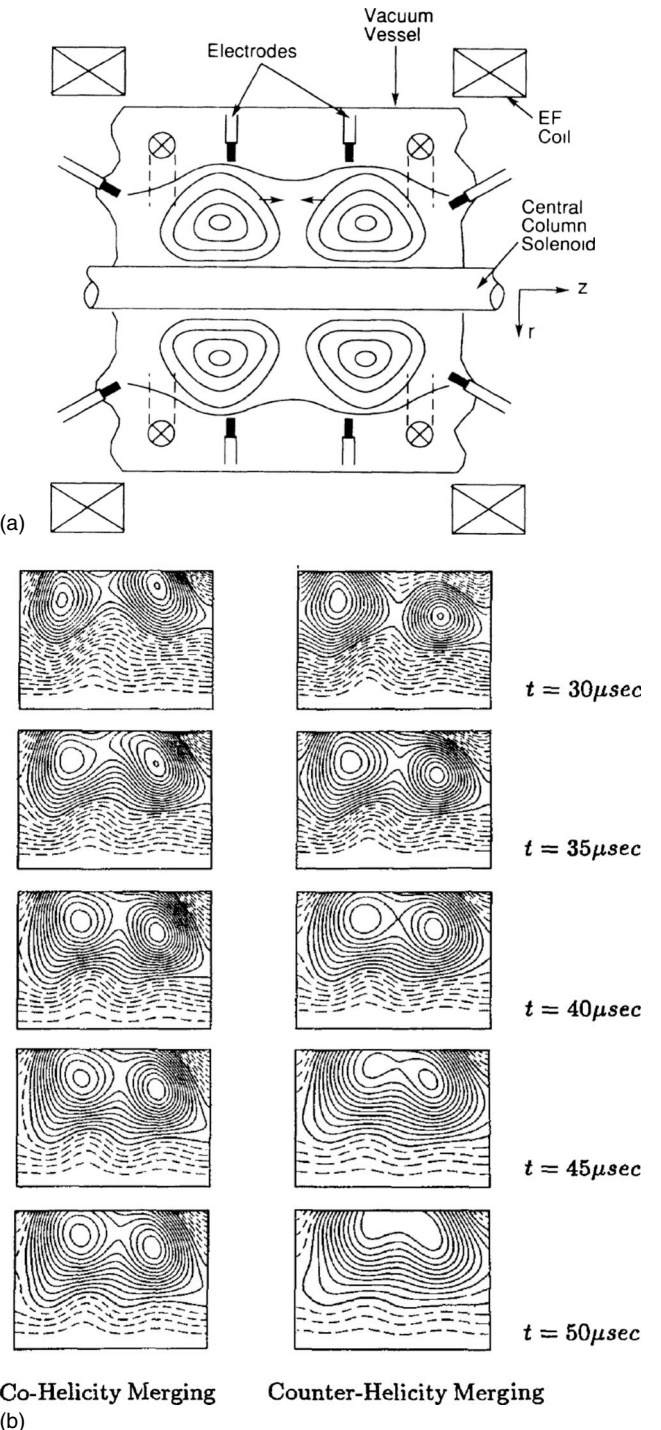


FIG. 19. Plasma merging experiment in TS-3. (a) Experimental setup. (b) Evolution of poloidal flux contours for cohelicity (left) and counterhelicity merging (right). The plasma parameters are kept roughly the same for the two cases. From Yamada *et al.*, 1990 and Ono *et al.*, 1993.

Many optical diagnostics were utilized in this device. The line-averaged electron density is monitored with a HeNe laser interferometer (Brown *et al.*, 2002). Plasma parameters are similar to those of TS-3, $n_e = (1\text{--}10) \times 10^{14}\text{ cm}^{-3}$, $T_i = 40\text{--}80\text{ eV}$, $T_e = 20\text{--}30\text{ eV}$ (inferred from soft-x-ray radiation), with typical magnetic fields of 0.1 T. The ion gyroradius is much smaller than the ra-

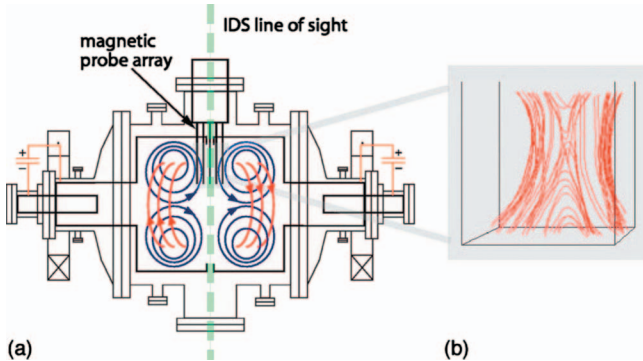


FIG. 20. (Color) The SSX device for studies of local and global dynamics of magnetic reconnection. From [Brown et al., 2006](#).

dius of the outer flux-conserving boundary of the plasma (defined by a cylindrical copper wall). The Lundquist number S ranges 100–1000, making the global structure of SSX spheromaks fully in the MHD regime ($S \gg 1, \rho_i/L \ll 1$).

Alfvénic outflow has been measured with both electrostatic ion energy analyzers ([Kornack et al., 1998](#)) and spectroscopically ([Brown et al., 2006; Cothran et al., 2006](#)). The line-averaged ion flow and temperature T_i at the midplane are measured with a 1.33 m ion Doppler spectrometer.

3. Controlled driven reconnection experiments

A series of dedicated laboratory experiments has been performed to investigate the fundamental processes of reconnection by making a prototypical reconnection layer in a controlled manner. Their goal is not to simulate specific reconnection events in space or in fusion devices but to provide key data to understand the fundamental process of reconnection. In these experiments, a reconnection layer can be created by driving oppositely directed field lines into the neutral sheet generating a reconnection region in a controlled setting with varying plasma parameters.

a. MRX facility

The MRX device was built at Princeton Plasma Physics Laboratory in 1995 to investigate the fundamental physics of magnetic reconnection. Another goal is to gain understanding of self-organization phenomena of fusion plasmas as well as space and astrophysical plasmas. The analysis focuses on the coupling between local microscale features of the reconnection layer and global properties such as external driving force and the evolution of plasma equilibrium. The local features of the reconnection layer have been extensively studied. The overall initial geometry is axisymmetric (and hence two-dimensional) but can be made nonaxisymmetric to study 3D characteristics of merging. The global plasma properties can be described by MHD ($S > 10^3$) with the ion gyroradius (1–5 cm) being much smaller than the plasma size ($R \sim 30$ –50 cm).

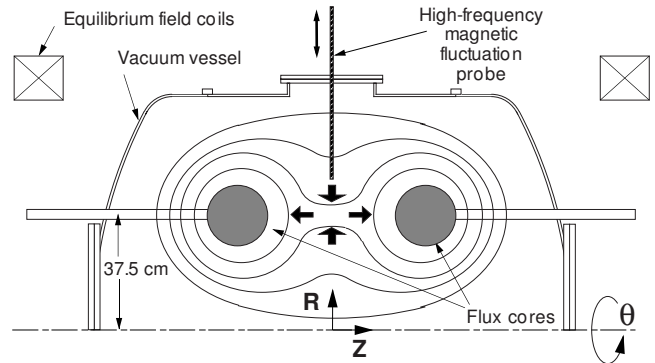


FIG. 21. Experimental setup for the MRX and illustration of pull driven reconnection in the double annular plasma configuration. Adapted from [Yamada et al., 1997b](#).

Experiments have been carried out in the double annular plasma setup in which two toroidal plasmas with annular cross section are formed independently around two flux cores and magnetic reconnection is driven in the poloidal field shown in Fig. 21. Each flux core (darkened section in Fig. 21) contains a toroidal field (TF) coil and a poloidal field (PF) coil to generate plasma discharges ([Yamada et al., 1981](#)). At first a quadrupole poloidal magnetic field is established by the PF coil currents (which flow in the toroidal direction); plasma discharges are created around each flux core by induction of two pulsing currents in the TF coils ([Yamada et al., 1997a](#)). After the annular plasmas are created, the PF coil current can be increased or decreased. For rising PF current, the poloidal flux in each plasma increases and is pushed toward the X point (push mode). For decreasing PF current, the poloidal flux in the common plasma is pulled back toward the X point (pull mode) (Fig. 21). For standard conditions [$n_e \sim (0.1\text{--}1) \times 10^{14} \text{ cm}^{-3}$, $T_e = 5\text{--}15 \text{ eV}$, $B = 0.2\text{--}1 \text{ kG}$, $S > 500$], the MRX creates strongly magnetized MHD plasmas. The mean free path for electron-ion Coulomb collisions is in the range 0.1–20 cm.

To measure the internal magnetic structure on a single discharge, a two-dimensional magnetic probe array is placed in the R - Z plane or toroidal cutoff plane, where Z is the axis of the vacuum vessel. The profile of the neutral sheet was measured and different shapes of neutral-sheet current layers were identified, depending on the third (toroidal) vector component of the reconnecting magnetic fields. As poloidal flux is driven toward the diffusion region, a neutral sheet is formed as seen in Fig. 21. Without the third component (called null-helicity reconnection), a thin double-Y-shaped diffusion region has been experimentally documented as seen in Figs. 5 and 13. With a significant third component (co-helicity reconnection), an O-shaped sheet current appears ([Yamada et al., 1997b](#)). The recent results from the MRX are discussed in subsequent sections.

b. Versatile Toroidal Facility

The Versatile Toroidal Facility (VTF) magnetic reconnection experiment ([Egedal et al., 2000](#)) was developed

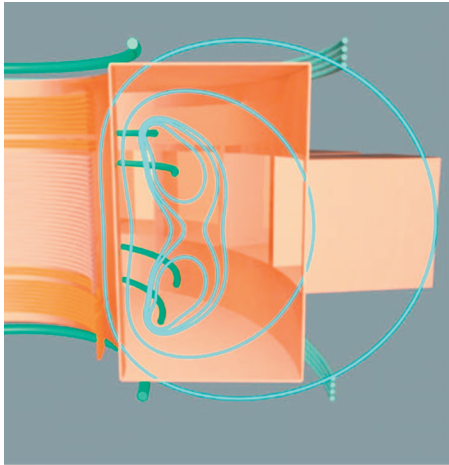


FIG. 22. (Color) Poloidal cross section of the VTF. The solid blue lines show the poloidal field geometry (courtesy of J. Egedal).

at the Plasma Science and Fusion Center of the Massachusetts Institute of Technology. The VTF experiment explores fast magnetic reconnection in collisionless plasma, where the mean free path between electron and ion collisions is much larger than the dimensions of the plasma for a configuration with a strong variable guide magnetic field. The VTF geometry and a poloidal cross section are shown in Fig. 22. The vertical orange structures are field coils capable of producing a toroidal magnetic field up to 10 kG. The understanding gained from research on reconnection in the VTF was recently applied to an interpretation of recent *in situ* measurements of electron phase space distribution during reconnection in the deep magnetotail. This is of particular relevance to the reconnection event observed by the WIND satellite as discussed in Sec. VII.B.

Table I summarizes major devices currently dedicated to the study of the physics of magnetic reconnection. The 3D aspects of magnetic reconnection were studied in two linear devices (Stenzel *et al.*, 2003; Gekelman *et*

al., 2007). Two new linear devices, rotating wall experiment (Bergerson *et al.*, 2006) and reconnection scaling experiment (Furno *et al.*, 2007), have recently been used in the study of magnetic reconnection, in particular, on line-tying effects.

B. Satellites for study of magnetic reconnections

A number of satellites have been launched to study the behavior of solar flares and the dynamics of the Earth's magnetosphere. Many significant findings have been made on magnetic reconnection phenomena in the solar atmosphere and the magnetosphere. The recent satellites such as TRACE and Hinode have shown most vividly the topological changes of solar flares with fine space resolution of less than an arcsecond (700 km). This section highlights the major satellites used for the study of magnetic reconnection phenomena. They are divided into two types: solar satellites with multiple optical and x-ray diagnostics, and space satellites with a variety of *in situ* diagnostics to measure local magnetic fields and particles velocity distribution functions with time resolution of less than a millisecond.

1. Solar satellites

(a) *Yohkoh*. The Japanese solar-physics satellite Yohkoh (Sunlight in Japanese) was launched in 1991 and observed the solar corona in x rays and gamma rays for more than ten years until December 2001. This corresponds to nearly a full solar activity cycle. Yohkoh revealed that the solar corona was very dynamic (Fig. 23), that magnetic reconnection plays an essential role in the energy release mechanism of solar flares through observations of various coronal activity, such as microflares, x-ray jets, and CMEs. Yohkoh's observations stimulated much researches of magnetic reconnection, leading to the launch of the next Japanese solar satellite Hinode.

(b) *Soho*. The Solar and Heliospheric Observatory was launched in December 1995 to study the Sun. It is a

TABLE I. Dedicated experiments currently operating for reconnection research.

| Facility | Main features | Main references |
|-------------------------------|---|--|
| 3D-CS at GPI, Russia | Liner geometry Guide field | Frank <i>et al.</i> , 2005 Frank <i>et al.</i> , 2006 |
| TS-3/4 at University of Tokyo | Plasma merging Compact torus | Yamada <i>et al.</i> , 1990 Ono <i>et al.</i> , 1993, 1996 |
| MRX at PPPL | Driven reconnection | Yamada <i>et al.</i> , 1997a, 2006 |
| SSX at Swarthmore | Plasma merging | Ji <i>et al.</i> , 2004, 1998 |
| VTF at MIT | Plasma merging Compact torus Strong guide field | Brown, 1999 Brown <i>et al.</i> , 2006 Egedal <i>et al.</i> , 2000 |
| RSX at LANL | Particle dynamics Current channel merging | Egedal <i>et al.</i> , 2005 Furno <i>et al.</i> , 2007 |
| RWX at Wisconsin | Line tying | Bergerson <i>et al.</i> , 2006 |

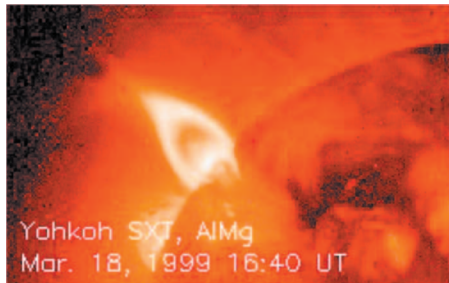


FIG. 23. (Color) Image from Yohkoh.

joint project for the European Space Agency (ESA) and NASA. Originally planned as a two year mission, SOHO has provided much useful data on magnetic reconnection through soft-x-ray pictures. In 2003, the SOHO spacecraft captured one of the most powerful solar flares ever recorded in recent years.

(c) *Trace*. Transition Region and Coronal Explorer, which was launched in April 1998, is a NASA space telescope to investigate the connections between fine-scale magnetic fields and the associated plasma structures on the Sun by providing high resolution images and data of the solar photosphere and transition region to the corona. A main focus is the fine structure of coronal loops low in the solar atmosphere. The telescope takes correlated images in a range of wavelengths corresponding to plasma emission temperatures from 0.3 to 300 eV. An image of the solar corona by TRACE is shown in Fig. 1.

(d) *Hinode*. Hinode (sunrise in Japanese) is a Japan Aerospace Exploration Agency Solar mission with US and UK collaboration. It is the followup to the Yohkoh mission which revealed the essential features of magnetic reconnection and it was launched in September 2006. The satellite was maneuvered to the quasicircular sun-synchronous orbit over the day-night terminator, which allows near-continuous observation of the Sun. Hinode carries three main instruments: a solar optical telescope (SOT), an x-ray telescope, and an extreme-ultraviolet imaging spectrograph.

2. Space satellites

(a) *International Sun-Earth Explorer*. The International Sun-Earth Explorer (ISEE 1 and 2) satellites were launched in October 1977 and provide data on magnetic reconnection in the magnetosphere [see, e.g., Russell and Elphic (1979)]. The data showed evidence for patchy impulsive reconnection. The flux transfer rate was measured to be similar to rates deduced for magnetopause erosion events.

(b) *Geotail*. The GEOTAIL satellite, a collaborative US-Japan research project, was launched in 1992 and provided key data on reconnection. The primary purpose was to study the structure and dynamics of the tail region of the magnetosphere with multiple instruments [see, e.g., Murata *et al.* (1995)]. The orbit covered the magnetotail over a wide range of distances: $8\text{--}210R_E$ from the Earth where R_E ($=6371\text{ km}$) is the Earth ra-

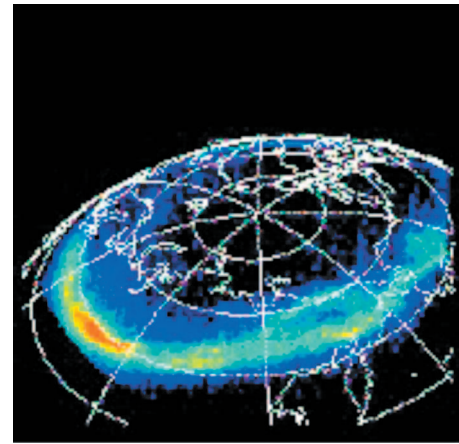


FIG. 24. (Color) Image of aurora from POLAR satellite. From www.physics.umn.edu/

dius. This orbit allows a study of the boundary region of the magnetosphere.

(c) *Wind*. The WIND satellite was launched on November 1994 and is the first of two NASA spacecraft in the Global Geospace Science initiative. The main science objectives were to (1) provide plasma, energetic particle, and magnetic field data for magnetospheric and ionospheric studies; and (2) investigate basic plasma processes occurring in the near-Earth solar wind. Recent observations [see, e.g., Mozer *et al.* (2002), Øieroset *et al.* (2002), and Phan *et al.* (2006)] from this satellite are discussed in Secs. V–VII.

(d) *Polar*. The POLAR satellite, launched in February 1996, is in a highly elliptical, 86° inclination orbit with a period of about 17.5 h. It provided multiwavelength imaging of the aurora (Fig. 24), measuring the entry of plasma into the polar magnetosphere and the geomagnetic tail. POLAR has studied the polar magnetosphere and, as its orbit has precessed with time, has observed the entire equatorial area of the magnetosphere. Data from POLAR on reconnection in both the magnetopause and magnetotail are described in Sec. VI.

(e) *Cluster*. CLUSTER is a ESA mission to study the Earth's magnetosphere using four identical spacecrafts flying in a tetrahedral formation. The four satellites launched in 2000 investigate the magnetosphere by measuring three-dimensional data from the interaction of the solar wind with the Earth's magnetic field and the effects on near-Earth space and its atmosphere, including auroras. The interspacecraft distances can be varied from around 100 to 10 000 km. The highly elliptical orbits of the spacecraft reach a perigee of around $4R_E$ and an apogee of $19.6R_E$.

(f) *Themis*. The THEMIS mission, launched in 2007, uses a constellation of five NASA satellites to study energy releases from the Earth's magnetosphere or substorms, magnetic phenomena that intensify auroras near Earth's poles. The name of the mission is an acronym for time history of events and macroscale interactions during substorms, alluding to the Titan, Themis. Each satellite carries identical instrumentation, including a flux-

gate magnetometer, an electrostatic analyzer, a solid-state telescope, a search coil magnetometer, and an electric field instrument.

C. Numerical modeling of magnetic reconnection

The numerical simulations of magnetic reconnection in the past two decades have generated significant new results. This section summarizes the recent progress. It is not meant to review numerical methods.

The simulation codes can be broadly divided into the three categories: (1) continuum codes, (2) particle codes, and (3) hybrid codes that treat one species, typically ions, as particles and another species, typically electrons, as a continuum. The most common continuum codes are based on fluid models, which can be traditional single-fluid MHD or two-fluid models. There are efforts, such as those by [Silin and Büchner \(2003\)](#), to simulate reconnection based on Vlasov codes where distribution functions are solved in both real and velocity spaces. But these studies are relatively rare and will not be included here.

1. Fluid models

Early MHD simulations of magnetic reconnection began with attempts to reproduce [Petschek \(1964\)](#) and other MHD solutions of fast reconnection by [Sonnerup \(1970\)](#), [Vasyliunas \(1975\)](#), and others. These early MHD work successfully generated solutions numerically either by introducing local anomalously large resistivity ([Ugai and Tsuda, 1977](#); [Hayashi and Sato, 1978](#)) or by imposing specific inflow boundary conditions ([Priest and Forbes, 1986](#)). While numerical confirmations of analytic models are highly valuable, it was realized that they did not agree with theory. Using a uniform resistivity, Biskamp could not find the Petschek solution numerically ([Biskamp, 1986](#)), triggering reassessments of analytic models. Since then numerical modeling has been established as a mainstream tool in studying magnetic reconnection.

Since the 1990s, MHD modeling of magnetic reconnection has seen explosive growth because of rapid progress in computing power and numerical techniques. Descriptions of these technical details are beyond the scope of this review, but the following general trends in the present frontier of MHD code development are worth mentioning. MHD simulations use increasingly realistic global boundary conditions. Examples include 3D simulation of the magnetosphere in the presence of the solar wind, high-temperature fusion plasmas, interacting magnetic networks on the solar surface, and disruptive coronal mass ejections. These 3D MHD simulations are used to predict global consequences of magnetic reconnection in situations such as in space weather. They are less often used to study detailed dynamics in the reconnection regions. Local dissipations are often approximated at a simple level.

Another trend is to model local dynamics in the current sheets or dissipation region. Instead of using a sim-

plified model of anomalous resistivity, Hall terms are added to the MHD Ohm's law. The $\mathbf{j} \times \mathbf{B}/en$ term is added in Hall-MHD models. It does not increase the number of unknowns in the equations but substantially increases the requirements for spatial and temporal resolution. This limits their application to very large systems, atypical of astrophysical plasmas.

The next level of sophistication includes the second Hall term $\nabla P_e/en$ in Ohm's law. Here P_e is the scalar electron pressure and can be different from its ion counterpart. Treating ion and electron fluids separately is the key feature of the two-fluid model, although most published work has been in the isothermal limit of $T_e=T_i$. Advancing electron and ion pressures separately requires models of electron and ion heat flux, which can be highly anisotropic with respect to the magnetic field. Implementing anisotropic heat transport during magnetic reconnection, where field lines lose their identities at the X line, represents a numerical challenge but has been implemented in some two-fluid numerical models. Some important features of fast reconnection in collisionless plasmas have been successfully captured by Hall-MHD and two-fluid models.

2. Particle models

The justification for using fluid models is based on frequent collisions between (at least) like particles. These are often absent in relatively collisionless plasmas where fast reconnection is observed. There are important aspects of magnetic reconnection that cannot be properly described by fluid models. Recent efforts have been made to include correction terms in the fluid equations to account for kinetic effects (see, e.g., [Kuznetsova et al., 2007](#)). Kinetic effects beyond two-fluid descriptions include acceleration or heating of charged particles, nongyrotropic pressure, and instabilities due to inhomogeneities in velocity space (microinstabilities).

The effects due to the off-diagonal terms in the electron pressure tensor or the electron nongyrotropic effects can only be studied in kinetic models. This can be seen when the generalized Ohm's law

$$\mathbf{E} + \mathbf{V}_e \times \mathbf{B} = -\frac{\nabla \cdot \mathbf{P}_e}{en} - \frac{m_e}{e} \left(\frac{\partial}{\partial t} + \mathbf{V}_e \cdot \nabla \right) \mathbf{V}_e \quad (14)$$

is used in Faraday's law. In fluid models, \mathbf{P}_e degenerates to a scalar pressure P_e . Since $\nabla \cdot \mathbf{P}_e = \nabla P_e$ is curl-free, it has no effect on the magnetic field evolution in the electron frame. The electron inertia only breaks the frozen-in condition in this case.

To model the fully kinetic behavior of highly nonlinear phenomena such as magnetic reconnection, a full analytic theory becomes extremely difficult. The only practical method is based on numerical simulations using the particle-in-cell (PIC) technique ([Birdsall and Langdon, 1985](#)) where the simulated "macroparticles" represent many plasma particles. Due to large-scale separation both in time (between electron plasma oscillation time and reconnection time) and in space (between Debye length and system size), which is typically

on the MHD scale), various approximations or compromises have to be used in order for a simulation run to finish in a realistic time period even with modern massively parallelized cluster computers.

One common compromise in the PIC simulation studies is the removal of fast electron plasma oscillations using large macroparticles. The effective dimensionless parameter ω_{pe}/ω_{ce} is often much smaller in the simulation (on the order of unity) than in real plasmas (on the order of 100). Though this approximation is used commonly, its physical effects are still unclear.

The large mass ratios between ions and electrons provide an additional difficulty. The spatial and temporal dimensions of the simulation domains are limited by fast electron gyration over a small spatial scale. To overcome this difficulty, there are two approaches: treating electrons as a fluid or using artificially heavy electrons. The former is commonly referred to as a hybrid model since ions are treated kinetically while electrons are treated as a fluid. Kinetic ion physics can be studied in these hybrid models while electron kinetic effects are ignored.

There are new types of hybrid codes: using MHD codes to model large-scale plasma dynamics and using PIC codes to model small-scale kinetic dynamics near the reconnection region. The challenges are to make numerically feasible and physical sound approximations for the connections between the regions modeled by MHD codes and the regions modeled by PIC codes. Some first successes have been reported (Sugiyama and Kusano, 2007).

V. MHD ANALYSIS OF RECENT EXPERIMENTAL RESULTS AND OBSERVATIONS

Important progress has been made using MHD models in analyzing the reconnection processes observed in laboratory experiments and *in situ* measurements by space satellites. Such analysis quantitatively tests the validity of the primary MHD models and provides insight into non-MHD effects. This section presents the MHD analysis of magnetic reconnection recently observed in laboratory and space plasmas.

A. Experimental observations and MHD analysis of magnetic reconnection

Quantitative tests of MHD models were not conducted in a laboratory plasma until the last decade despite the long time history of MHD models since Sweet and Parker. In this section, we summarize recent results on these tests followed by observations of ion heating and flow acceleration.

1. MHD analysis with effective resistivity

A first question is whether classical MHD theory can quantitatively describe the reconnection process in highly collisional plasmas in which the single-fluid assumption holds. The neutral-sheet experiment (Syro-

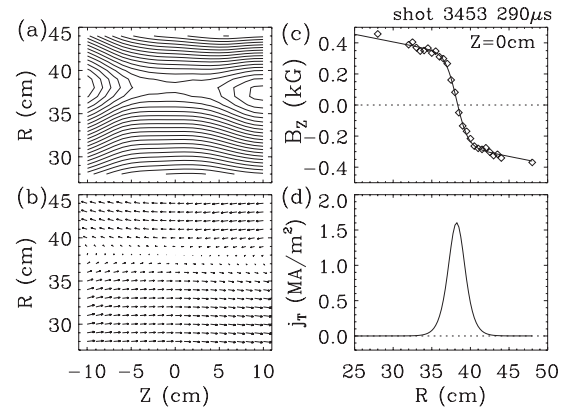


FIG. 25. An example of magnetic profile measured in the MRX (a) vector plot of poloidal field, (b) poloidal flux contours, (c) measured radial profile of B_Z fitted to $\tanh[(R - R_0)/\delta]$, and (d) deduced current-density profile. From Ji *et al.*, 1999.

vatskii, 1971; Frank, 1974) was carried out in a collisional plasma in which the electron mean free path is much shorter than the plasma size. A quantitative analysis of the reconnection rate was not made. The reconnection speeds, inferred from the evolution of reconnected flux, were reported from the collisional experiments on TS-3 (Yamada *et al.*, 1991; Ono *et al.*, 1993) with and without a guide field. The reconnection speed was much faster without a guide field (see Sec. V.B.1).

The first quantitative tests of the classical Sweet-Parker model were performed on the MRX (Ji *et al.*, 1998, 1999), where all important quantities were measured or inferred. Figure 25 shows an example of magnetic profile in the MRX at high collisionality. The prototypical rectangular shape of the diffusion region is seen. The reconnection speed V_R was determined by E_θ/B_Z , where the reconnecting electric field $E_\theta \equiv -(\partial\Psi/\partial t)/2\pi R$ and B_Z is the upstream reconnecting magnetic field. The measured reconnection rate V_R/V_A did not agree with the predicted rate of $S^{-1/2}$ from the classical Sweet-Parker model. Causes of the discrepancies were found by examining the validity of assumptions made in each step of the derivation of the Sweet-Parker model.

Examining the continuity equation revealed effects due to plasma compressibility. The relation $V_R = (\delta/L)V_Z$ is replaced by

$$V_R = \frac{\delta}{L} \left(V_Z + \frac{L}{n} \frac{\partial n}{\partial t} \right) \quad (15)$$

when the density within the current sheet increases. This effect accelerates reconnection during the density buildup phase.

A downstream plasma pressure also plays a role. From the equation of motion, the outflow is reduced from the usual $V_Z = V_A$ to

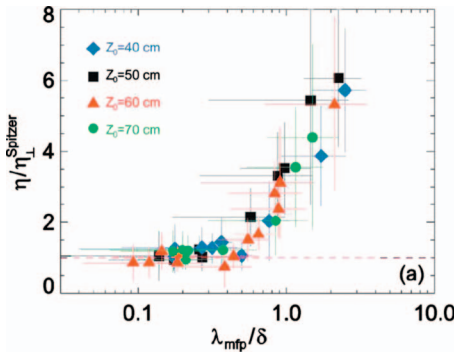


FIG. 26. (Color) Effective plasma resistivity normalized to the transverse Spitzer resistivity as a function of inverse collisionality $\lambda_{\text{mfp}}/\delta$ for different flux core separations Z_0 in no-guide-field cases. From Kuritsyn *et al.*, 2006.

$$V_Z^2 = V_A^2(1 + \kappa) - 2(p_{\text{down}} - p_{\text{up}})/\rho, \quad (16)$$

where $\kappa \equiv (2/B_Z^2) \int_0^L B_R (\partial B_Z / \partial R) dZ = 0.2 - 0.3$ represents the relative importance of the downstream tension force, which is omitted in the Sweet-Parker model. The higher downstream pressure ($p_{\text{down}} \gg p_{\text{up}}$) substantially reduces the outflow to 10–20 % of V_A . This reduction indicates the importance of boundary conditions in determining local reconnection rates. More discussions on these effects can be found in Sec. VIII.C.

Ohm's law along the current (toroidal) direction was examined. Outside of the current sheet, $(\mathbf{V} \times \mathbf{B})_\theta$ balances with the reconnecting electric field E_θ but has to be balanced by other terms within the current sheet. In MHD models, the balancing term is the resistive term, and thus an effective resistivity can be determined by $\eta^* = E_0/j_0$ (Ji *et al.*, 1998). When the plasma is collisional, i.e., the electron mean free path is much shorter than the current sheet thickness, the effective resistivity η^* agrees well with the transverse Spitzer resistivity (Spitzer, 1962) within 30% error and it varies as $T_e^{-3/2}$ (Trintchouk *et al.*, 2003). In the relatively collisionless regime where the mean free path is much larger than current sheet thickness, a significant resistivity enhancement over the classical values was measured as shown in Fig. 26.

The Sweet-Parker model was generalized (Ji *et al.*, 1998, 1999) to incorporate the above three modifications, i.e., plasma compressibility, higher downstream pressure than upstream, and effective resistivity larger than the Spitzer resistivity,

$$\frac{V_R}{V_A} = \frac{1}{\sqrt{S^*}} \sqrt{\left(1 + \frac{Ln}{nV_Z}\right) \frac{V_Z}{V_A}}, \quad (17)$$

where S^* is the Lundquist number calculated from the effective resistivity. Figure 27 shows good agreement between the observed reconnection rate and that predicted by the generalized model. This result shows that the reconnection process can be described by the Sweet-Parker model, with generalizations, in a stable 2D reconnection neutral sheet with axisymmetric geometry. This generalized Sweet-Parker model applies to both

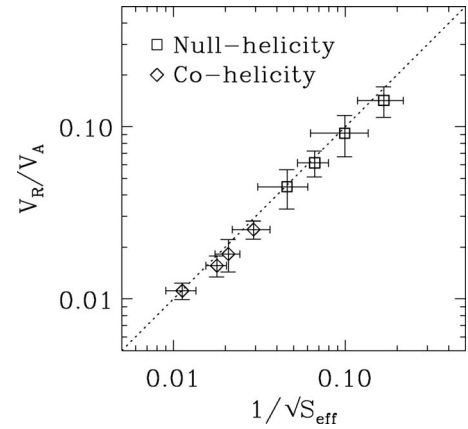


FIG. 27. Comparisons between the experimentally measured reconnection rates and predictions by generalized Sweet-Parker model at the MRX. From Ji *et al.*, 1999.

cases with and without a guide field (cohelicity and null helicity, respectively).

2. Effects of guide field

The third vector component of the magnetic field plays an important role in the reconnection process (Kivelson and Russell, 1995). In the dayside reconnection region of the terrestrial magnetosphere the southward interplanetary magnetic field (IMF), which merges antiparallel to the Earth's northward dipole field, reconnects much faster at the meridian plane than the northward IMF.

In the MRX, the reconnection resistivity was measured both with and without a guide field (Kuritsyn *et al.*, 2006). In antiparallel reconnection without guide field, the transverse Spitzer resistivity was measured. With a sizable guide field, the measured resistivity was a factor of 2 smaller consistent with parallel Spitzer resistivity. Spitzer calculated that $\eta_\perp = 1.96 \eta_\parallel$. In the relatively collisionless cases, a significant enhancement over the Spitzer values was seen in both cases.

Merging experiments showed that magnetic reconnection is influenced by the merging angle of the field lines (Ono *et al.*, 1993; Yamada *et al.*, 1997a, 1997b; Brown, 1999; Cothran *et al.*, 2003). To determine the dependence of the reconnection speed on merging angles of reconnecting lines, the magnitude of external guide field was varied in TS-3 and the MRX while the reconnecting field was kept roughly constant (Yamada *et al.*, 1990, 1997a, 1997b; Ono *et al.*, 1993). When the guide field is near zero (the reconnecting angle is near 180°), the reconnection speed is maximized. As the reconnecting angle is reduced with increasing guide field, the reconnection speed decreases substantially. In the MRX it was observed that the presence of guide field broadens the neutral sheet substantially changing the 2D profile from the double Y shaped to an O shaped (Yamada *et al.*, 1997a, 1997b). This transition of the neutral sheet was first recorded by UCLA group in the EMHD regime (Gekelman *et al.*, 1982).

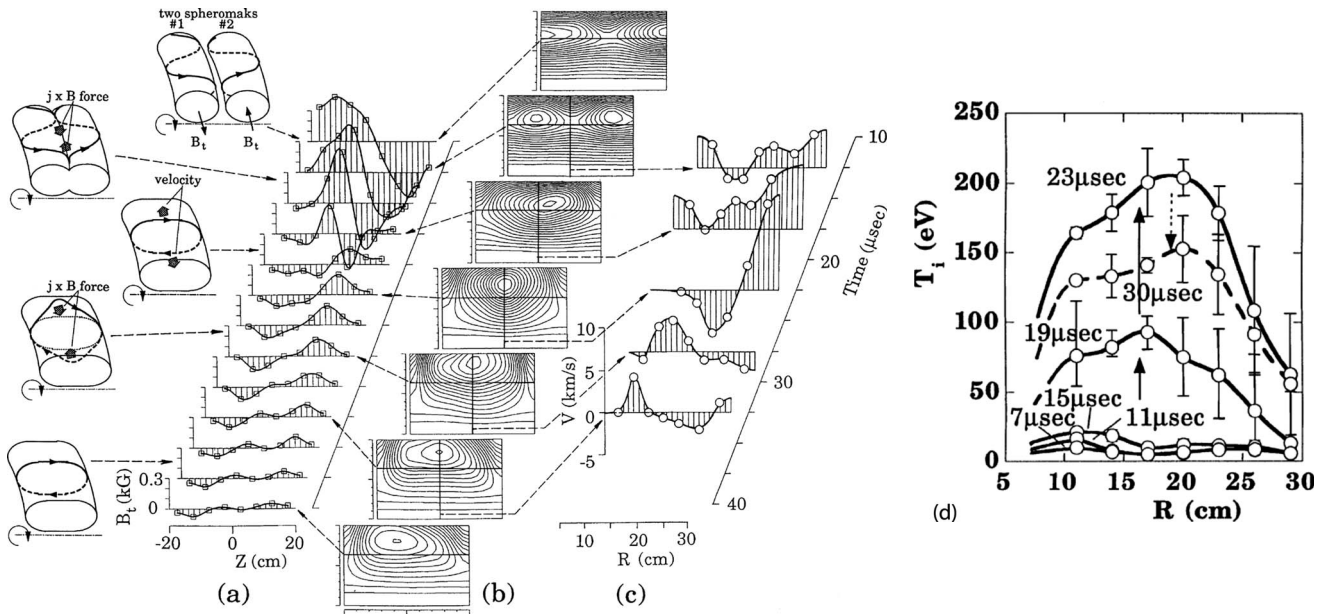


FIG. 28. Counter-helicity plasma merging experiment. (a) Axial profiles of the toroidal magnetic field B_t at $r=18$ cm, (b) poloidal flux contours on the R - Z plane, (c) radial profiles of the ion global velocity V in the toroidal direction on the midplane, and (d) radial profiles of ion temperature T_i on the midplane during the reconnection of two merging spheromaks with equal but oppositely directed B_t . From Ono *et al.*, 1996.

Generally, the reconnection rates in guide-field reconnection are notably smaller than no-guide-field cases. The observed slower rates are attributed to (1) smaller resistivity for a neutral-sheet current parallel to the guide field, (2) suppression of plasma flow by the guide field, and (3) less compressibility of the plasma due to presence of a guide field. The first factor could be due to the current flow along field lines that cause less micro-turbulence and less Hall effects. The second and third factors can be due to the guide field confining the plasma locally, increasing downstream pressure and reducing plasma compressibility. Further study is necessary to assess the physics of guide-field effects, particularly in the two-fluid regime discussed in Sec. VI.

An important question here is why reconnection occurs so fast in tokamak sawtooth crash where the guide field is very strong. This may be due to 3D global MHD instabilities that drive a fast magnetic reconnection in a localized region, as described in Sec. VIII.

B. Plasma heating and acceleration

One of the most important physics issues for magnetic reconnection is how magnetic energy is converted into plasma thermal and kinetic energy. A significant amount of magnetic energy is seen to be converted to thermal energy during reconnection and that the energy conversion rate is much larger than expected from classical dissipation mechanisms.

1. Plasma heating during plasma merging

A violent plasma acceleration is expected in the toroidal direction as the field lines contract after the merging of two toroidal plasmas of the opposite helicity. Evi-

dence of this was observed in the TS-3 experiment (Ono *et al.*, 1993). Figure 28(a) shows the time evolution of the profile of the toroidal field B_t vs Z (axial) direction for the counterhelicity merging discussed in Sec. IV.A.2. This result was obtained by a B_t probe array axially inserted at the radius $R=14$ cm (that matches the magnetic axis). Initially, the merging plasmas formed the B_t profile shown in the figure, positive on the left and negative on the right side. As reconnection progressed, the value of B_t decreased as expected but then the B_t profile flipped (changed its polarity) between $t=20$ and $30 \mu\text{s}$. This overshoot is regarded as evidence of the toroidal slingshot effect (Yamada *et al.*, 1990) as shown in Figs. 28(a) and 28(c). Figure 28(a) describes schematically the dynamic (3D) evolution of magnetic field lines during and after the reconnection. Numerical MHD simulations show similar 3D effects in solar flare processes (Matsutomo *et al.*, 1993) and in magnetospheric physics (Hawkins *et al.*, 1994). Energy transfer from magnetic to plasma thermal energy is expected in this dynamic toroidal field annihilation process. Strong plasma acceleration and ion heating were documented during counter-helicity merging (Ono *et al.*, 1996) as shown in Figs. 28(c) and 28(d).

Local ion heating due to reconnection has been measured (Hsu *et al.*, 2000) in the MRX using an ion dynamic spectroscopy probe (Fiksel *et al.*, 1998) placed inside the neutral sheet. The ion heating rate was found to be much larger than the values predicted by classical dissipation. The SSX experiment was also utilized to study ion heating during merging (Kornack *et al.*, 1998). While their results are consistent with the results from TS-3 and the MRX, a burst of plasma flow at the Alfvén speed was observed in the reconnection plane.

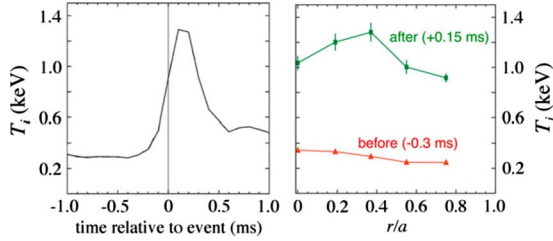


FIG. 29. (Color online) Ion heating during reconnection. Left: Carbon ion temperature vs time at the core. Right: Ion temperature vs radius before and during the reconnection event. From Den Hartog *et al.*, 2007.

2. Strong ion heating during reconnection in RFP

There is a strong correlation between reconnection and ion heating in a RFP but the exact mechanism is unknown. Ion heating is particularly strong in the case of multiple reconnection events—the temperature quadruples in 100 μ s throughout the entire plasma (Den Hartog *et al.*, 2007). The temporal and radial dependence of the ion temperature through a reconnection event is shown in Fig. 29. The multiple reconnections are characterized by a large increase in the amplitude of tearing modes at the locations of the resonant surfaces, which nonlinearly drives MHD modes at the outer radius of the plasma. During multiple reconnections there is a notable change in the magnetic field equilibrium and a large decrease in the stored magnetic energy.

In a helium plasma the bulk ion (He^{2+}) temperature increase is higher than the bulk ion temperature in a deuterium plasma (D^+). However, the impurity ion (C^{6+}) temperature is the same in both plasmas. Differential heating of minority ions is also observed in the solar wind.

The cause of the observed anomalous heating is yet to be determined. A theoretical calculation (Svidzinski *et al.*, 2008) for viscous ion heating was made. It was found that when the radial gradient of the flow velocity is sufficiently large, the calculated heating rate is comparable to that found in experiment. However, such steep flow profiles have not been seen experimentally. The heating rate for impurities was found to be much greater than that for the lighter bulk ions. More study is needed to determine the cause of the observed ion heating.

C. Observation of accelerated plasmas in the exhaust of reconnection site in space

The recent findings of reconnection exhausts in the solar wind provide a good test bed to verify the typical picture of a neutral sheet in which the magnetic field is reversed together with acceleration of ions in the exhaust region (Gosling *et al.*, 2005; Phan *et al.*, 2006). Solar-wind reconnection is usually generated by the interplay of the two solar winds originated by coronal mass ejection. Magnetic field orientations of the two merging plasmas are well defined. The presence of accelerated ions in the reconnection X line has been ob-

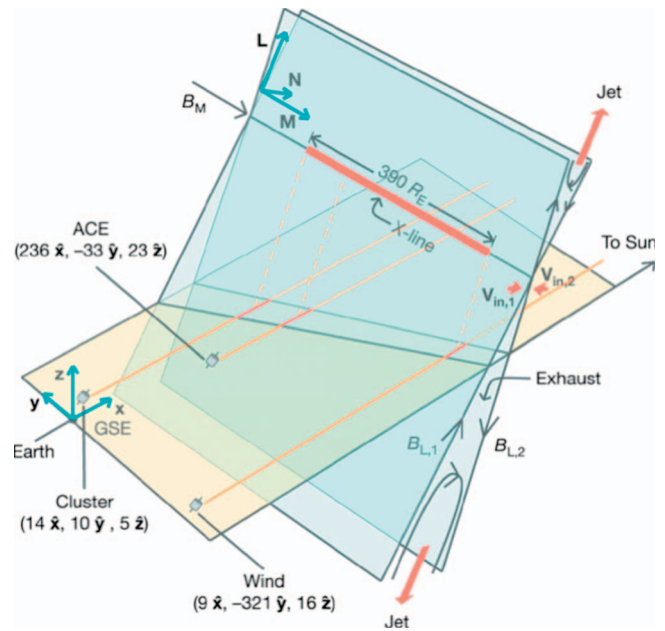


FIG. 30. (Color) Diagram of the encounters of three satellites with regard to contemplated reconnection X lines. From Phan *et al.*, 2006.

served by coordinated measurements from the three satellites, ACE, CLUSTER, and WIND (Fig. 30).

Reconnection in the current sheet (shown in blue in the figure) is considered to occur at the X line between magnetic field lines with large antiparallel components $B_{L,1}$ and $B_{L,2}$; the resulting bidirectional plasma jets (confined to the reconnection exhausts) are observed far from the X line. The three spacecraft positions are shown in units of R_E and in geocentric solar ecliptic (GSE) coordinates with the x axis pointing from Earth to Sun, the y axis pointing toward dusk, and the z axis parallel to the ecliptic pole. All three spacecrafts were relatively close to the ecliptic plane (in yellow). ACE was $222R_E$ upstream of CLUSTER, while WIND was $331R_E$ “downward” of CLUSTER. Also shown is the LMN current sheet coordinate system, with N along the overall current sheet normal, M along the X-line direction, and L along the antiparallel magnetic field direction. The current sheet is tilted 45° relative to the Sun-Earth line. The thick solid red line is the hypothesized $(390R_E)$ portion of the X line whose effect is observed by the three spacecrafts. The solid orange lines denote the spacecraft trajectory relative to the solar wind, with the red line portion marking the intersection of the exhaust with the spacecraft.

All three satellites detected typical signatures which would support, in the profiles of magnetic field ion velocity vectors, the passage of the same bifurcated current sheet. Although a direct measurement of a shock structure in the reconnecting region (near an X line) was not made, it was suggested that the data were consistent with the Petschek MHD model in which plasma acceleration is generated by the tension force of the reconnecting field at the exhaust.

Most of the observations mentioned here have been analyzed in the context of MHD, but it is quite obvious that two-fluid physics analysis is needed to accurately describe the results since the size of the reconnection regions are comparable to the ion skin depth or the ion gyroradii. In the next section, we focus our discussion on two-fluid physics.

VI. TWO-FLUID PHYSICS OF THE RECONNECTION LAYER

As presented in the preceding sections, magnetic reconnection was described primarily through the MHD theory which was developed in the early phase of the plasma research, treating the plasma as a single fluid (Parker, 1957; Sweet, 1958; Petschek, 1964). The MHD framework is based on the assumption that electrons and ions move together as a single fluid even in the presence of internal currents. This formulation has been re-evaluated by a realization that the MHD condition does not hold in a thin reconnection layer such as those seen in the magnetosphere, where ions become demagnetized and the relative drift velocity between electrons and ions can be large. Reconnection layers, such as those created at the magnetopause (Vasyliunas, 1975; Dungey, 1995; Kivelson and Russell, 1995), have thicknesses that are comparable to the ion skin depth (c/ω_{pi}). Because of the force balance between the magnetic field and the plasma kinetic pressure, the ion skin depth is comparable to the ion gyroradius ($B^2/8\pi \sim nT_i$ leads to $c/\omega_{pi} \sim \rho_i$) and only electrons are magnetized, leading to strong two-fluid effects, especially the Hall effect, in the neutral sheet. This effect is considered to allow a large reconnection electric field at the reconnection region and is thus responsible for speeding up the rate of reconnection over Sweet-Parker rate. Generally speaking, two-fluid effects come into play due to the different behaviors of large orbit ions and strongly magnetized electrons. Electromagnetic or electrostatic turbulence at high frequencies ($\omega > \omega_{ci}$) can also be excited and can increase the reconnection rate, as discussed in VII.

A. Numerical simulation of two-fluid reconnection

In the past 12 years, numerous two-dimensional numerical simulations (Mandt *et al.*, 1994; Ma and Bhattacharjee, 1996; Biskamp *et al.*, 1997; Horiuchi and Sato, 1999; Birn *et al.*, 2001) of the collisionless neutral sheet have demonstrated the importance of the Hall term ($\mathbf{j} \times \mathbf{B}$) based on two-fluid or kinetic codes. In the generalized Ohm's equation, it allows a steady (laminar) cross-field current of electrons, which contributes to a large apparent resistivity and generates fast reconnection. Extensive numerical work has been done by Shay and Drake (1998), Shay *et al.* (1998), Horiuchi and Sato (1999), Pritchett (2001), Daughton *et al.* (2006), and many others with periodic and open boundary conditions. Particularly, under a collaboration entitled "The Geospace Environmental Modeling (GEM) Magnetic Reconnection Challenge," a concerted effort was made

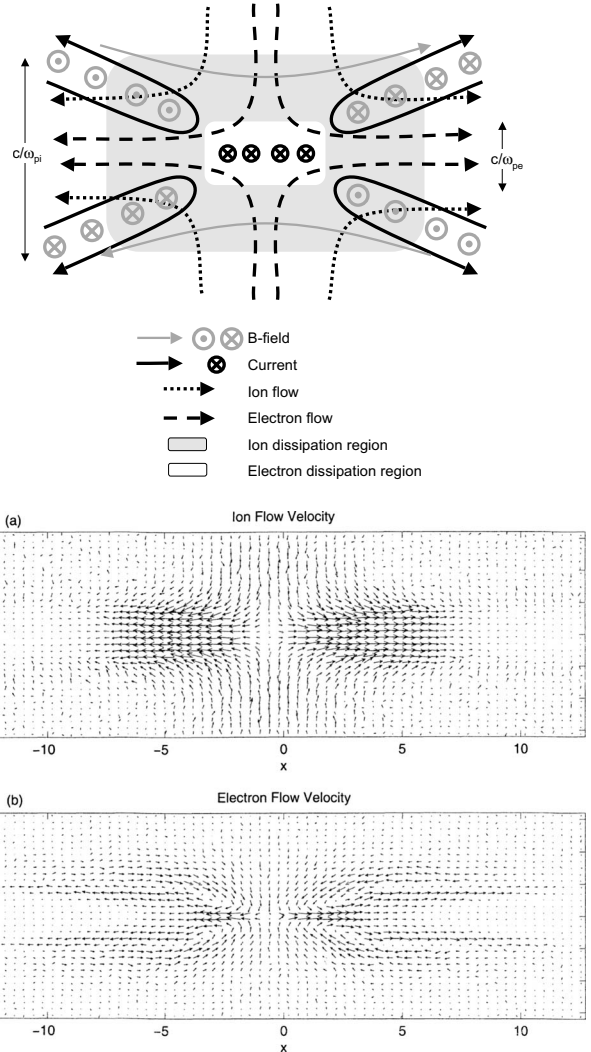


FIG. 31. Two-fluid dynamics in the reconnection layer. (Top) Schematic diagram of the neutral sheet. From Drake and Shay, 2007. (Bottom) Patterns of ion and electron flows in the neutral sheet. From Pritchett, 2001.

to determine the physical mechanisms and rates of two-fluid reconnection (Birn *et al.*, 2001) and to apply it to the Earth's magnetosphere. For this purpose, antiparallel (without guide field) reconnection was extensively studied in collisionless plasmas.

A common picture has emerged from numerical calculations which utilized benchmarking studies of reconnection. Figure 31(a) shows a schematic diagram for the field structure and the dynamics of ion and electron flows in a typical neutral sheet (Drake and Shay, 2007) together with the results from the PIC simulation by Pritchett (2001). As seen in Fig. 31(b), ions become demagnetized as they enter the neutral sheet, turn 90° in the reconnection plane (x, z) of their coordinate system, and then flow outward to the exit direction. In contrast, the magnetized electrons mainly flow inward along the separatrices toward the X point. As the electrons $E \times B$ motion makes them migrate toward the X point, the magnetic field weakens. The electron drift (E_y/B_x) due to the reconnection electric field E_y becomes larger near

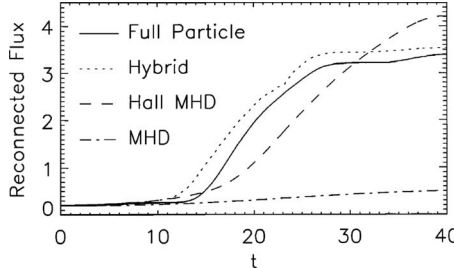


FIG. 32. Reconnected magnetic flux vs time for four different codes for GEM projects: MHD, Hall MHD, hybrid, and full particle codes. From [Birn et al., 2001](#).

the X point and electrons are ejected out to the exit. The electron flow patterns shown in Fig. 31 generate net circular currents in the reconnection plane and create an out-of-plane magnetic field with a quadrupole profile, a signature of the Hall effect. Similar results were obtained by a simpler Hall MHD code which did not include particle dynamics of electrons and ions ([Breslau and Jardin, 2003](#)). The increased electric field caused by the strong Hall term ($\mathbf{j} \times \mathbf{B}/en$) producing a steady laminar cross-field current of electrons represents a fast motion of flux lines ($E = -d\Psi/dt$) in the reconnection plane, a fast rate of magnetic reconnection.

An important question is how the reconnection rate depends on the dissipation mechanism. An important conclusion of GEM challenge ([Birn et al., 2001](#)) is that the reconnection speed is insensitive to the dissipation mechanism and much larger than the resistive MHD reconnection rate. In Fig. 32, the reconnected flux is shown as a function of time for different simulations using a MHD code, a Hall MHD code (including $\mathbf{j} \times \mathbf{B}$ and $\nabla \cdot \mathbf{P}$ terms in Ohm's law), a hybrid code (massless electrons and particle ions), and a PIC code. All runs were carried out with the same Harris equilibrium with finite initial perturbations. The rate of reconnection is the slope of the rising reconnected flux. As seen in Fig. 32, all models but the MHD model show indistinguishable rates of reconnection and are significantly faster than that of the MHD model.

Since the mechanism for breaking field lines in various models differs (electron inertia in PIC and hyper-resistivity in the other non-MHD models), their results support the idea that the reconnection rate is insensitive to the dissipation mechanism. It is argued that because of the dispersion relationship of whistler waves $\omega/k \propto k$ the total outflow flux of electrons from the dissipation region $n_e v_x \delta$ is constant since $v_x \approx \omega/k$ and $\delta \approx 1/k$. It was thus concluded that the reconnection rate is primarily determined by the Hall term and insensitive to the dissipation mechanisms. It is considered that the dissipation of magnetic energy in their simulations occurs only in the vicinity of the X point within the distance of a few electron skin depths. There still remains a question of whether the GEM challenge properly addressed a general problem of reconnection, particularly the dissipation mechanism which causes field-line breaking and the conversion of magnetic energy to plasma energy. Re-

cently, further efforts have been made using PIC numerical codes to investigate the effects of boundary conditions (periodic versus open) ([Daughton et al., 2006](#)), which will be discussed in Sec. VIII. The effects of the electron pressure tensor term in the presence of a guide field ([Hesse, 2006](#)) are described in Sec. VII.

A group of two-fluid numerical calculations has been carried out to assess the Hall effect in the presence of collisions or resistivity. [Ma and Bhattacharjee \(1996\)](#) reported that the neutral-sheet profile changes from a double Y shape to an X shape with impulsive reconnection features as two-fluid effects were turned on with a constant resistivity. When the resistivity was set to be uniform in space and sufficiently large, the familiar rectangular-shaped Sweet-Parker layer was obtained (Fig. 33). When the resistivity is reduced, characteristic features of the two-fluid dynamics appear with the double-wedge-shaped neutral sheet (Fig. 33). This result is in good agreement with the recent observation in the MRX as described later.

Impulsive reconnection was observed ([Cassak et al., 2005](#)) when the Hall effect was turned on, on the top of slow resistive reconnection. For a given set of plasma parameters they observed two stable reconnection solutions: a slow (Sweet-Parker) solution and a fast Hall reconnection solution. Below a certain critical resistivity, the slow solution disappears and fast reconnection occurs suddenly and dominates.

The GEM challenge program ([Birn et al., 2001](#)) found that reconnection proceeds much faster than resistive MHD reconnection, and the reconnection rate is determined primarily by the Hall term, not by dissipation. Some argued that this results in a separation of the dissipation region of line breaking from the global region. The dissipation region is shorter than the global length and so the problem of transporting plasma a long distance faced by Sweet-Parker and Petschek models is eased. Figure 34 shows that there are long separatrices attached to the dissipation region much as pictured in the Petschek model.

This argument is borne out by the simulations of [Daughton et al. \(2006\)](#), who extended the simulation box and allowed open boundary conditions. They found that the reconnection rate first followed that of the periodic box simulations but later slowed down as the plasma reached the new wall. This simulation itself does not allow for any back pressure since, once the plasma reaches the wall, its dynamics are no longer considered.

The GEM simulations seem adapted to the magnetosphere, where the change of topology is the prime reason for reconnection, but are not well adapted to the solar problem where the conversion of a large amount of magnetic energy is the main concern. Thus, in the latter case incoming lines of force must be very long, and if the matter they bring in is not moved out of the way by a large longitudinal distance, then the matter on the first reconnected lines will bottle up the reconnection and stop it. The problem of back pressure along the separatrix was considered in the MHD context by [Uzdensky and Kulsrud \(2000\)](#) who were able to obtain an analytic

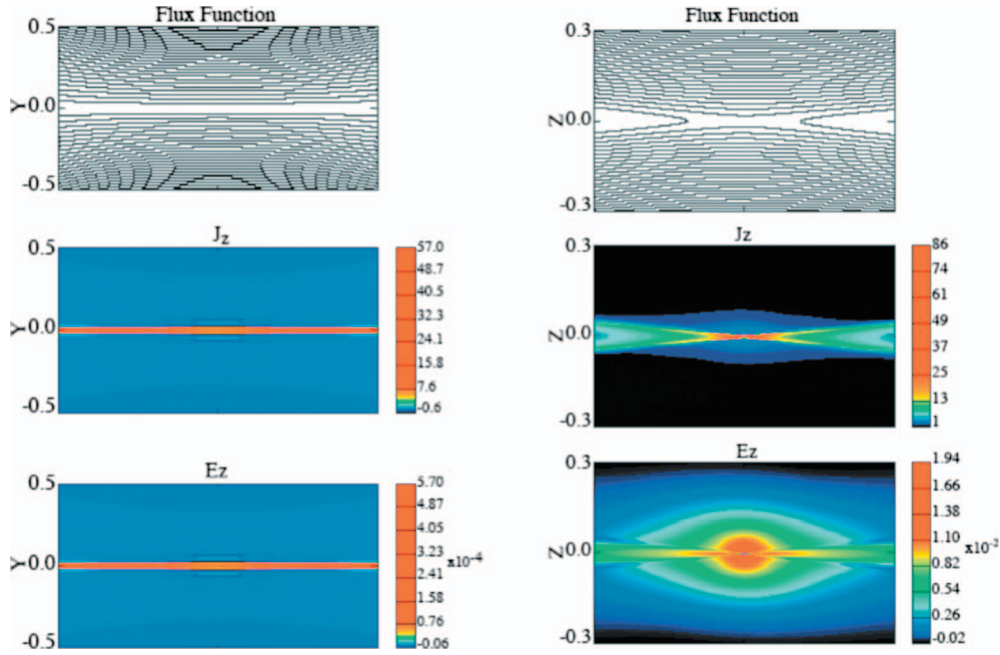


FIG. 33. (Color) Change of reconnection layer profile. Comparison of numerical simulation with (a) resistive MHD and (b) Hall MHD codes in which the electron pressure gradient is included. Without a guide field, the measured profile of the MRX neutral sheet is in good agreement with these results of numerical simulations. Adapted from [Ma and Bhattacharjee, 1996](#).

solution for flow in the separatrix that separates the upstream and downstream equilibria outside of the current layer.

B. Analytical theory for two-fluid reconnection

In the MHD equations, it is assumed that the electron and ion velocities are equal, so that one needs to keep only one of their velocities, usually the ion velocity. This occurs if the scale size of spatial variations is larger than the ion skin depth $\delta_i = c/\omega_{pi}$, where $\omega_{pi} = \sqrt{4\pi ne^2/M}$. If the current j is constant over a current layer thickness δ , the magnetic field changes by $\Delta B \approx 4\pi\delta j$. If $v_i - v_e \approx \sqrt{T/M}$, the ion sound speed, and if δ is larger than the ion skin depth,

$$\Delta B > 4\pi n e \frac{v_i - v_e}{c} \frac{c}{\omega_{pi}} \quad (18)$$

or

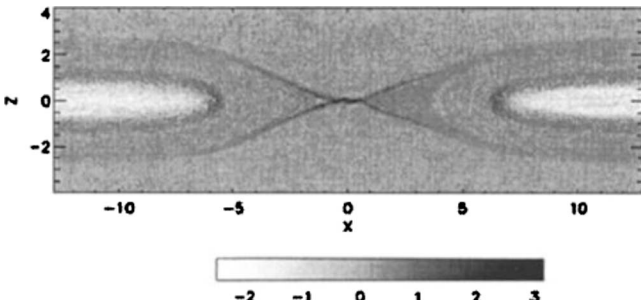


FIG. 34. Out-of-plane electron current from a hybrid simulation. From [Shay et al., 2001](#).

$$(\Delta B)^2 > \frac{4\pi n^2 T M}{M} = 4\pi n T \approx 2B_0^2, \quad (19)$$

where B_0 is the field outside of the layer. Thus, if the ion and electron velocities were to differ by more than the ion sound speed, the change in magnetic field ΔB is larger than B_0 .

In many space and astrophysics cases the calculated thickness of the Sweet-Parker layer thickness δ_{SP} is less than the ion skin depth δ_i . Hence, there is no guarantee that the two velocities are close or that the Sweet-Parker theory is applicable. The ions and electrons can move independently of each other, and the reconnection physics in the layer will differ from that given by the Sweet-Parker model, allowing the layer thickness to be the thicker ion skin depth. For example, the ions could flow in the thicker layer while the electrons flow in a thinner layer. The ion mass flow can be larger than the flow in the Sweet-Parker layer, while the thinner electron layer can allow the lines to break fast enough to accommodate this faster downstream mass flow. We only need the continuity equation in the more general Sweet-Parker model while the undetermined thinness of the electron layer is determined by Ohm's law. The resulting reconnection velocity under this simplified model is

$$v_R \approx (\delta_i/L)v_A, \quad (20)$$

which is faster than the corresponding Sweet-Parker reconnection velocity ($\delta_{SP}/L)v_A$.

The mathematical difference between one- and two-fluid theory appears in the different Ohm's laws. The one-fluid Ohm's law [Eq. (1)] differs from the two-fluid Ohm's law,

$$\mathbf{E} + \frac{\mathbf{v} \times \mathbf{B}}{c} - \frac{\mathbf{j} \times \mathbf{B}}{nec} + \frac{1}{ne} \nabla \cdot \mathbf{P}_e + \frac{m d\mathbf{v}}{e dt} = \eta \mathbf{j}, \quad (21)$$

where \mathbf{P}_e is the electron pressure tensor. Equation (21) is correct even for one-fluid MHD and is reduced to the ordinary Ohm's law by setting $\mathbf{v}_e = \mathbf{v}_i = \mathbf{v}$ and neglecting the electron inertia and the pressure tensor terms.

The generalized form of Ohm's law is identical to the equation of motion for electrons,

$$nm \frac{d\mathbf{v}_e}{dt} = -\nabla \cdot \mathbf{P}_e - ne \left(\mathbf{E} + \frac{\mathbf{v}_e \times \mathbf{B}}{c} \right) \quad (22)$$

because $\mathbf{j} = ne(\mathbf{v}_i - \mathbf{v}_e)/c$ and $\mathbf{v} = \mathbf{v}_i$.

It is necessary to apply two-fluid dynamics to magnetic reconnection when the Sweet-Parker layer is thinner than the ion skin depth δ_i . The ratio of the Sweet-Parker layer thickness to the ion skin depth is $\approx 0.2\sqrt{L/\lambda}$, where λ is the mean free path and L is the global length of the current layer (Yamada *et al.*, 2006). The two-fluid regime is closely related to the collisionless regime. The Hall effect becomes dominant when the mean free path is longer than the global length by a factor of 1/25.

The two-fluid effect is brought out by the example of a 2D reconnection problem in the x - z plane where the reconnection field is along the z direction. If the initial B_y is zero (no guide field), then in ordinary MHD there can be no B_y field because of a symmetry in MHD theory that separates the toroidal y component and the poloidal xz components. In two-fluid theory this symmetry is broken by the $\mathbf{j} \times \mathbf{B}$ Hall term and a toroidal B_y component is produced. This was noticed by Sonnerup (1979) in an early discussion of two-fluid theory applied to magnetic reconnection. The same B_y field was found by Terasawa (1983) in a two-fluid investigation of the tearing mode.

A physical interpretation of the origin of a toroidal field was given by Mandt *et al.* (1994), who ascribed it to the toroidal motion of electrons which by flux freezing "pull" poloidal magnetic field lines into the toroidal direction. This interpretation needs further considerations. Inspection of Eq. (21) shows that, in absence of the pressure term, electrons are indeed frozen in the electron fluid. However, the main toroidal motion of the electrons is due to the diamagnetic current of the electrons produced by their pressure gradient and it can be argued that this motion cannot drag the field lines. Additional poloidal electron flows, driven by a poloidal electric field (Yamada *et al.*, 2006), are necessary for toroidal pulling the lines of force.

A second interpretation is that the toroidal field would arise from Ampere's law and poloidal motion of the electrons. This picture is closer to the equations that Sonnerup and Terasawa used to show the B_z field's existence. This second interpretation due to Uzdensky and Kulsrud (2006) is elaborated below (Fig. 35).

If the magnetic field is purely poloidal with no externally applied B_y guide field, the ion gyration radius is comparable with the current layer thickness δ , and the

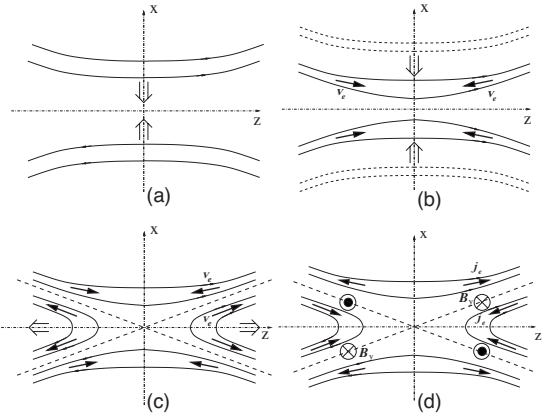


FIG. 35. The basic idea of out-of-plane field generation. Adapted from Uzdensky and Kulsrud, 2006.

ions are essentially unmagnetized. The electron gyration radius is much smaller so that the electrons are tied to the lines everywhere except where the magnetic field is very small, near $x=0$.

As the reconnection proceeds, the lines of force move into the reconnection current layer, with the electrons tied to them. Their transverse $\mathbf{E} \times \mathbf{B}$ velocity brings them into the region where the ions are unmagnetized and the ion density is unaffected by the reconnection processes. The electron and ion motions are not entirely decoupled because, by charge neutrality, their densities must be equal to avoid large poloidal electric fields. This *quasineutrality* condition cannot be accomplished by the transverse electron velocities alone. The electrons must develop velocities parallel to the lines of force and these velocities are strongly constrained by charge neutrality.

In Fig. 35(b), the volume per flux of the field-line tubes increases strongly as the lines approach the separatrix with most of the volume concentrated near the midplane $z=0$. Without the parallel electron flow the density near the midplane would drop because the $\mathbf{E} \times \mathbf{B}$ flow diverges so there must be a parallel electron current that produces a the toroidal magnetic field. (The ion current is assumed small.) The figure shows that this toroidal field has a quadrupole character reversing across the axes. Downstream from the separatrix the electrons flow away from the $x=0$ plane because the flux tubes contract as they move, so the parallel electron current reverses sign.

However, near the separatrix the volume per flux diverges as does the parallel electron flow. Because of the toroidal field this flow has a diverging toroidal flow accelerated in the toroidal direction. As a consequence, the toroidal field also diverges in turn forcing the electrons tied to the lines to accelerate infinitely fast in the toroidal direction. Consequently, the toroidal inertial force becomes comparable to the toroidal electric force in Ohm's law. The poloidal velocity of the electrons is no longer tied to the lines which can slip off the lines where their magnetization fails. This leads to a boundary layer about the separatrix in which the lines of force can move faster than the electrons and break.

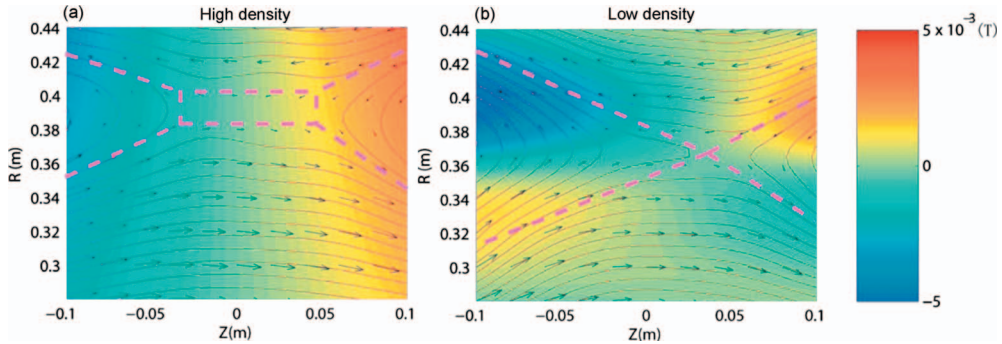


FIG. 36. (Color) Comparison of the experimentally measured reconnection layer profile for two cases: (a) collisional regime ($\lambda_{\text{mfp}} \ll \delta_{\text{sheath}}$) and (b) nearly collisionless regime ($\lambda_{\text{mfp}} > \delta_{\text{sheath}}$). In-plane magnetic field is shown as arrows and out-of-plane field component is shown by the color codes ranged from -5 to 50 G. Dashed pink lines show that the magnetic configuration changes from an elongated current sheet [Sweet-Parker type in (a)] to a double-wedge shape (Petschek-like) as collisionality is reduced. The predicted quadrupole structure of the out-of-plane magnetic component, a signature of Hall effects, is observed in (b). From Yamada *et al.*, 2006.

For any point $P(x, z)$, we define the volume per flux $V(x, z)$ as the volume contained in a flux tube of unit magnetic flux which passes through P , contained between it and the x axis.

The toroidal field is

$$B_y(x, z) = -4\pi n e E_y V(x, z), \quad (23)$$

where E_y is the reconnecting electric field.

If the ion density is constant throughout the current layer, then the electron behavior can be treated quantitatively. Uzdensky and Kulsrud (2006) found the following results in the first quadrant ($x > 0, z > 0$) and outside the separatrix boundary layer. Results in the other quadrants can be found by symmetry.

On any line ψ , the toroidal position is

$$y^2 - y_0^2 = 2\pi n e E_y (V^2 - V_0^2), \quad (24)$$

where y_0 is the toroidal coordinate where the line ψ leaves the current layer and $V_0(\psi)$ is the volume per flux at this point.

The toroidal velocity and acceleration are

$$v_y = dy/dt = 4\pi n e c E_y^2 (dV_0^2/d\psi) \quad (25)$$

and

$$a_y = d^2 y/dt^2 = 4\pi n e c E_y^3 (d^2 V_0^2/d\psi^2). \quad (26)$$

Close to the separatrix $m a_y \approx e E$ when

$$\psi - \psi_S \approx \sqrt{\frac{m}{M} \ln \frac{M}{m}} B_0 \delta \approx 0.06 \delta B_0, \quad (27)$$

where ψ_S is the value of ψ on the separatrix. δ is the thickness of the current layer and M is the ion mass. This result is valid only for a particular model.

The thickness of this region along the x axis for the simple poloidal field layer is $\Delta y \approx 0.25 \delta$, where δ is the thickness of the entire current layer [Fig. 35(d)].

C. Experimental observations of two-fluid effects in the reconnection layer

In the past two decades, a number of laboratory experiments have provided important data contributing to the understanding of the local two-fluid physics of reconnection. Table I shows a number of recent experimental devices dedicated to the study of magnetic reconnection. In this section, we review the observations from these devoted laboratory studies that lead to improved understanding of the two-fluid physics in the reconnection layer. Recent major observations from space satellites are also described. The observations are compared with the numerical simulation results mentioned earlier.

1. Measurements of profile of reconnection layer

The detailed study of the 2D profiles of reconnection layer provides a clue to the physics mechanisms acting in the region. Since the 1970s, the profile of the reconnection layer has been studied in many laboratory plasmas by generating it in a controlled manner (Stenzel and Gekelman, 1981; Ono *et al.*, 1993; Yamada *et al.*, 1997a, 2000). In the driven reconnection in the MRX, profiles of the neutral sheets have been investigated by changing its plasma parameters such as density and temperature (Yamada *et al.*, 2006; Yamada, 2007).

It is observed that the 2D profile of the neutral sheet changes significantly from the rectangular shape in the collisional regime ($\lambda_{\text{mfp}} \ll \delta_{\text{sheath}}$) to a double-wedge shape in the collision-free regime ($\lambda_{\text{mfp}} > \delta_{\text{sheath}}$). Simultaneously, the reconnection rate is seen to increase as the collisionality is reduced. Figure 36 shows how the profile of the MRX neutral sheet depicted by the measured magnetic field vectors and flux contours changes with respect to collisionality condition. In the high plasma density case where the mean free path is much shorter than the sheet thickness, a rectangular-shaped profile of the Sweet-Parker model of Fig. 14 type is identified and the classical reconnection rate is measured. In

the case of low plasma density where the electron mean free path is longer than the sheet thickness, an X-shaped profile appears as shown in Fig. 36(b) and the Hall MHD effects become dominant as indicated by the notable out-of-plane quadrupole field depicted by the color code. There is no recognizable out-of-plane Hall field in the collisional case of Fig. 36(a), where the weak dipole toroidal field profile is only a remnant of the field created by initial poloidal discharges around the two flux cores. The X-shaped profile of the Petschek type, seen in Fig. 36(b), differs significantly from that of the Sweet-Parker model [Fig. 36(a)], and a fast reconnection rate is measured in this low collisionality regime. This result is an experimental demonstration of how collisionality changes the shape of the reconnection layer, simultaneously affecting the reconnection rate. A slow shock, a key signature of the Petschek model, is not identified in this regime. This observation is consistent with the recent numerical results that included both two-fluid effects and resistivity (Ma and Bhattacharjee, 1996; Bhattacharjee *et al.*, 2001). Without a guide field, the measured profile of the MRX neutral sheet is in remarkable agreement with these numerical simulation results.

It is difficult to directly measure the 2D spatial profiles of the reconnection region in the magnetosphere because of the limited number of measuring locations by satellites. In the solar atmosphere, 2D neutral-sheet-like patterns have been sometimes recognized through soft-x-ray satellite images of solar flares, but their exact magnetic profiles are unknown. It appears that a reconnection process is underway throughout this area based on the sequence of the high energy electron flux hitting the footpoints at the photosphere. In order to describe the observed reconnection rate (Yokoyama *et al.*, 2001) by the Sweet-Parker model and to explain the apparent fast flux transfer, the plasma resistivity or energy dissipation has to be anomalously large throughout a wide region.

2. Verification of Hall effects in the reconnection layer

The two-fluid dynamics of reconnection, shown in Fig. 31, predict the presence of strong Hall effects due to decoupling of electron flow from ion flow. In a collisionless neutral sheet such as seen in the magnetosphere, this situation is equivalent to magnetized electrons pulling magnetic field lines in the direction of the electron current and thus generating an out-of-plane quadrupolar field.

a. Observation of Hall effects in space

In the magnetosphere, the two-fluid physics of magnetic field reconnection was analyzed in terms of the ion diffusion region of scale size $c/\omega_{pi} \sim 100$ km in the sub-solar magnetopause (Mozer *et al.*, 2002).

A symbolic hyperbolic tangent in-plane field and a sinusoidal out-of-plane Hall magnetic field were observed near the separatrices of the current sheet. Signatures of Hall MHD and the ion diffusion region [the lightly tinted region in Fig. 37 (top)] were seen in the Y component of the magnetic field (into and out of the

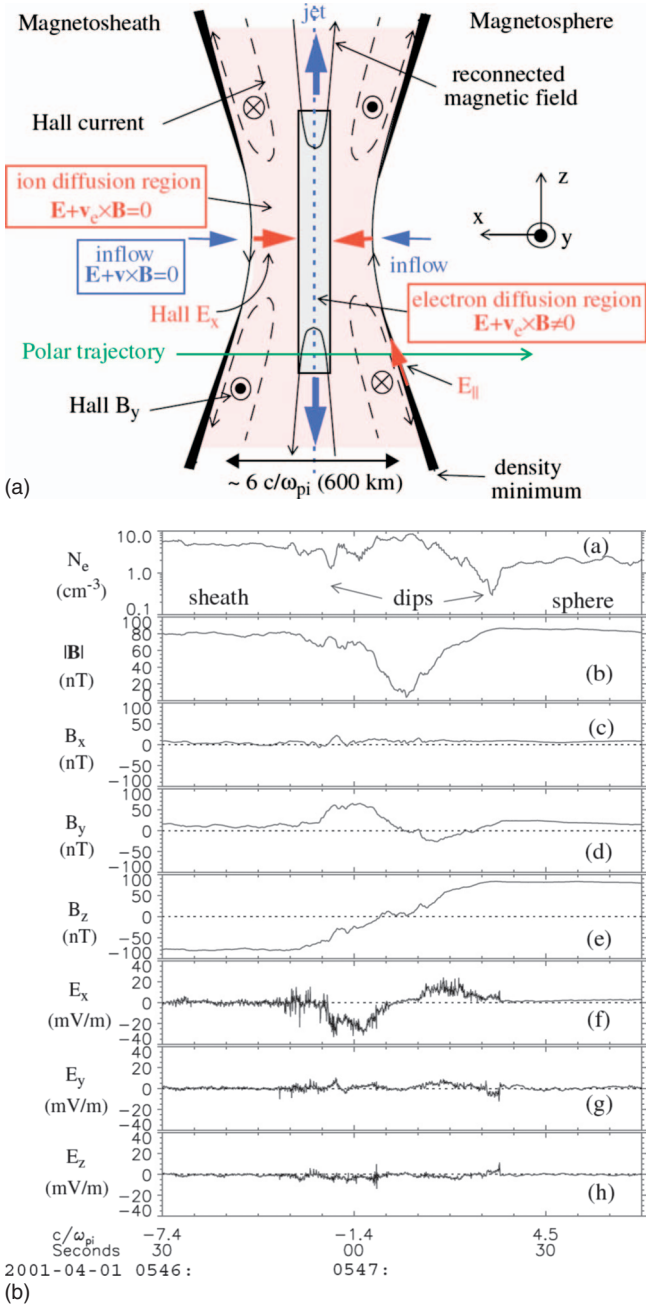


FIG. 37. (Color) Conjecture flight path of the POLAR satellite in the modeled diffusion region (top) and data collected on 1 April 2001 (bottom). (a) The plasma density. (b)–(e) The magnitude and three components of the measured magnetic field at a rate of 8 samples/s, respectively. (f)–(h) The three components of the electric field in a frame fixed to the magnetopause. The electric field data rate was 40 samples/s. From Mozer *et al.*, 2002.

paper), the X component of the electric field (the red horizontal arrows), and the disagreement between the measured perpendicular ion flow and MHD based $\mathbf{E} \times \mathbf{B}/B^2$. The detailed data are shown in Fig. 37 (bottom). The amplitude of the Hall field B_Y was 45 nT or $\sim 0.55 B_{X0}$, where B_{X0} is the asymptotic magnetic field in the magnetosheath.

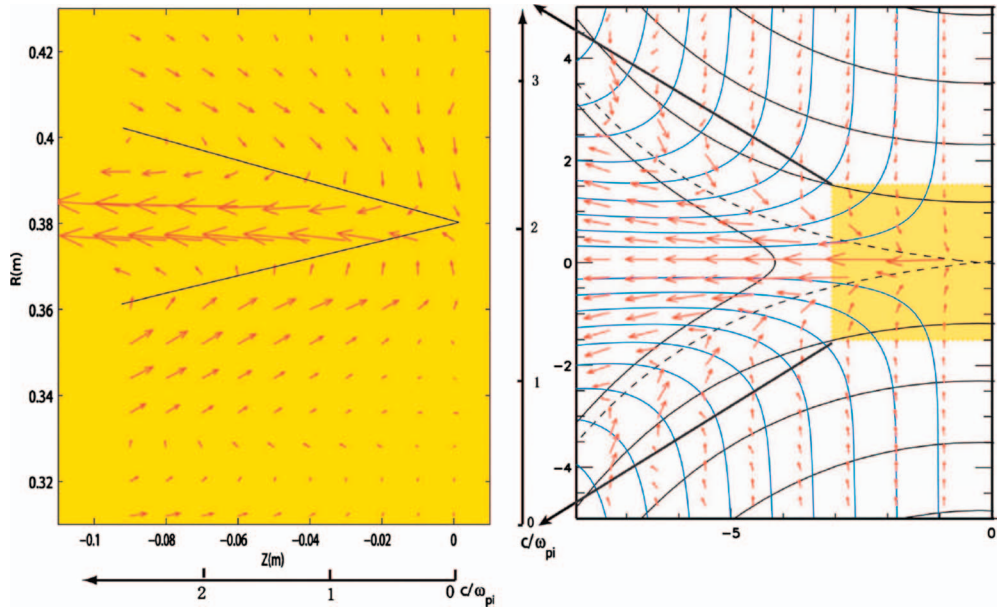


FIG. 38. (Color) Comparison of 2D profiles of electron flow vectors from the MRX data measured by fine scale probes (left panel) and numerical simulation (right panel); the MRX data should be compared with the yellow-coded region in the right panel for the same spatial coverage in terms of c/ω_{pi} . In the right panel, patterns of ion flows (blue lines) and electron flows (red arrows) are superposed on the flux plot of reconnection field line (black lines). From Yamada *et al.*, 2006.

The maximum normal electric field E_x was ~ 30 mV/m or $\sim 0.5 V_A B_{x0}$, which is consistent with the recent numerical simulations that demonstrated a large negative potential well around the X point. The ion diffusion region had a width of about six magnetosheath ion skin depths (or approximately six magnetospheric ion skin depths) at the location of the spacecraft crossing. About the same time as their report, evidence of Hall effect was reported through the detection of a quadrupolar B_y field after analyzing the data from GEOTAIL skimming in January 1997 along the dayside magnetopause (Deng and Matsumoto, 2001). Another report of the out-of-plane quadrupolar field was made from the data from the WIND satellite which traveled in the reconnection sheet of the magnetotail (Øieroset *et al.*, 2001). Recently a reconnection electric field was studied to deduce a reconnection speed when a satellite flew through the ion diffusion region (Mozer and Retinò, 2007).

b. Observation of Hall effects in laboratory experiments

More conclusive quantitative study of Hall effects has been carried out in the MRX by comparing the results of a two-fluid simulation for the MRX geometry with the experimental results (Ren *et al.*, 2005; Yamada *et al.*, 2006). Aided by the numerical work, a deeper understanding of the two-fluid reconnection dynamics has been obtained. The results from this study are shown in Fig. 38.

As shown in Fig. 38 (right), the reconnecting field lines move into the neutral sheet (reconnection layer) of width comparable to the ion skin depth. As they approach the X point, ions become demagnetized. The ion flows gradually change direction by 90° from the x to the

z direction in the reconnection (x, z) plane (the blue lines). It is shown that magnetized electrons flow quite differently (the red vectors) still following magnetic field lines until they approach the X -point or separatrix surfaces.

The MRX experimental data in Fig. 38 (left) show that as electrons flow through the separatrix regions of reconnection sheet, they are first accelerated toward the X point. After making a sharp turn at the separator lines, they then flow outward in the Z direction. When one compares the corresponding flow patterns between the experimental data and the numerical simulation (in the yellow section), one finds excellent agreement and that the data illustrate the essence of the Hall effects. The vectors of electron flow in the MRX data illustrate that, after the initial acceleration, electrons are further accelerated as they pass through the narrow channel section around the central separatrix. The initial acceleration may be due to a larger $\mathbf{E} \times \mathbf{B} (\sim E_y/B_z)$ velocity as the reconnection magnetic field diminishes near the origin ($B_z \sim 0$) with uniform reconnection electric field E_y . To date these MRX data provide the most quantitative data of Hall currents in a real plasma.

The measured electron flow pattern generates a circular net current pattern in the reconnection plane and thus creates an out-of-plane magnetic field with a quadrupole profile. A 2D profile of the out-of-plane quadrupole magnetic field was measured in the MRX by scanning the 90-channel probe array. Figure 36(b) shows the color contours of this out-of-plane quadrupole field in the diffusion region during collisionless reconnection together with the vectors of the reconnection magnetic field in the reconnection ($R-Z$) plane. This has been regarded as a hallmark of the Hall effect (Birn *et al.*, 2001;

[Shay et al., 2001](#)). This process can be interpreted as a mechanism in which the electrons, which are flowing in the y direction of the neutral-sheet current, tend to pull magnetic field lines toward the direction of electron sheet current. The spatial resolution of this figure is 4 cm in the Z direction (grid size) and is 1 cm in the R direction which are obtained by radially scanning the probe array and averaging several discharges at each position. The amount of Hall field is consistent with the results from the numerical simulation ([Ren et al., 2005; Yamada et al., 2006](#)).

In the different geometry of the plasma merging experiment SSX ([Matthaeus et al., 2005; Brown et al., 2006](#)), the observation of a similar out-of-plane field was reported. It was argued that an in-plane Hall electric field was measured based on the $\mathbf{j} \times \mathbf{B}$ force balance. However, a more precise documentation of the in-plane pressure gradient and a direct measurement of plasma space potential is needed to verify their argument since in the neutral sheet the $\mathbf{j} \times \mathbf{B}$ force should generally balance with ∇p as described by the Harris equilibrium.

In the MST reversed field pinch ([Ding et al., 2004](#)) device, experimental measurements in the collisionless reconnection region with a strong guide field were carried out in the center core using Faraday rotation of a far-infrared laser and in the edge with magnetic probes. In the plasma core, the measured magnetic field indicated that the Hall effect is strongly localized to the reconnection layer of a helical structure at the resonance flux surface of $m/n=1/6$.

3. Identification of the electron diffusion layer

Another important prediction of the 2D numerical simulations is the existence of a two-scale diffusion layer in which an electron diffusion layer resides inside of the ion diffusion layer whose width is the ion skin depth (see, e.g., [Pritchett, 2001](#)). More exact profiles of electron flow vectors have been recently measured in a laboratory plasma. In the neutral sheet of the MRX, the electron diffusion region was identified and it was found that demagnetized electrons are accelerated in the outflow direction in the reconnection plane, as shown in Fig. 39 ([Ren et al., 2008](#)). The width of the electron diffusion region, which is identified by the profile of electron outflow, scales with the electron skin depth as $(5.5-7.5)c/\omega_{pe}$. The electron outflow velocity scales with the electron Alfvén velocity $[(1.2-1.6)V_A]$. But the thickness of the electron diffusion layer is three to five times larger than the values ($\sim 1.5c/\omega_{pe}$) obtained by 2D numerical simulations (see Sec. VII).

A careful check of the effects of collisions has been made to determine how much of the enhancement of the thickness should be attributed to them ([Ji et al., 2008; Ren et al., 2008](#)). While the electron outflow seems to slow down by dissipation in the electron diffusion region, the total electron outflow flux remains independent of the width of the electron diffusion region. We note that even with presence of the sharp electron diffusion region, the reconnection rate is still primarily de-

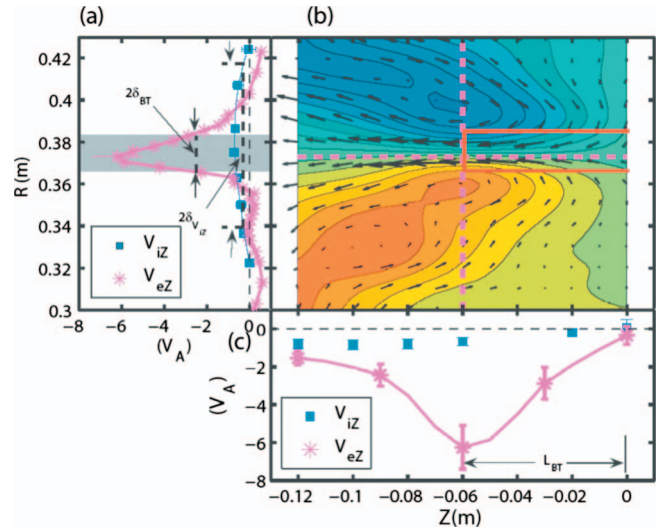


FIG. 39. (Color) Experimental identification of electron diffusion layers. (a) The radial profiles of the electron outflow velocity V_{eZ} (magenta asterisks) and ion outflow velocity V_{iZ} (blue squares) measured in a helium plasma. (b) The two-dimensional profile of the out-of-plane field B_T (color-coded contours) and the in-plane electron flow velocity V_e (black arrows). (c) V_{eZ} and V_{iZ} as a function of Z . The magenta dashed lines in (b) represent the cuts at $Z=-6$ cm and at $R=37.5$ cm along which the profiles in (a) and (c) are taken. From [Ren et al., 2008](#).

termined by the Hall electric field as concluded by the GEM project. The ion outflow channel is shown to be much broader than the electron channel, also consistent with the numerical simulations. A more comprehensive study is required to determine how the profiles of the electron diffusion layer affect overall reconnection dynamics including energy dissipation.

4. Scaling of the reconnection rate with collisionality

We observe that the reconnection rate, which is represented by an effective local resistivity, increases significantly as the collision mean free path increases and the plasma enters the two-fluid physics regime. How does it quantitatively scale with respect to the collisionality of the plasma? In the MRX, a scaling for reconnection resistivity was obtained with respect to the ratio of characteristic scale length for two-fluid theory, the ion skin depth c/ω_{pi} , and for MHD theory, the Sweet-Parker width δ_{SP} . The classical reconnection rate with the Spitzer resistivity is obtained in the regime of $c/\omega_{pi} < \delta_{SP}$. When the ion skin depth becomes larger than δ_{SP} , the reconnection rate is larger than the classical rate ([Yamada et al., 2006](#)). Figure 40 presents the MRX scaling for effective resistivity $\eta^*=E/j$ normalized to the Spitzer value η_{SP} in the center of reconnection region; η^* is measured as discussed in Sec. V. Shown for comparison is a scaling obtained by a recent Hall MHD numerical simulation results using ([Breslau and Jardin, 2003](#)). This figure exhibits a criterion for the Hall effects to become important, namely, the reconnection resistiv-

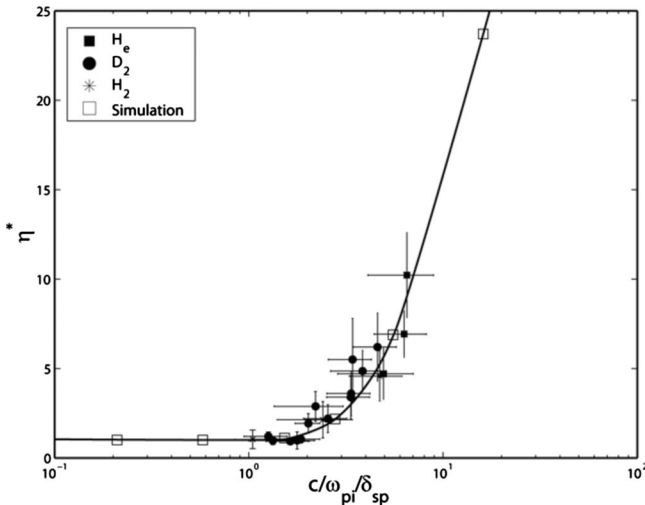


FIG. 40. MRX scaling. Effective resistivity $\eta^* (=E/j)$ normalized by the Spitzer value η_{SP} vs the ratio of the ion skin depth to the Sweet-Parker width (δ_i) becomes larger than the Sweet-Parker width (δ_{SP}) by a factor of 2. The apparent agreement of the MRX scaling with the Hall MHD code indicates that the enhanced resistivity is primarily due to the laminar Hall effect. In the numerical simulation (Birn *et al.*, 2001), it was also concluded that the reconnection electric field is primarily generated by the laminar Hall effect, namely, the $\mathbf{j} \times \mathbf{B}$ term.

ity (or reconnection speed) takes off from the classical Spitzer value (or the Sweet-Parker reconnection rate) when the ion skin depth (δ_i) becomes larger than the Sweet-Parker width (δ_{SP}) by a factor of 2. The apparent agreement of the MRX scaling with the Hall MHD code indicates that the enhanced resistivity is primarily due to the laminar Hall effect. In the numerical simulation (Birn *et al.*, 2001), it was also concluded that the reconnection electric field is primarily generated by the laminar Hall effect, namely, the $\mathbf{j} \times \mathbf{B}$ term.

Using the ratio of the ion skin depth to the Sweet-Parker width, the relationship is translated into the square root of the ratio of the electron mean free path to the system size (L , sheet length) as shown by Yamada *et al.* (2006),

$$\frac{c}{\omega_{pi}} \frac{1}{\delta_{SP}} = 4.5 \left(\frac{\lambda_{mfp}}{L} \right)^{1/2} \left(\frac{m_i}{m_{iH}} \right)^{1/4}, \quad (28)$$

where m_i and m_{iH} are mass of the plasma ions and protons with $T_e \sim T_i$, $\eta_{\perp} = 2\eta_{\parallel}$, and $V_A \sim v_{thi}$ ($\beta \sim 1$) assumed. The above MRX scaling suggests that the reconnection rate would increase when this ratio exceeds about 2, which is where the length of reconnection layer becomes comparable to five to ten times the electrons mean free path. This criterion has been repeatedly seen in antiparallel reconnection in the MRX. This verifies that the enhanced resistivity observed in the MRX is primarily facilitated by the Hall effect. In the low collisionality regime, where $\delta/\lambda_{mfp} < 1$ (note that the axis representing collisionality is flipped from Fig. 26), the Hall field accounts for almost all of the reconnection field except just around the X point. This scaling study of reconnection rate should be extended to the case of guide field reconnection (Yamada, 2007).

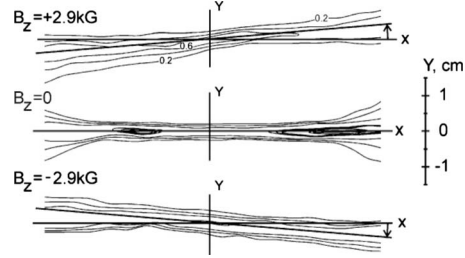


FIG. 41. Density contours of the TS-3D neutral sheet for Kr plasma with different guide fields $B_g = 2.9, 0, -2.9$ kG. Fill gas pressure p is about 20 mTorr. From Frank *et al.*, 2006.

It should be noted that fluctuations can still be responsible for fast reconnection since the electromagnetic fluctuations appear when Hall effects become dominant. They can even be coupled to each other. The anomalous resistivity, if large enough, can dominate the Hall term and change the two-fluid physics. While the magnitude of this laminar Hall effect becomes nearly zero at the X point, anomalous resistivity caused by turbulence is expected to support the reconnection electric field around the X line and separatrices. Bursty lower hybrid wave turbulence is observed in the center of the reconnection region of the MRX (Ji *et al.*, 2004; Ren *et al.*, 2008). In a reconnection experiment in the EMHD regime (Stenzel *et al.*, 1982), ion acoustic waves were observed in the hot electron plasma ($T_e \gg T_i$) and were attributed to the observed anomalous resistivity (see Sec. VII).

5. Effects of guide field

A 3D PIC simulation study carried out by Pritchett and Coroniti (2004) in an open geometry investigated the effects of a guide field on collisionless magnetic reconnection. The quadrupole B_y pattern is replaced by an enhancement of the guide field component between the separatrices due to a paramagnetic effect. The enhanced parallel electric field and electron velocity are confined in one pair of separatrices, while the electron current-density peaks on the other pair. This may explain two early observations made by Yagi and Kawashima (1985) and Frank *et al.* (2005, 2006) (shown in Fig. 41) that, with the presence of a sizable guide field, the current sheet appears to tilt in the reconnection plane. This observation was explained by $\mathbf{j} \times \mathbf{B}$ force working on the outgoing electron flux in the reconnection plane from the center of the neutral sheet. The current sheet broadens and the density decreases with increasing guide field. More discussions of the effects of a guide field are found in Sec. VII.B.2.

In the presence of a strong guide field ($B_y \gg B_x$), the reconnection rate is reduced by factor of 2–3 (Yamada *et al.*, 1990, 1997a; Ji *et al.*, 1998). This is consistent with the results from a 2D particle simulation by Horiuchi and Sato (1997). The agreement between the experimental data in a collisional plasma and the theoretical results in a collisionless regime may hint an answer to the question what basic physics mechanism is responsible for the slower rate in guide reconnection case. The magnetic

pressure of the compressed guide field can be responsible for slowing down the incoming magnetized plasma at the reconnection layer.

6. Observation of two-fluid effects in the magnetotail

In a substorm, an explosive release of magnetic energy is considered to occur due to magnetic reconnection in the magnetotail as described in Sec. III. During the substorm period, magnetic noise bursts at lower hybrid frequencies were observed in the neutral sheet. It was reported that a current sheet structure caused by Hall effects was identified around the near-Earth neutral-sheet line during a substorm based on the data from the GEOTAIL satellite (Asano *et al.*, 2004). A negative potential well, a signature reported by numerical simulations of two-fluid reconnection, was measured. They found a double peaked current sheet away from X line and attributed its cause to Hall current profiles at the separatrices around the neutral sheet.

The detailed characteristics of the neutral sheet in the near-Earth magnetotail was also measured by the CLUSTER spacecraft (Wygant *et al.*, 2005). The measurements of electric fields, magnetic fields, and ion energy are used to study the structure and dynamics of the reconnection region in the tail at the distances of $18R_E$. They investigated the structure of electric and magnetic fields responsible for the acceleration of ions and the formation of the electron current layer during the process of magnetic reconnection in the Earth's geomagnetic tail.

Electric and magnetic field measurements from the thinnest current sheet obtained during 0940–0950 UT time are presented in Fig. 42. The electric field has a bipolar signature coinciding with a flip in the direction of the magnetic field. The electric field reversal occurs at the center of the current sheet suggesting the presence of a strong potential well predicted by numerical simulations. Attention was focused on the measurements of the large amplitude normal component of the electric field observed near the reconnection X line, the structure of the associated potential drops across the current sheet, and the role of the potential structure in the ballistic acceleration of ions across the current sheet. The measured width of the individual current sheet was often very thin in the range of 60–100 km [$(3\text{--}5)c/\omega_{pe}$]. The observed high electric field structure would lead to a large 4–6 kV electric potential well centered in the separatrix region and over 8 kV near the exhaust of the neutral sheet. Measured H^+ velocity space distributions obtained inside the current layers provide evidence that the H^+ ions are accelerated into the potential well along the z axis, producing a pair of counterstreaming double-peaked energetic H^+ beams. These results reveal important signatures of the two-fluid reconnection dynamics: the strong potential well and a very thin (electron) current sheet. This is good evidence that the flows of electrons and ions are quite decoupled. Based on the observations, they proposed the following mechanisms for

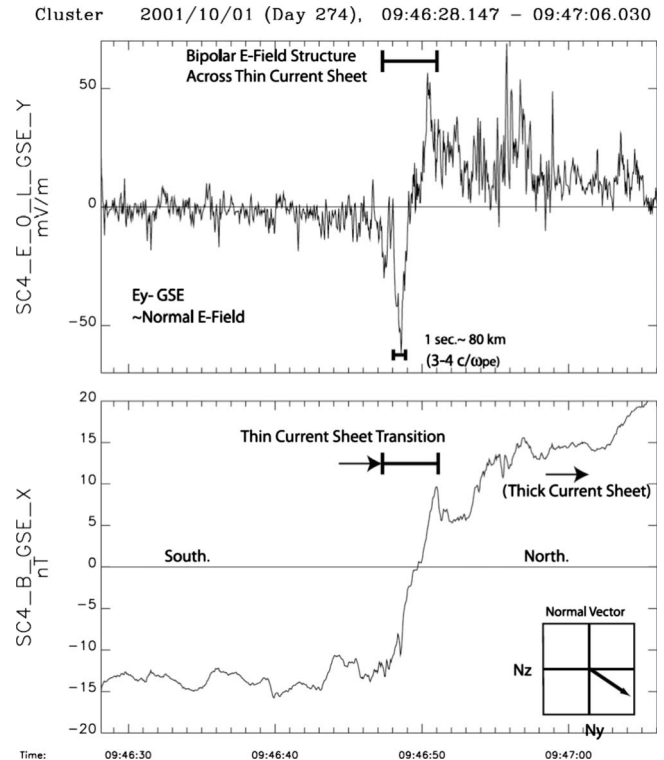


FIG. 42. Electric and magnetic field data from the CLUSTER spacecraft 4 from a “thin” ($\delta \sim 4c/\omega_{pe}$) current sheet on 1 October 2001 at 0946:50 UT. Measurements are (top) E_y GSE dominated by the normal component of the electric field and (bottom) B_x GSE showing current sheet. Distance scale determined from normal velocity, $V_n \sim 80$ km/s. From Wygant *et al.*, 2005.

acceleration of ions in the neutral sheet in the magnetotail.

- (1) Incoming field lines bring magnetized electrons to the X line, compress them, and create a strong negative well near the $z=0$ lines (Fig. 42).
- (2) Nonmagnetized ions are accelerated along the z axis toward the center, overshoot, and bounce back. During this process ions are accelerated toward the exit along the x axis because of the wedge-shaped structure of the potential well. Schematic diagrams based on this proposed scenario are shown in Fig. 43. By these dynamics, generation of the observed counterstreaming ion beams was explained.

Although magnetic measurements by space satellites are not as conclusive as laboratory results, for which multiple reproducible plasma experiments can be carried out, the space satellite diagnostics for the particle energy distribution function compensate for their weakness and contribute importantly to the understanding of collisionless reconnection. Multiple satellite observations also improve the reliability of space data analysis.

VII. KINETIC EFFECTS OF MAGNETIC RECONNECTION

As described, the MHD and two-fluid models have captured some of the most important physics underlying

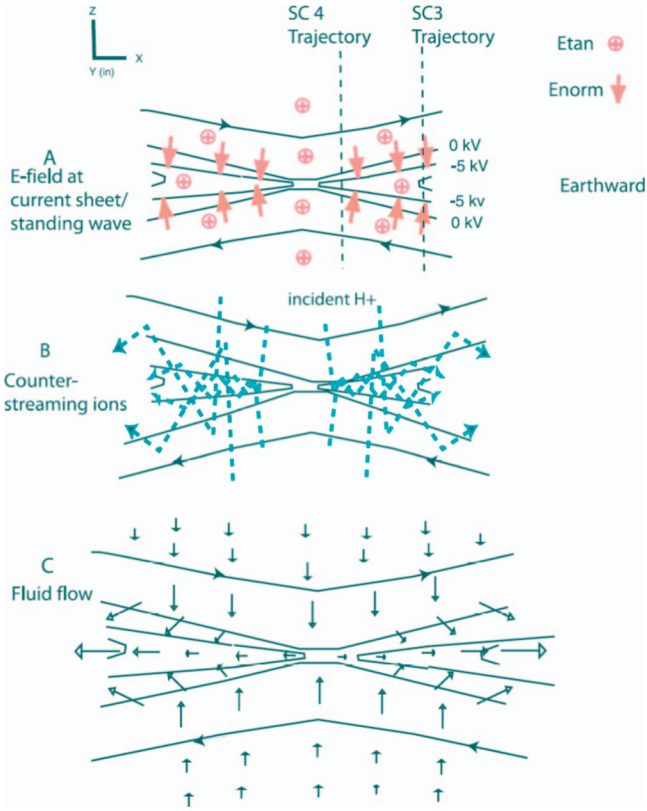


FIG. 43. (Color) Schematic diagrams of ion acceleration mechanism. (a) Presence of strong normal component of the electric field was observed with standing wave or current layer near x line. (b) Trajectory of representative ions ballistically accelerated into 46 kV potential well forming quasitrapped counterstreaming beams. Counterstreaming beams produce effective pressure; deceleration of ion fluid across potential drop; and jet at $1V_A$ along outflow direction. (c) Schematic of ion fluid flow vectors consistent with averaging over single particle trajectories. From [Wygant et al., 2005](#).

the fast reconnection processes. In the direction perpendicular to magnetic field, MHD models effectively describe the dynamics on scales larger than ion skin depth or ion gyroradius. When the current sheet thickness becomes comparable with the ion scales, two-fluid models become necessary to describe the separate dynamics of electrons and ions. Below the ion scales, ion kinetic effects becomes important, although electrons can still be modeled by fluid approximations. Below the electron skin depth or the electron gyroradius, even electrons must be treated kinetically. In the direction parallel to the magnetic field, both ion and electron kinetic effects can be important even on the global MHD scales due to lack of constraints on their movement in that direction. Samples of kinetic effects beyond two-fluid descriptions include accelerations or heating of charged particles, effects due to nongyrotropic pressure, and instabilities due to inhomogeneities in velocity space (microinstabilities). Understanding of kinetic effects is less mature than the physics of two-fluid dynamics.

This section describes the present understanding of kinetic aspects of magnetic reconnection. One-

dimensional kinetic equilibria often serve as a basis for the further analyses. The kinetic effects within the reconnection plane are discussed, focusing on the effects due to electron nongyrotropic pressure in balancing reconnection electric field. Kinetic effects due to instabilities along the reconnecting current are discussed as a possible origin for anomalous resistivity.

A. Kinetic equilibrium

1. Harris solutions and its generalizations

Analytic solutions of time-independent kinetic equilibria in a neutral sheet confined between oppositely directed magnetic fields provide a convenient basis for theoretical analyses and numerical simulations of kinetic effects of magnetic reconnection. Such solutions are difficult to find because the Vlasov-Maxwell system is nonlinear even in the simplest case of a steady state in one dimension. Using the constants of motion, [Harris \(1962\)](#) found an elegant solution using shifted Maxwellian distribution functions with spatially constant drift velocity $V_i = -V_e \equiv V$ and temperature $T_i = T_e \equiv T$,

$$B_z = -B_0 \tanh(x/\delta), \quad (29)$$

$$j_y = (B_0/\mu_0\delta) \operatorname{sech}^2(x/\delta), \quad (30)$$

$$n = n_0 \operatorname{sech}^2(x/\delta), \quad (31)$$

while E_x vanishes. δ is the current sheet thickness given by $\delta = (c/\omega_{pi})\sqrt{T/m_i}/V$. In more general cases ([Yamada et al., 2000](#)) when $V_i \neq -V_e$ and $T_i \neq T_e$, these solutions are unaffected, but E_x becomes

$$E_x = \frac{T_e V_i + T_i V_e}{T_e + T_i} B_0 \tanh\left(\frac{x}{\delta}\right) \quad (32)$$

and δ is given by

$$\delta = \frac{c}{\omega_{pi}} \frac{\sqrt{2(T_e + T_i)/m_i}}{V_i - V_e} = \frac{c}{\omega_{pi}} \frac{\sqrt{2}V_s}{V_{drift}}, \quad (33)$$

where $V_s \equiv \sqrt{(T_e + T_i)/m_i}$ and $V_{drift} \equiv V_i - V_e$ is the relative drift between ions and electrons. The Harris model was generalized ([Mahajan, 1989; Mahajan and Hazeltine, 2000](#)) to include time dependence, cylindrical geometry, and sheared velocity profiles. The solutions must be determined numerically.

To provide analytic models for the magnetospheric tail current sheet, where the Earth's dipole field needs to be superimposed, the Harris solutions have been generalized to two dimensions using shifted Maxwellian distribution functions ([Kan, 1973](#)). Velocity shears are introduced by two-component drift Maxwellians. This model was extended to include an X point or an O point ([Brittnacher and Whipple, 2002; Yoon and Lui, 2005](#)).

When the temperature is anisotropic in the magnetic field ([Cowley, 1978](#)) or the distribution functions are non-Maxwellian ([Schindler and Birn, 2002](#)), different classes of kinetic equilibria can be found numerically. Another class of current sheet equilibria has been devel-

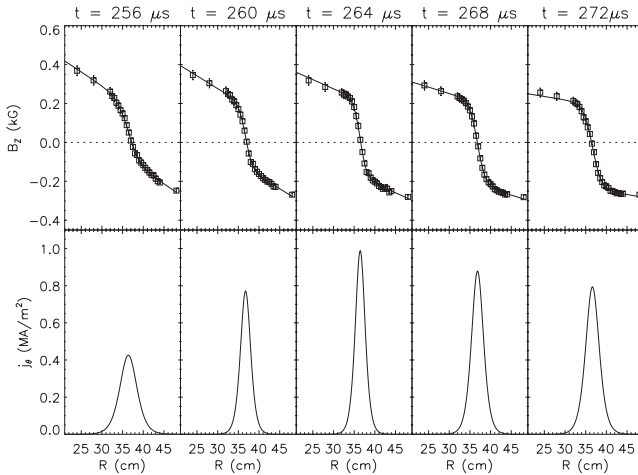


FIG. 44. An example of driven magnetic reconnection in the MRX: time evolution of radial profiles of reconnecting magnetic field (top raw) and current density (bottom raw). From Yamada *et al.*, 2000.

oped to take into account boundary conditions, the so-called forced current sheet (Kropotkin and Domrin, 1996; Sitnov *et al.*, 2000). Semianalytic and numerical solutions have been found (Sitnov *et al.*, 2003, 2006) using anisotropic and nongyrotropic variations for applications to the bifurcated current sheets observed in magnetospheric tails.

2. Experimental observations of the Harris sheet

The hyperbolic tangent shape of reconnecting magnetic field was observed in the MRX neutral sheets. Figure 44 shows a measurement and its fit to

$$B_Z(R) = -B_0 \tanh[(R - R_0)/\delta] + b_1 R + b_2. \quad (34)$$

The factors b_1 and b_2 are determined by the background quadrupole and equilibrium fields. The latter is an applied field necessary to keep the plasma in a desirable position. The cylindrical factor b_1 does not appear in j_θ because it is canceled exactly by $\partial B_R / \partial Z$ of the background quadrupole field. It was found that the static force balance, $\mathbf{j} \times \mathbf{B} = j_y B_z = \nabla p$, is maintained between the incoming magnetic field and the plasma pressure during the quasi-steady-state phase of reconnection since the inflow speed is much slower than Alfvén speed. The measured magnetic field profiles agree well with the prediction by a generalized Harris theory for nonequal temperatures and drift speeds of ions and electrons (Yamada *et al.*, 2000).

An important finding in the laboratory neutral sheets is that the measured δ scales with the ion skin depth (Yamada *et al.*, 2000). These results were consistent with earlier data (Ono *et al.*, 1997; Kornack *et al.*, 1998), where δ was measured to be on the order of the ion gyroradius and the ion skin depth. This indicates that two-fluid effects are important in the neutral sheet, as summarized in the last section. This implies that the relative drift is as the same order of the ion sound speed, which can be a consequence of 3D instabilities.

One interesting experimental observation is that the measured reconnecting magnetic field has a shape close to the hyperbolic tangent despite the many simplifications used to derive this functional shape. The local Maxwellian shape of the distribution function is justified by collisions between like particles while uniform temperatures can be justified by rapid heat transport (Yamada *et al.*, 2000). It was shown (Ji *et al.*, 2001) that the field profile is insensitive to the normalized drift velocities of charged particles by investigating a nonlinear equation derived from the force balance $\partial B / \partial x = -V(1 - B^2)/\sqrt{2}$, where x and B are normalized by c/ω_{pi} and $\sqrt{2\mu_0 n_0(T_e + T_i)}$, respectively, and $V \equiv V_d/V_s$. When $T_e + T_i$ is a constant, the magnetic profile is

$$B_z = B_0 \tanh\left(\int_0^x \frac{V}{\sqrt{2}} dx\right). \quad (35)$$

Because V occurs in the integration, the B profile is insensitive to the V variations. As long as V is a reasonably smooth function of x , the magnetic profile will be close to the hyperbolic tangent shape (Ji *et al.*, 2001).

Neutral sheets are observed in magnetospheric plasmas in both the magnetopause and magnetotail sides. As shown in Fig. 37, the reconnecting magnetic field profile measured by the POLAR satellite matches well with the hyperbolic tangent form (Bale *et al.*, 2002; Mozer *et al.*, 2002). In the magnetotail, thin current sheets were observed by IMP spacecraft (Fairfield *et al.*, 1981) that include information on the pitch angle distribution function of protons. Detailed observations were made by two ISEE spacecraft (McComas *et al.*, 1986; Sergeev *et al.*, 1993).

Detailed observations were reported by CLUSTER spacecraft which detected for the first time the substructures within the current sheets. A bifurcated state of the current sheets was observed (Runov *et al.*, 2003), sometimes accompanied by flapping motions (Sergeev *et al.*, 2003). These fine structures and fast dynamics can be causes and/or consequences of magnetic reconnection activity in the magnetospheric tail.

B. Kinetic effects within the reconnection plane

In this section, we focus on two-dimensional effects within the reconnection plane, first where there is no substantial guide field, followed by the case where there is a substantial guide field.

1. Kinetic effects without guide field

We discuss the leading 2D kinetic mechanism supporting the reconnecting electric field. Vasyliunas (1975) first pointed out the importance of anisotropic pressure in balancing the reconnecting electric field near the X line. Dungey (1989) and Sonnerup (1988) followed up with the so-called gyroviscosity or off-diagonal elements of the electron pressure tensor. Lyons and Pridmore-Brown (1990) provided a detailed analysis showing that the nongyrotropic pressure element can support the re-

connecting electric field near the X line. It was modeled in hybrid simulations of collisionless ion tearing (Hesse and Winske, 1993). The first direct numerical evidence of its importance was found (Cai *et al.*, 1994) for *ions* (rather than electrons) in self-consistent calculations using a hybrid code that treats ions kinetically in a fluid electron background.

In fully kinetic models where both ions and electrons are treated as particles, the first clear identification of the force due to electron nongyrotropic pressure in balancing reconnecting electric field was found by Cai and Lee (1997). The simulations were made in a small 2D box with dimensions of only eight electron gyroradii, with a small number of grid points in space, and a small number of particles, but with a realistic mass ratio. The size of $\nabla \cdot \mathbf{P}_e/en$ was shown to be comparable to the reconnecting electric field. Electron inertial effects were large due to the transient nature of the simulated reconnection.

The importance of electron nongyrotropic pressure was unambiguously shown in fully kinetic 2D simulations for both ions and electrons (Hesse *et al.*, 1999; Kuznetsova *et al.*, 2001; Pritchett, 2001). Since these simulations were performed with larger boxes with more spatial grids with large mass ratios, a quasi-steady-state for magnetic reconnection was reached. It was found that the reconnecting electric field is balanced by forces due to electron nongyrotropic pressure, and electron inertial effects were unimportant near the X line. The predicted half thickness of such layers is one to two times the electron skin depth. This 2D mechanism has been observed to survive in 3D particle simulations at limited mass ratios or spatial dimensions in the third direction.

The nongyrotropic pressure is closely related to particle meandering motion near the center line. This was pioneered by Biskamp and Schindler (1971) and later investigated numerically by Horiuchi and Sato (1994). When charged particles reach the neutral line, their gyromotion reverses direction and they drift in the out-of-plane direction. The breakdown of gyrotropic symmetry in the inflow direction can explain one part of the force due to nongyrotropic pressure in the generalized Ohm's law. The nongyrotropic pressure is also related to the Speiser orbits (Speiser, 1965) which describe ejection of charged particles from the current sheet due to transverse field in the reconnection plane.

Direct observations of electron nongyrotropic pressure during reconnection in space plasmas are challenging. There has been only one documented attempt (Scudder *et al.*, 2002) and the results are not very clear as to whether these off-diagonal terms are important in the vicinity of the X line. In reconnecting laboratory plasmas, direct measurements of these terms are equally challenging owing to the difficulties in resolving both pitch angles in velocity space and small electron layers in physical space. The effects due to electron nongyrotropic pressure have been indirectly evaluated. Using a transport model for the off-diagonal terms (Kuznetsova *et al.*, 2000), a simple but fairly accurate expression has

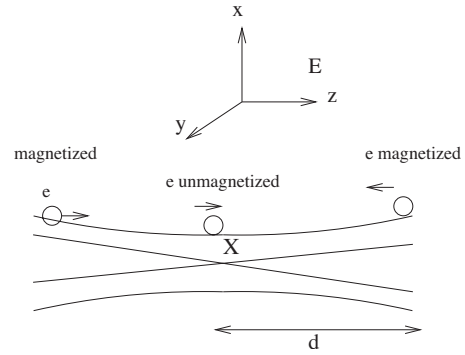


FIG. 45. Illustration of electron acceleration in the diffusion region. Adapted from Kulsrud *et al.*, 2005.

been obtained (Hesse *et al.*, 1999) in terms of electric field,

$$E_{NG} = \frac{m_e}{2e} V_{th,e} \left(\frac{\partial V_x}{\partial x} - \frac{\partial V_z}{\partial z} \right) = \frac{m_e}{e} V_{th,e} \frac{\partial V_z}{\partial z}. \quad (36)$$

This expression was also obtained by Dorfman *et al.* (2008). All quantities in Eq. (36) can be directly measured (Ji *et al.*, 2008) in the electron-scale layer of the MRX near the X line. It was found that the force due to electron nongyrotropic pressure was sizable but not enough to explain the observed reconnecting electric field. This is consistent with the fact that the observed half thickness of the electron layer [$(5.5\text{--}7.5)c/\omega_{pe}$] is much thicker than predicted. Interestingly, similar electron layer thicknesses were reported from the CLUSTER observations (Wygant *et al.*, 2005; Phan *et al.*, 2007). Since both residual classical resistivity due to Coulomb collisions and electron inertial effects are small in these plasmas, it has been suggested that some other forces, including ones due to 3D effects (discussed later in this section), must exist.

The role of the pressure tensor can be understood from the following approximate physical picture by Kulsrud *et al.* (2005) (Fig. 45), neglecting any toroidal guide field. At the X point where the magnetic field is zero, an electron at rest would be accelerated along the reconnection electric field E_y in the y direction, and with collisions it would attain the velocity $v_y = -eE_y\tau/m$, before making a collision, where τ is the electron-ion collision time. If collisions are rare or absent, v_y would be very large.

Very few electrons are actually at rest, most of them having a thermal velocity $\approx v_{th}$ along \mathbf{B} . Because the field is very weak near the X point the electrons are effectively unmagnetized. If the extent of this region is $2d$, then during the passage of an electron over this length, it would be freely accelerated along the y direction and in the absence of collisions would gain a velocity $v_y = -eE_y(2d/v_{th})/m$ and at the X point would be half this value. If the mean free path is less than d its velocity (at X) would be the same as the one at rest. If $\lambda > d$ its velocity would be smaller by approximately d/λ . This means that if the current density at X was limited then

E_y could be stronger by the reciprocal factor $\lambda/2d$. In the entire absence of collisions E_y would be finite and the magnetic flux lines would be broken at a finite rate.

Consider the electron velocity distribution at a point $z=d$. At this point there is an off-diagonal contribution P_{yz}^e to the pressure tensor, due to a correlation between the y and z velocities, because electrons with positive v_z have passed through the unmagnetized region and gained a v_y contribution to their guiding center while electrons with negative v_z remain magnetized and their guiding center has zero v_y . A simple estimate shows that $P_{yz}^e = mn\langle v_y v_z \rangle \approx \frac{1}{2}mnV_y v_{th} \approx -neE_y d$. By symmetry P_{yz}^e at $z=-d$ is equal to the negative of this value and thus the gradient of P_{yz}^e at X is the difference of these values divided by $2d$ or $(\nabla \cdot P^e)_y \approx -neE_y$ the value necessary to balance E_y at X . These off-diagonal components are the nongyroscopic parts of the pressure tensor.

For ions, the importance of nongyrotropic pressure has been studied numerically. By comparing hybrid simulations and Hall-MHD simulations, the ion nongyrotropic pressure accelerates momentum transport away from the X line (Yin and Winske, 2003). Fully kinetic simulations with large mass ratios have revealed (Ishizawa and Horiuchi, 2005) that the off-diagonal ion pressure terms cancel the Hall effects outside of ion meandering orbit size, determining ion dissipation region. The same cancellation should happen to the electron layers although less clearly.

2. Kinetic effects with guide field

The imposition of a substantial guide field, compared to the reconnecting field, magnetizes the electrons within the electron diffusion region and reduces the electron nongyrotropic effects. This was first studied by Horiuchi and Sato (1997) using a PIC code with open and driven boundary conditions. A decrease of the electron layer thickness was observed and the reconnection rate was determined by the external drive.

Effects of a guide field were investigated extensively by a series of numerical studies during spontaneous reconnection (Hesse *et al.*, 2002, 2004, 2005; Pritchett and Coroniti, 2004; Pritchett, 2005; Swisdak *et al.*, 2005; Hesse, 2006). With a strength of the guide field on the order of 0.2 of the reconnecting field, electrons begin to be magnetized in their diffusion region (Swisdak *et al.*, 2005). With a stronger guide field, the thickness of the electron layer decreases and scales as the electron gyroradius in the guide field. Within this scale, the electron nongyrotropic pressure remains important in balancing the reconnecting electric field (Hesse *et al.*, 2005). The reconnection rate slows with guide field, consistent with MHD simulations. Tilt of the separatrices was observed due to the guide field and can be attributed to the Hall effect.

In generating electron nongyrotropic pressure, it was found that the electron heat flux plays an important role (Hesse *et al.*, 2004). This heat flux is a result of mixing in the electron layer between incoming electrons, which are less energetic, and outgoing electrons, which have

been accelerated (Hesse, 2006). This picture remains relatively unchanged in 3D simulations (Hesse *et al.*, 2005) despite the observation of waves propagating along the third direction (Pritchett and Coroniti, 2004).

The prediction by 2D numerical simulations that the thickness of the electron diffusion region is the order of electron gyroradius has not been verified in either the space or laboratory in the presence of a strong guide field. In the VTF experiment, reconnection is driven in the presence of a strong guide (toroidal) field in a cusp-like X -point configuration. An electron current channel was detected near the X point and its size was found to scale with the geometric mean of electron gyroradius and cusp field gradient scale (Egedal *et al.*, 2003). Perhaps due to the electrostatic sheath of the nearby conducting boundaries, the current flowing in these layers is very small, and thus the associated magnetic dissipation is expected to be small.

The complicated electron trajectories near the X line have profound effects on the electron distribution function $f(\mathbf{v}_e)$ and the detailed analysis techniques were applied to the measurements by the WIND satellites (Egedal *et al.*, 2005). The analysis was carried out by solving Liouville's equation $df/dt=0$ for electron trajectories in specified magnetic and electrostatic fields. Agreement between the predicted distributions and the measured ones was possible by assuming the reconnection region to be positively charged to about 1 keV [see Figs. 46(a) and 46(b)], electrostatically trapping the thermal electrons in trajectories that bounce numerous times inside the reconnection region [see Fig. 46(c)].

C. Mechanisms for anomalous resistivity

In plasma physics it is generally the case that when the relative motion of ions and electrons exceeds the ion acoustic speed there is a two-stream instability that leads to a strong anomalous resistivity. The relative ion-electron motion in the reconnection layer when the thickness is less than the ion skin depth should increase the reconnection rate through the resistivity enhancement.

This anomalous resistivity should have several important effects that would aid the magnetic reconnection process. It should keep the reconnection layer as thick as the ion skin depth. A much thinner layer would increase the resistivity by a large amount and the increased magnetic diffusion would force the layer thickness back to the ion skin depth. Since the layer is thicker than the Sweet-Parker thickness, it would allow a faster outflow of the plasma. The increased resistivity should heat the incoming plasma to a point where its pressure balances the outside magnetic pressure. Most of other collisionless plasma and two-fluid effects such as the Hall effect do not lead to plasma heating.

The increased resistivity would increase the rate of breaking of field lines at the X point. Field-line breaking is accomplished by the nongyrotropic component of the electron pressure tensor as described in the last section,

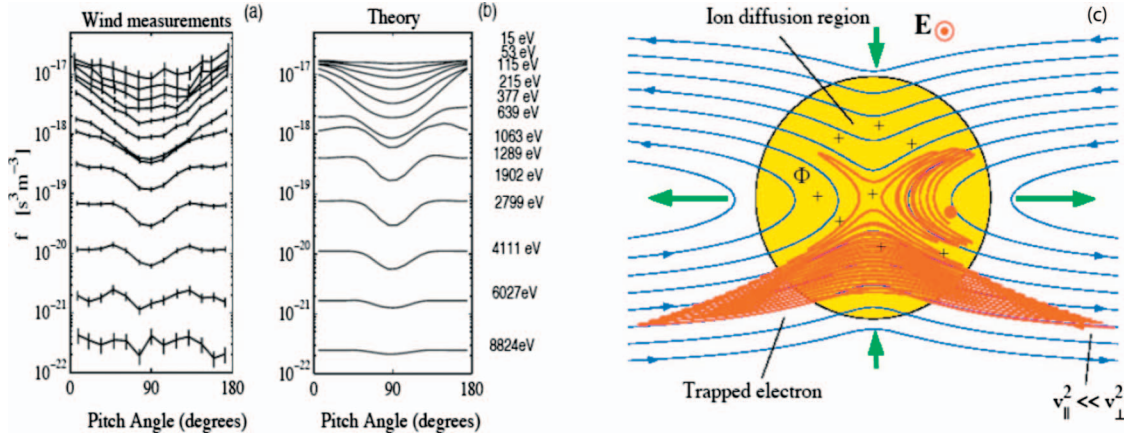


FIG. 46. (Color) Electron energy distributions measured in space. (a) Electron pitch angle distributions measured by the 3D plasma and energetic particle instrument on the WIND spacecraft. (b) Theoretical distribution approximating the distribution measured by WIND. (c) Trapped electron trajectory inside the reconnection region. From Egedal *et al.*, 2005.

although this effect could be modified by the presence of anomalous resistivity at X .

Anomalous resistivity allows the electrons to flow across the field lines, weakens the argument for quadrupolar magnetic fields, and interferes with other two-fluid collisional effects. It is sometimes observed that when magnetic fluctuations occur in magnetic reconnection experiments, indicating the presence of instabilities, the quadrupolar magnetic fields are absent. When two-fluid effects are seen, the fluctuations are sometimes absent or weak. In the latter case fluctuations may be too weak to produce much anomalous resistivity.

Although there is strong evidence for the existence of anomalous resistivity in reconnection, so far no convincing instability has been found that can explain it. A large number of suggestions have been made for instabilities in reconnection, but none seems to be a convincing source for anomalous resistivity. In the case without a guide field, the plasma beta in the reconnection layer is generally very large compared to unity in regions away from the current layer boundary. This means that in the body of the current layer any instability must be electromagnetic. This rules out the simpler electrostatic instabilities. Applying theories of local instabilities does not generally work since they are often convective and propagate out of the instability region of the layer before they can grow. This occurs because the current layers are found to be even thinner than the ion skin depth by a factor of as much as 3, and the instability regions are a good deal thinner.

Most research on plasma instabilities has been devoted to instabilities in collisionless shocks, and other discontinuous regions, rather than those in reconnection layers. A survey of the literature on such instabilities finds that many are not appropriate for reconnection. In reconnection layers one finds that the relative ion-electron drift velocity is a good deal larger than the ion acoustic speed, so the appropriate instabilities have not been examined in the correct parameter regime.

Historically the most widely quoted instability is that of Krall and Liewer (1971). Although this is a purely

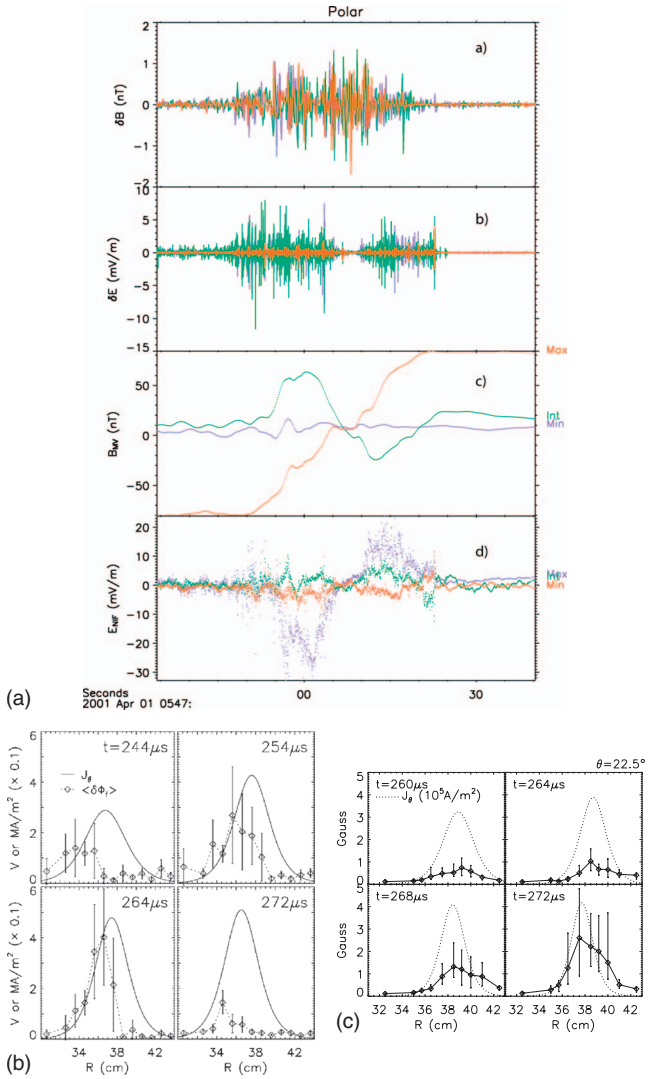


FIG. 47. (Color) Electrostatic and electromagnetic fluctuations from POLAR satellite at magnetopause (top panels adapted from Bale *et al.*, 2002) and reconnecting current sheets in the MRX (bottom panels from Carter, Yamada, *et al.*, 2002 and Ji *et al.*, 2004).

electrostatic instability, it is important as the first instability that brings out qualities that an instability driving anomalous resistivity should have. It has been detected in the MRX in the lower beta outer boundaries of the reconnection layer (Carter, Ji, et al., 2002). The original treatment of the instability is fully kinetic and because its wavelength is of the order of the electron gyroradius the treatment is complicated. For a wavelength slightly larger than the electron gyroradius, it can be correctly treated by a simple fluid theory (Krall and Liewer, 1971).

Guided by the difficulties found in earlier theories, Wang et al. (2008) discovered a local instability that has the desirable property of a very small group velocity across the layer. It does not propagate out of the instability region before growing enough to generate appreciable anomalous resistivity. The instability turns out to be a normal mode, but the quasimode treatment brings out the physics more clearly and is much easier both linearly and nonlinearly. The instability itself is not a strong generator of resistivity but it can nonlinearly drive a magnetohydrodynamic mode. These nonlinear coupled modes can lead to a solution to the anomalous resistivity problem. These modes have properties consistent with the experimentally observed fluctuation in the MRX and with the numerical simulations (Daughton, 2003).

A similar instability called modified two-stream instability was reported [see, e.g., McBride et al. (1972); Lemons and Gary (1977)]. This instability is driven by a local ion current unrelated to the diamagnetic drift, a situation that can occur in collisionless shocks, but does not generally apply to the reconnection current sheets. Full electromagnetic effects were taken into account in the treatments by Silveira et al. (2002) and Yoon and Lui (2004), and a self-consistent pressure gradient was incorporated by Ji et al. (2005). This instability also suffers from a large group velocity of the order of the Alfvén speed in the \hat{x} direction, which limits its growth and thus its importance in the reconnecting current sheets (Wang et al., 2008).

Global eigenmode analyses in a Harris sheet (Harris, 1962) of the current driven instabilities (Daughton, 1999, 2003; Yoon et al., 2002) have been carried out to take into account the effects of boundary conditions of a Harris current sheet. This followed similar work on the same subject (Huba et al., 1980). It was found that for short wavelengths ($k\lambda_e \sim 1$, $\lambda_e \equiv c/\omega_{pe}$), the unstable modes concentrate at the low- β edge and are predominantly electrostatic lower hybrid drift instability (LHDI). For relatively longer wavelengths ($k\sqrt{\lambda_e \lambda_i} \sim 1$), unstable modes with significant electromagnetic components, which may be explained by an electromagnetic LHDI (Wang et al., 2008), develop in the center region. For even longer wavelengths ($k\lambda_i \sim 1$), a drift kink instability (Daughton, 1999) exists but has a slower growth rate at realistic ion-electron mass ratios.

Particle simulations under various limited conditions have been carried out in three dimensions to study the stability of a Harris current sheet (Horiuchi and Sato, 1999; Lapenta and Brackbill, 2002; Daughton, 2003; Scholer et al., 2003; Daughton et al., 2004; Ricci et al.,

2004, 2005; Silin et al., 2005; Moritaka et al., 2007). It was found that at first the electrostatic LHDI-like instabilities at $k\lambda_e \sim 1$ are active only at the low- β edge. These edge instabilities grow to large amplitudes to heat electrons anisotropically, thin the current sheet, and induce ion flow shear. These modifications to the background state lead to secondary electromagnetic instabilities localized at the center of the current sheet. These instabilities are identified as drift kink instabilities (Horiuchi and Sato, 1999; Moritaka et al., 2007), Kelvin-Helmholtz instabilities (Lapenta and Brackbill, 2002), or collisionless tearing modes (Daughton et al., 2004; Ricci et al., 2004). Combinations of these instabilities are considered to cause substantial increases in the reconnection rate.

High-frequency electrostatic and electromagnetic fluctuations have been detected in the reconnecting current sheets in both space (Shinohara et al., 1998; Bale et al., 2002) and the laboratory (Carter, Ji, et al., 2002; Carter, Yamada, et al., 2002; Ji et al., 2004). In agreement with the numerical predictions, it was found that electrostatic fluctuations peak at the low beta edge of the current sheet, while the electromagnetic fluctuations peak at the center of current sheet, as shown in Fig. 47.

The measured frequency spectra show that most fluctuations are in the lower hybrid frequency range, but it was found that the electrostatic fluctuations did not correlate with the observed enhanced resistivity or the fast reconnection rate (Carter, Ji, et al., 2002). With the use of the hodogram probe (Ji et al., 2004), the observed electromagnetic waves were found in the lower hybrid frequency range and appeared in an impulsive manner in all three magnetic components when the current sheet forms. They persisted as long as the reconnection proceeds. The dispersion relation of the waves was measured from the phase shift between two spatial points. The fluctuations have large amplitudes and appear consistently near the current sheet center with peak $\delta B/B_0 \sim 5\%$, where B_0 is the upstream reconnecting magnetic field. A correlation has been found between the wave amplitudes and the fast reconnection rates in the low-density regime. A question remains as to how these electromagnetic waves compare to the waves seen in numerical simulations. To find the causes of the observed enhanced dissipation at the center of the current sheets, another step is needed to clarify the interrelationships between laminar Hall dynamics and magnetic fluctuations at the sheet. There is no clear consensus with regard to how the observed waves are excited and how they affect the reconnection rate or dissipation.

In a reconnection experiment in the EMHD regime (Stenzel and Gekelman, 1981), where the electrons were magnetized and the ions were not magnetized, their gyro-orbit exceeded the size of the plasma. Ion acoustic waves were observed in their hot electron plasma ($T_e \gg T_i$) and the observed anomalous resistivity was attributed to them (Gekelman et al., 1982).

Imposing a strong guide field can qualitatively alter the kinetic stability properties of a reconnecting current sheet. Due to strong ion Landau damping, electrons need to drift by their thermal speed relative to ions for a

Buneman-like instability to take place. [Drake et al. \(2003\)](#) performed 3D particle simulations of magnetic reconnection with a guide field and found that such instabilities can lead to the development of electron holes, where the electron density is substantially depleted in a highly nonlinear state. Such electron holes can be a source of anomalous resistivity. Similar waves were observed in other 3D particle simulations with a strong guide field ([Pritchett and Coroniti, 2004](#)), but electron holes were not specifically identified. In space, electron holes have been observed by the CLUSTER satellite ([Cattell et al., 2005](#)), and they propagate rapidly along the current direction in a reconnecting magnetotail current sheet, especially near the separatrix. Lower hybrid drift waves, although not predicted in the simulations, were observed. In the VTF, electrostatic structures, similar to electron holes, have been measured near the X line where a strong guide field was present during driven reconnection ([Fox et al., 2008](#)).

VIII. MAGNETIC SELF-ORGANIZATION AND RECONNECTION

In the previous sections, the physics of magnetic reconnection in the vicinity of the neutral sheet or the diffusion regions has been discussed in detail. Plasma dynamics in these narrow diffusion regions are extremely important in determining the rate at which magnetic fields reconnect and magnetic energy is released. In most cases, however, the cause of magnetic reconnection does not originate in these spatially localized regions. Rather, magnetic reconnection takes place because there is a need for magnetic field to release its excessive energy stored on global scales. When an external force is applied to the plasma, the magnetic configuration gradually changes to a new equilibrium while plasma parameters slowly adjust. When this new state becomes unstable, the plasma reorganizes itself rapidly to a new MHD equilibrium state, through forming current sheets, driving magnetic reconnection, and changing magnetic topology. The excess magnetic energy is converted to plasma kinetic energy, and the plasma magnetically relaxes or self-organizes to a lower magnetic energy state. This global view of magnetic reconnection phenomena, including its causes, dynamics, and consequences, applies to almost all cases covered by this review, i.e., laboratory fusion plasmas, magnetospheric plasmas, solar plasmas, and some of the more distant astrophysical plasmas. In this section, the global aspects of magnetic reconnection are discussed focusing primarily on results from the laboratory fusion plasmas in which the global conditions are well defined and the global and local plasma parameters are quantitatively monitored.

The underlying global instability for magnetic reconnection is determined by magnetic structures and boundary conditions. Magnetic fields in toroidal plasmas consist of those produced by both external and internal currents. The magnetic energy of the internal origin is free energy and is released when the plasma is unstable.

In tokamak plasmas, the internal magnetic field is typically much smaller than the external one, while in the RFP and spheromak plasmas they are comparable. Magnetic reconnection due to these instabilities can cause only relatively small change in the magnetic field profile (or a localized change in the radial q profile) of tokamaks, while it can reorganize the whole magnetic structure of the RFP and spheromak plasmas. A significant effort has been devoted to studies of sawtooth relaxation of these current carrying plasmas. In the following sections, the relaxation phenomena in tokamaks (Sec. [VIII.A](#)), RFP, and spheromak plasmas (Sec. [VIII.B](#)) are examined. The common paradigm is “as magnetic energy is stored in a magnetic equilibrium configuration via slow adjustment of an external parameter, plasma often reorganizes itself suddenly to a new MHD equilibrium state, which forms current sheets and drives magnetic reconnection.” The effects of global boundaries on local reconnection are discussed in Sec. [VIII.C](#) and applications to astrophysical plasmas are discussed in Sec. [VIII.D](#).

A. Sawtooth reconnection in tokamaks

As discussed in Sec. [III](#), a sawtooth relaxation oscillation in a tokamak is characterized by a periodic peaking and sudden flattening of the electron temperature (T_e) profile. It presents a typical example of global magnetic reconnection in a laboratory plasma ([Kadomtsev, 1975](#); [Wesson, 1987](#)). Recent progress in analyzing this magnetic self-organization phenomena caused by magnetic reconnection in the internal flux surface of tokamak discharges in which the safety factor q is near unity is presented.

1. Electron temperature evolution

An axisymmetric tokamak plasma consists of nested flux surfaces on each of which T_e can be assumed constant because of high parallel heat conductivity of electrons. Electron cyclotron emission (ECE) diagnostic systems were developed to measure the T_e profile as a function of radial position. Since the predominant toroidal field varies as $B_t \propto 1/R$ with plasma major radius R , this diagnostic provides the features of flux surfaces or electron temperature contours using an equilibrium code. The 2D electron temperature profile on a poloidal plane of the plasma has been measured with a rigid body rotation model for a circular cross-section tokamak. The sawtooth crash phase which takes 100–500 μs has been studied extensively with this technique as shown in Fig. 48 ([Edwards et al., 1986](#); [Nagayama et al., 1991](#); [Yamada et al., 1992](#)). By color coding the change of the electron temperature (transfer of heat), a fast electron heat transfer was documented. Just before the crash, a shrinking circular hot peak shows up and a crescent-shaped flat island grows inside the $q=1$ region with a kink structure of $m/n=1/1$ (Sec. [II.C](#)). During the crash phase, a fast heat transfer from inside to outside the $q=1$ surface was observed and was attributed to magnetic reconnection.

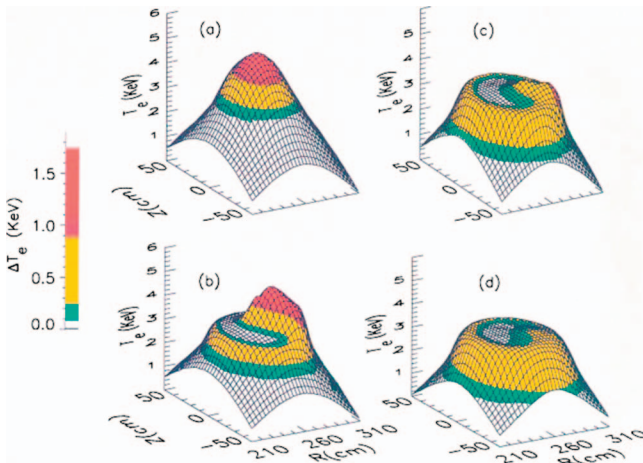


FIG. 48. (Color) Two-dimensional profile of T_e over the minor cross section of the TFTR tokamak plasma at four times during a sawtooth crash phase. The time interval between each profile is 120 μs . From Yamada *et al.*, 1994.

The T_e profile inside the $q=1$ radius becomes flat after the crash, consistent with the Kadomtsev prediction (Kadomtsev, 1975).

2. q profile evolution

The motional Stark effect diagnostic was employed to measure the magnetic pitch angle profile and hence the q profile [$q(R)$ is the local safety factor] based on an equilibrium for a circular tokamak. This diagnostic system is based on polarimetry measurements of the Doppler shifted D_α emission from a neutral deuterium-beam injection heating line (Levinton *et al.*, 1993). This technique is noninvasive and nonperturbative. The field-line pitch is localized to the geometric intersection of the field of view with the neutral beam lines leading to good spatial resolution of $\delta r = 3-5$ cm. If the plasma has good axisymmetric flux surfaces, the measured field-line pitch profile can be translated into a radial profile of the field-line pitch, namely, the reverse rotational transform or $q(R)$, making use of tokamak equilibrium calculations (Yamada *et al.*, 1994). The measured central q values shown in Fig. 49 indicate that central q values increase

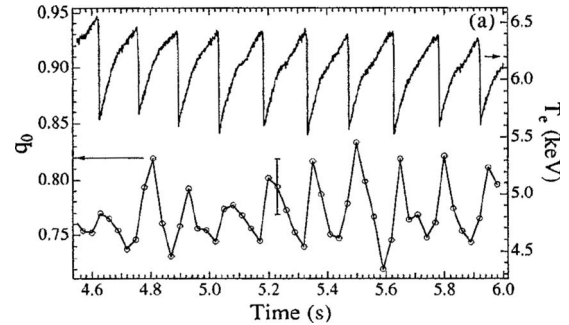


FIG. 49. Time evolution of peak electron temperature and central q value associated with sawtooth crash. From Yamada *et al.*, 1994.

by 5–10 %, typically from 0.7 to 0.75, during the sawtooth crash phase but do not relax to unity even while the pressure gradient disappears inside the $q=1$ region. In this case, as well as most tokamak sawtooth discharges, q_0 stays below unity throughout the sawtooth cycle, contrary to Kadomtsev's model. The increase of q_0 is more than the statistical error of the measurement. Because only field-line breaking and rearrangement can make a $q(R)$ change on such a short time scale, this verifies a magnetic field-line reconnection.

3. Physical processes during sawtooth reconnection

The observations raise an important question as to why the magnetic field lines inside the $q=1$ region do not form a flat $q \sim 1$ inner region after the crash as suggested by Kadomtsev (1975), while the temperature gradient diminishes to zero as predicted by his full reconnection theory. Simultaneous measurements of $T_e(r, \theta)$ and $q(R)$ profile evolutions (Levinton *et al.*, 1993; Yamada *et al.*, 1994) were made in TFTR tokamak. Based on these results, a heuristic model was proposed for the sawtooth crash. The plasma is viewed as two concentric toroidal plasmas separated by the $q=1$ flux surface. A kink mode develops due to a strong peaking of toroidal current and displaces the pressure contours on an ideal MHD time scale with a helical ($m=1, n=1$ poloidal and toroidal mode numbers) structure, inducing a forced re-

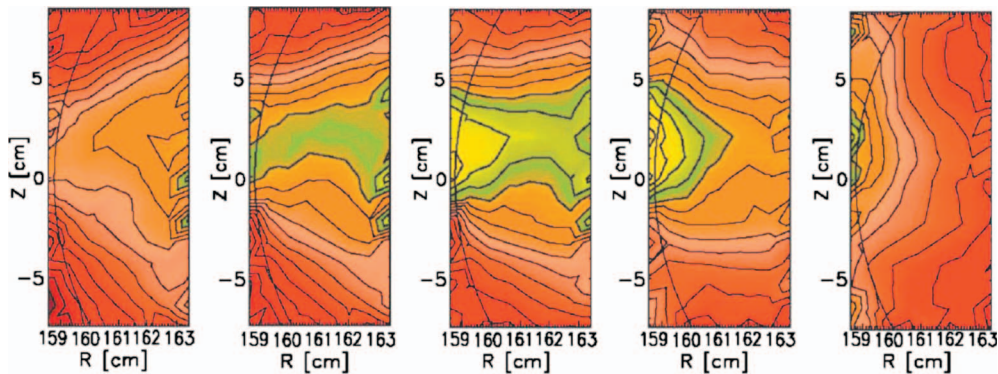


FIG. 50. (Color) Time evolution of hot region (yellow) during 50 μs in the sawtooth crash in TEXTOR. Circle lines show inner $q=1$ surface (high field side). From Park, Luhmann, *et al.*, 2006.

connection at the $q=1$ surface in both toroidal and poloidal directions. If ballooning modes, which can become unstable with high mode numbers, trigger reconnection, it could occur preferentially in the outer part of the displaced surface. This nonaxisymmetric deformation of toroidal plasma destroys the nested flux surfaces of different electron temperatures inside the $q=1$ flux surface making the T_e profile uniform inside $q=1$. Simultaneously, a rapid reflux of thermal energy occurs through the reconnection region along newly connected field lines which connect the inside and the outside of the $q=1$ surface (Lichtenberg, 1984). The precipitous drop of the pressure gradient, which occurs within a short period of $100-200 \mu\text{s} \ll \tau_{\text{Sweet-Parker}}$, removes the free energy to drive the kink instability inhibiting the full reconnection process proposed by Kadomtsev.

Similar changes of central q values were measured in the sawtooth plasmas of circular cross-section tokamaks (Soltwisch, 1988; Levinton *et al.*, 1993; Yamada *et al.*, 1994; Nagayama *et al.*, 1996). Although the final values of the central q after the crash are different, all reported $\Delta q < 0.1$ during sawteeth. Magnetic reconnection in tokamak plasmas is driven by an internal MHD mode (driven reconnection) and is determined by the growth rate of the MHD instabilities. The plasma's stability depends on the plasma parameters [$n_e(R)$, $T_e(R)$, and $T_i(R)$], current profiles (q profiles), and 3D boundary conditions.

Park *et al.* (Park, Donné, *et al.*, 2006; Park, Luhmann, *et al.*, 2006) measured the 2D electron temperature profiles in the TEXTOR tokamak using sophisticated 2D arrays of ECE spectroscopy (Fig. 50). The magnetic reconnection occurs very fast, in $<100 \mu\text{s}$, much shorter than the Sweet-Parker time. This confirmed that reconnection occurs in a localized region in agreement with earlier models (Park *et al.*, 1995). They found the reconnection region to be distributed on both the high and low toroidal field sides of tokamak contrary to the ballooning-based models which predict that reconnection occurs predominantly on the lower field side.

The recent extensive study of sawtooth relaxation in tokamaks has revealed the following:

- (1) Magnetic reconnection is often driven by an ideal kink-type MHD instability excited after a gradual change of tokamak equilibrium and the reconnection time is much faster than the Sweet-Parker time. With the recent understanding of two-fluid physics in the collisionless plasmas, this is not surprising since the Sweet-Parker model is only applicable to collisional plasmas, while tokamak plasmas are collisionless, $\lambda_{\text{mfp}} \gg R$.
- (2) Heat diffusion transport can occur much faster than the magnetic reconnection, namely, on the time scale of parallel electron heat conduction, and influence the evolution of global reconnection phenomena or magnetic self-organization. Kadomtsev-type full reconnection is truncated because the high pressure gradient that drives a kink mode is reduced due

to fast heat conduction through reconnection region.

B. Magnetic reconnection in reversed field pinch and spheromak plasmas

The energy of the internal magnetic field is comparable to that of the external magnetic field in RFP and spheromak plasmas. This internal magnetic energy can be released through magnetic reconnection once the plasma is unstable. Global magnetic structures are reorganized into a state with lower magnetic energy. This is called magnetic relaxation, flux conversion, or dynamo activity (Taylor, 1974, 1986). Magnetic reconnection does not occur arbitrarily in these global relaxation processes; it must satisfy certain global constraints.

Considering the global aspects of local magnetic reconnection, the first question is whether global ideal MHD conservation laws can still hold. Magnetic flux is conserved since magnetic reconnection is only capable of dissipating parts of any given magnetic field line, in contrast to simple magnetic diffusion, which can destroy an entire field line, but at an extremely slow rate.

A well-conserved global quantity is magnetic helicity which is a measure of the “knottedness” and the “twistedness” of a magnetic field (Woltjer, 1958). It is defined by $K = \int \mathbf{A} \cdot \mathbf{B} dV$, where \mathbf{A} is the vector potential of the magnetic field \mathbf{B} and the integration is over a volume V . The magnetic helicity is an invariant within a flux tube in a perfectly conducting plasma. A question is whether magnetic helicity is still conserved in a highly conducting plasma undergoing reconnection.

The essence of the Taylor relaxation theory (Taylor, 1974, 1986) is that the plasma has a tendency to relax toward the minimum (magnetic) energy state while conserving total magnetic flux and helicity. Experimentally, magnetic helicity was observed to change little compared to magnetic energy which decreases substantially during RFP relaxation (Ji *et al.*, 1995; Anderson *et al.*, 2004). A simple estimate of helicity change due to magnetic reconnection is given by Ji (1999). It is argued that the total magnetic helicity is a well conserved quantity with $\delta K \ll K$ during magnetic reconnection if the thickness of diffusion region is much smaller than the global size.

Magnetic reconnection is perhaps the only process (other than self-similar expansions) that can release magnetic free energy while conserving flux and helicity. Thus, magnetic reconnection is strongly implied, although not explicitly specified, in the process of Taylor relaxation.

The predicted relaxed states (Taylor, 1974) are described by the force-free equilibria given by $\nabla \times \mathbf{B} = \mu \mathbf{B}$, where $\mu [= (\mathbf{j} \cdot \mathbf{B})/B^2]$ is a spatial constant along and across field lines. This prediction explains a common feature of both RFP and spheromak plasmas, which after an initial highly turbulent state the plasma settles into a more quiescent state in which μ tends to be spatially uniform (Bodin, 1990; Bellan, 2000).

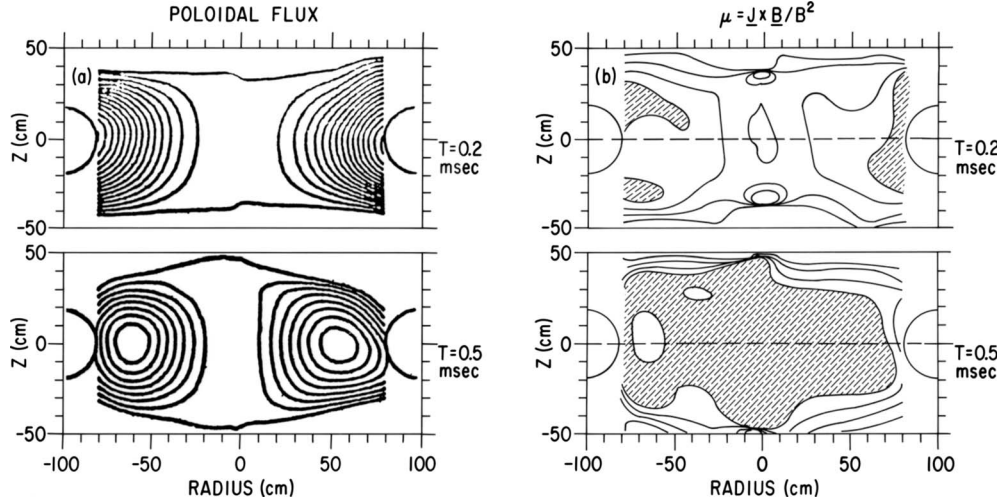


FIG. 51. Contours of poloidal flux (left panels) and μ (right panels) during and after formation of S-1 spheromak, measured by internal probes. Shaded regions refer to the value of $\mu = 5.5 \text{ m}^{-1}$ (Taylor value) within 15% errors. From Hart *et al.*, 1986.

An example is shown in Fig. 51, where a constant- μ Taylor state is experimentally verified (Hart *et al.*, 1986). The turbulent initial state undergoes violent reconnection to form a spheromak configuration, the minimum energy state. After this initial formation process, the relaxation or reconnection activity occurs in a cyclic or continuous fashion. The plasma is driven away from the relaxed state, and the relaxation opposes this tendency. During the drive period, the plasma slowly evolves away from the relaxed state as μ becomes spatially peaked. During the relaxation period through the onset of instabilities, the plasma rapidly returns to a relaxed state as μ becomes flatter. Peaking and flattening of the μ profile over the relaxation cycles have been experimentally verified in both RFP (Ji *et al.*, 1995) and spheromak (Yamada, 1999a) plasmas.

The underlying instabilities for reconnection and relaxation are driven by excess internal current within the plasma. In spheromaks, a kink instability can be destabilized. The instability is no longer localized to the central region but occupies the entire plasma and causes global reorganization (Bellan, 2000). In the RFP plasmas, the underlying instability is a tearing mode instability (Furth *et al.*, 1963) occurring at multiple radii, with each radial location corresponding to rational surfaces, in which the safety factor is m/n . During a relaxation event, impulsive reconnection takes place at a single radial location or at multiple locations simultaneously to reorganize the plasma back to a relatively stable state (Ortolani and Schnack, 1993).

The process of flattening of the μ profile due to these instabilities is a redistribution of the current parallel to the mean magnetic field over the plasma radius. Insights can be gained by examining parallel components of Ohm's law,

$$\langle \mathbf{E} \rangle_{\parallel} + \langle \tilde{\mathbf{V}} \times \tilde{\mathbf{B}} \rangle_{\parallel} = \langle \eta \mathbf{j} \rangle_{\parallel}, \quad (37)$$

where $\langle \cdots \rangle$ is ensemble average over the fluctuations associated with reconnection processes. The fluctuation-

induced electromotive force $\langle \tilde{\mathbf{V}} \times \tilde{\mathbf{B}} \rangle$ is called the α dynamo effect (Ji and Prager, 2002), derived from the same notion in a mean-field theory (Krause and Rädler, 1980) of dynamo action or generation of magnetic field from a turbulent flow. In the MHD frame, a nonzero component of $\langle \tilde{\mathbf{V}} \times \tilde{\mathbf{B}} \rangle$ along the mean field was predicted by a nonlinear computation (Ortolani and Schnack, 1993), experimentally detected by Ji *et al.* (1994) and Fontana *et al.* (2000) in the edge of a RFP plasma, and by al Karkhy *et al.* (1993) in a spheromak.

A question is whether two-fluid effects are still important during magnetic reconnection on global scales. Theoretically, it was found that the tearing mode structures and growth rates can be significantly modified by two-fluid effects (Mirnov *et al.*, 2003, 2004). The Hall effect enters Eq. (37) as a new term on the left-hand side, $-\langle \tilde{\mathbf{j}} \times \tilde{\mathbf{B}} \rangle_{\parallel}/en$. It has been experimentally shown (Fig. 52) for a particular mode ($m=6, n=1$) in the core of MST plasmas (Ding *et al.*, 2004). The amplitude and time dependence of this term is just what is required to explain the flattening of the μ profile near the center of the plasma. Other two-fluid effects, such as the electron diamagnetic effect theoretically predicted (Lee *et al.*, 1989) and experimentally explored (Ji *et al.*, 1995), can play a role in global relaxation. It remains unclear

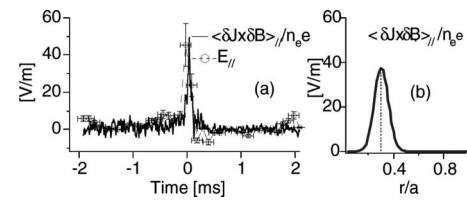


FIG. 52. Observation of Hall effects in RFP. (a) Time evolution of the Hall dynamo due to $(m=6, n=1)$ (solid line) and inductive electric field (dashed line) during a relaxation cycle. (b) Amplitude of Hall dynamo as a function of radius. From Ding *et al.*, 2004.

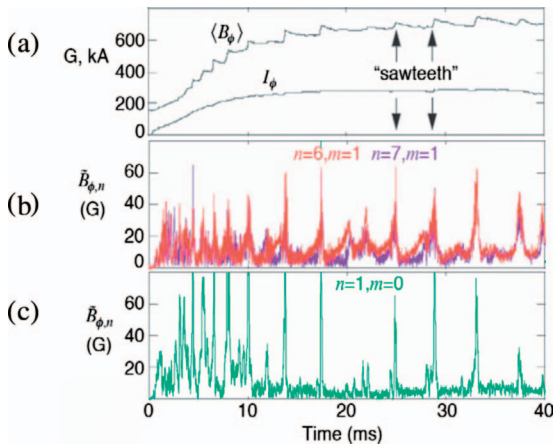


FIG. 53. (Color) Multiple reconnection in RFP. Time dependence of (a) toroidal flux and plasma current, (b) core-resonant magnetic fluctuations, and (c) edge-resonant magnetic fluctuations. From Prager *et al.*, 2005.

whether these two-fluid effects are important in determining global aspects of magnetic reconnection during relaxation.

In the central region where μ is peaked before relaxation, $\langle \tilde{V} \times \tilde{\mathbf{B}} \rangle$ has the opposite sign to that of the parallel current while it has the same sign at the edge region, and the μ profile flattens after a relaxation event. This process can be viewed as a flux conversion of poloidal flux to toroidal flux. Reducing parallel current at center, where the field lines are mostly toroidal, means reducing poloidal flux, and increasing parallel current at the edge, where field lines are mostly poloidal, means increasing toroidal flux. How exactly does magnetic reconnection accomplish this dynamo or flux conversion process in three dimensions? The answers to this crucial question seem to be rather complex and are yet to be fully resolved. In spheromaks, there have been suggestions (Ono *et al.*, 1988) that the kinked part of the plasma can twist itself so much that field lines change their orientation significantly. Through subsequent three-dimensional reconnections, field lines restore their axisymmetric state but with a different ratio of toroidal to poloidal fluxes. In RFP plasmas, magnetic islands growing out of tearing modes at each rational surfaces can flatten the current profile in its vicinity as shown in quasilinear calculations of Strauss (1985) and Bhattacharjee and Hameiri (1986). The flattening of the μ profile in the global scale has yet to be further studied.

Some important clues have been reported from the MST experiment on the nonlinear aspect of tearing mode interactions. During relaxation, there are several unstable $m=1$ tearing modes resonant near the center. When the $m=0$ mode is absent or weak, the resulted relaxation is milder as shown in Fig. 53 (Prager *et al.*, 2005). Around $t=20$ ms, the $m=0$ mode amplitude is small, and the relaxation is much weaker as indicated in the changes in the toroidal flux. The nonlinear interactions cause rapid momentum transport (Hansen *et al.*, 2000), which is related to charge transport (Ding *et al.*,

2007). Accompanying this rapid momentum transport during relaxation events, anomalous ion heating is observed (Den Hartog *et al.*, 2007) as shown in Fig. 29. No significant ion heating is observed without the nonlinear $m=0$ mode. A plausible scenario emerges in which multiple and interacting reconnection processes cause an efficient global relaxation to release magnetic energy under the constraints of flux and helicity conservation. Primary instabilities drive localized reconnections, resulting in transient flows and magnetic fields, which can lead to secondary reconnections. These secondary reconnections accelerate the rate of energy release and other nonlinear processes such as momentum transport and ion heating. A similar physics mechanism was proposed for solar flares to explain their impulsive nature (Kusano *et al.*, 2004). It is interesting to compare the relationship and time sequence between the spatial structures of spontaneous and driven reconnection regions of RFP plasmas with those of solar flare eruptions.

C. Effects of global boundaries on reconnection

1. The formation of a current layer

During magnetic self-organization, magnetic reconnection occurs through current sheets. The major questions are how a large-scale system generates local current structures and are they formed spontaneously or must they be forced to form by changing boundary conditions.

The aspect ratio of the current layers has generally been taken as the global length over some microscopic length such as the ion skin depth or Sweet-Parker layer thickness. For such aspect ratios the reconnection rate is much too small to account for the observations. When a current layer develops, its actual aspect ratio is of considerable importance.

There has been research on the origin and nature of the current layers (Syrovatskii, 1971; Rosenbluth *et al.*, 1973; Waelbroeck, 1989; Becker *et al.*, 2001; Jemella *et al.*, 2004) [see Biskamp (2000, p. 60)]. These studies can only be certain of their length in highly symmetric situations where the global length of the system is the natural length for the current layer. Situations such as that of the solar flare are far from symmetric. For these cases there is no reason to believe that current layers are as long as the global size. Parker (1979) attempted to show that in a fully three-dimensional equilibrium current layers are inevitable and their length is comparable with the local scales of the equilibria, the length over which the ambient field changes by a finite amount. Since the reconnection velocity goes inversely as the square root of the current length, these shorter lengths should lead to faster local reconnection.

Much less magnetic energy is released in each of the reconnections associated with these shorter current lengths. There could be so many of them that the total released energy could be very large. To get a rapid release of a lot of energy, the local reconnections have to interact and proceed almost simultaneously. Lu and

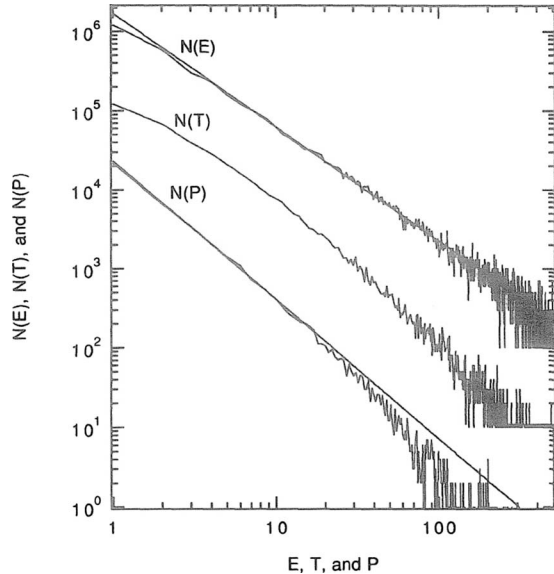


FIG. 54. Frequency distributions of avalanches as a function of energy E , peak flux P , and duration T . From [Lu and Hamilton, 1991](#).

[Hamilton \(1991\)](#) and [Lu \(1995\)](#) suggested such a rapid sequence of releases, as a self-organized effect, such as happens in avalanches or sand piles. Their idea is that first one local reconnection happens and the magnetic energy released triggers reconnection in neighboring current layers. Their released energy triggers more reconnection and so on. This model was inspired by the observation that the distribution function for the number of solar flares as a function of their peak power is a nearly perfect power law over many decades (Fig. 54). Such a power law cannot be produced in any other way.

This bears on two important puzzles: How are current layers formed and with what length? How is reconnection triggered in them? The details of the physics in a reconnection layer are now fairly well understood, and attention is turning to these more global questions.

In Sec. III, Sweet's qualitative picture of how current layers could form by two pairs of sun spots moving together carrying their dipole fields was presented. The dipole fields were pressed together and because of flux freezing a current layer was formed between them.

A similar but more quantitative model was developed by [Hahm and Kulsrud \(1985\)](#). (This model was originally suggested by Taylor in 1981.) Consider a magnetic field in the \hat{z} direction, varying linearly in x , as

$$B_z = (x/a)B_0, \quad (38)$$

and embedded in a plasma contained between two infinitely conducting plane plates at $z = \pm a$ (Fig. 55). If the plates are not planar but are suddenly indented by a small amount δ , so that their equation becomes

$$x = \pm [a - \delta \cos(kz)], \quad (39)$$

the magnetic field between the plates is changed by an equally small amount δB_1 .

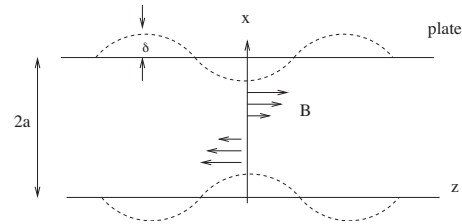


FIG. 55. The geometry of the problem. From [Hahm and Kulsrud, 1985](#).

The resulting steady-state solution is not unique ([Hahm and Kulsrud, 1985](#)). There is one with a surface current

$$4\pi j_z^* = (2B_0k\delta/\sinh ka)\cos kz \quad (40)$$

and no magnetic islands. There is a second one with no surface current but with a reconnected flux

$$\psi_{\text{rec}} = 2B_0\delta/\cosh ka \quad (41)$$

across the midplane. The time-dependent solution after the indentation is made first approaches the current layer solution until the layer is thin enough that reconnection occurs and the second solution is approached. The evolution of the reconnected flux is shown in Fig. 56. The time scale is the tearing mode time

$$t_{\text{rec}} = (a^2/\lambda)^{3/5}(a/v_A)^{2/5}. \quad (42)$$

In summary, by external forcing of the boundaries as shown in Fig. 55, a current sheet is formed. This current sheet disappears in a reconnection time. In the time-dependent solution, the current sheet is never singular but evolves to a very narrow high current-density sheet in which resistivity leads to reconnection. The solution evolves between two steady-state solutions.

The bounding sheets, moving to compress the plasma, are similar to Sweet's moving dipole fields. This process may be characteristic of how current sheets form in general three-dimensional nonsymmetric equilibria. This simple model is important because it is possible to present the formation of the current layer and its further reconnection in considerable analytic detail.

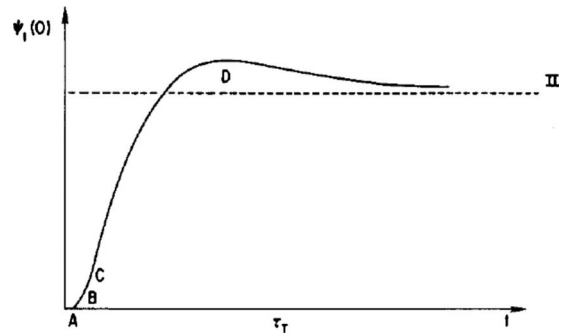


FIG. 56. The time solution of reconnected flux. From [Hahm and Kulsrud, 1985](#).

2. Effects of boundary conditions

Once a current sheet is formed by global instabilities, magnetic reconnection depends on the local dynamics as discussed and the boundary conditions. This area is being developed. In this section, a few cases that show the effect of boundary conditions on the local reconnection process are examined.

The dependence of reconnection rates on the system size, the scaling problem, is important since it involves application of the physics learned from the local dynamics in the vicinity of reconnection region to a large plasma. As discussed in Sec. VI, the thickness of the current sheet is determined by the ion skin depth in the two-fluid regime. A central question is how the current sheet length L is determined since the aspect ratio δ/L determines the reconnection rate in the steady-state Sweet-Parker model. In Sec. V, a wide span of δ/L values (0.1–0.5) were reported from the experiments of the MRX and TS-3 (Ono *et al.*, 1993; Ji *et al.*, 1998, 1999).

A systematic numerical study of the scaling problem was performed by Shay *et al.* (1999) using particle simulations in two dimensions with varying system size. It was shown that L is limited to $\sim 10\delta \sim 10c/\omega_{pi}$ resulting in a universal reconnection rate of ~ 0.1 , determined only by the local physics and insensitive to the system size. These results are consistent with the Hall-MHD simulations using open boundary conditions and various initial conditions (Huba and Rudakov, 2004). Similar results were obtained from two-fluid simulations based on a localized forcing (Sullivan *et al.*, 2005) where dependences on other parameters such as the upstream magnetic field strength were studied. Particle simulations in even larger periodic systems exhibit similar behavior of fast reconnection (Shay *et al.*, 2007).

Several analytic investigations (Wang *et al.*, 2001; Bhattacharjee *et al.*, 2005), based on the forced reconnection setup in Sec. VIII.C.1 (Hahm and Kulsrud, 1985), showed that the current sheet length and its reconnection rate are not universal constants, depending on the system size. These analyses were tested in Hall MHD (Wang *et al.*, 2000) in the presence of a variable guide field. Different scalings were obtained in a similar analysis in Hall MHD without (Fitzpatrick, 2004) and with (Porcelli *et al.*, 2002) electron inertia. Particle simulations using open boundary conditions (Daughton *et al.*, 2006; Fujimoto, 2006) showed that the current sheet extends toward the downstream boundary, resulting in slower reconnection rates.

There have been few studies on boundary condition effects in the laboratory experiments. The large downstream pressure in the MRX was found (Ji *et al.*, 1998) to slow the outflow and the reconnection rate, demonstrating the importance of boundary conditions. It was found that reconnection slows with increasing distance between flux cores or equivalently the system size (Kuritsyn *et al.*, 2007). The reduced reconnection rates in larger systems were attributed to longer current sheets. In addition to this dependence on the system size, the current sheet length L was found in the MRX (Kuritsyn

et al., 2007) to depend on the effective resistivity η^* (defined in Sec. V.B.1). For a given system size, the current sheet length anticorrelates with the effective resistivity: the current sheet length varies inversely with resistivity. The product η^*L tends to be a constant, independent of collisionality. The relation can be understood by a simple argument based on $V_R = \eta^*/\mu_0\delta$ and $V_R L = V_A \delta$. In the conventional Sweet-Parker model, V_R and δ are treated as unknowns while L is the system size. When two-fluid effects dominate, δ is limited by the ion skin depth and L is shortened from the system size. Eliminating V_R from the above relations yields $\eta^*L = \mu_0 V_A \delta^2$, which has been verified in the MRX (Kuritsyn *et al.*, 2007). These results illustrate the importance of interplay between local dissipation and global boundary conditions during magnetic reconnection. This anticorrelation between η^* and L could explain fast reconnection in solar flares if this scaling is confirmed in broader plasma parameter regimes. If one extends the order of magnitude estimate made by Kulsrud (1998) with the use of a reduced L from the system size by a factor of $\eta^*/\eta_{Spitzer}$, one could shorten the reconnection time by another square root of the same ratio, leading to an improved prediction of a few minutes for the flare time.

The back pressure effect was considered in the MHD context by Uzdensky and Kulsrud (2000) for the flow along the 2D separatrix that separates the upstream and downstream equilibria outside of the current layer. A snow-plow shock was found to propagate along the separatrices that only occur at the end of the global length. The separatrix is closed and the shocks from the two ends collide and are reflected back to give rise to back pressure. The delay in reflection turned out to be longer than the time for the field line to pull out of the reconnection layer and join the downstream plasma. Thus as far as the flow in the current layer is concerned, the back pressure from the reflected shocks has little effect.

Boundary effects are important when magnetic field lines are tied to an electrically conducting surface. This is particularly true in the solar corona where most, if not all, magnetic field lines intercept a conducting surface. To fully understand reconnection phenomena on the Sun, the effect of these boundary conditions must be understood. Recent linear analysis of the kink instability has shown that the growth rate is reduced for a sufficiently short distance between line-tied ends (Huang *et al.*, 2006) while the instability threshold may be lowered by a resistively slippery boundary (Ryutov *et al.*, 2006). In laboratory plasmas, the kink instability has been studied (Bergerson *et al.*, 2006; Furno *et al.*, 2007) in a linear geometry with partial line tying at the ends. The line-tied effects on the nonlinear stages of these instabilities during magnetic reconnection have yet to be investigated.

Boundary conditions may affect the reconnection process near 3D magnetic null points. This problem is motivated by the fact that these 3D null points are abundantly found in the solar corona where magnetic

TABLE II. Comparisons of magnetic reconnection in different plasmas.

| System | L (cm) | B (G) | $\delta_i = c/\omega_{pi}$ (cm) | δ_{SP} (cm) | δ_i/δ_{SP} |
|---------------|-------------|-------------|------------------------------------|-----------------------|------------------------|
| MRX | 10 | 100–500 | 1–5 | 0.1–5 | 0.3–10 |
| RFP/Tokamaks | 10/100 | $10^3/10^4$ | 10 | 0.1 | 100 |
| Magnetosphere | 10^9 | 10^{-3} | 10^7 | 10^4 | 1000 |
| Solar flare | 10^9 | 100 | 10^4 | 100 | 100 |
| ISM | 10^{18} | 10^{-6} | 10^7 | 10^9 | 0.01 |

structures are mapped from the measured surface fields (Brown and Priest, 2001). The electric current flowing on separators and separatrices is a source of magnetic reconnection and therefore corona heating (Longcope, 1998; Antiochos *et al.*, 2002). This subject has been largely theoretical and more recently numerical [see, e.g., Pontin (2007) for a recent summary], with limited data from direct observations in space or laboratory. 3D null points were reported in the magnetotail (Xiao *et al.*, 2006, 2007), but they were embedded in a largely 2D current sheet and were not very different from the quasi-2D cases covered here (i.e., two dimensions in large scales but possibly three dimensions locally within the current sheets). In the laboratory, the only experiment on this subject was performed in the electron MHD regime where ions are unmagnetized (Stenzel *et al.*, 2003). Overall, reconnection involving 3D null points is not well understood.

D. Magnetic reconnection in astrophysical plasmas

Astrophysical plasmas can be generally classified into low- β ($\ll 1$) plasmas where the magnetic field is dynamically important and high- β ($\gg 1$) plasmas where the magnetic field is dynamically unimportant in most regions of the plasma. (To be general, β includes the plasma flow energy in addition to the usual thermal energy.) Examples of low- β plasmas include stellar corona, magnetospheres of compact objects, accretion disk corona, and radio jet lobes from active galactic nuclei. High- β plasmas include interiors of stars and compact objects, most accretion disks, supernova remnants, and intergalactic plasmas. For the interstellar media, $\beta \approx 1$.

Magnetic reconnection is thought to be a dominant mechanism of magnetic energy release in low- β plasmas. The signatures of magnetic reconnection include fast plasma flows, heating, and particle acceleration. The analysis of stellar flares (Mullan, 1986) relies on the assumption that they are similar to solar flares but much larger and more energetic. The extreme remoteness of objects from our solar system makes it difficult to analyze the precise mechanisms of observed phenomena despite recent advances in Doppler imaging of microwave, optical, and x-ray signals. Laboratory results in low- β plasmas (Yamada *et al.*, 2006) can be related to magnetic reconnection phenomena in space and astrophysical plasmas. Table II illustrates the relative ratios of the ion

skin depth c/ω_{pi} to the Sweet-Parker width δ_{SP} for various laboratory, space, and astrophysical plasmas. If we apply the results from laboratory to space and astrophysical plasmas as discussed in Sec. VI.C.4, fast reconnection should occur when $c/\omega_{pi} \gg \delta_{SP}$. This inequality is valid in all the cases listed in Table II except the interstellar medium plasmas, suggesting that two-fluid effects may play an important role. Using this criterion for a transition from the MHD regime to the two-fluid regime, a self-regulation of the solar corona heating mechanism was proposed by Uzdensky (2007). Most regions of the interstellar medium are in the MHD regime, but the theory for magnetic reconnection requires a different MHD model than the classic Sweet-Parker model that predicts a long reconnection time.

In high- β plasmas, magnetic fields may not be energetically important in most regions. These plasmas may be good electrical conductors and can generate strong magnetic fields at certain locations. Magnetic reconnection may play an important role in determining the state at which the magnetic energy saturates. Examples include stellar, galactic, and accretion disk dynamos where magnetic reconnection can remove small-scale magnetic structures and irreversibly alter the magnetic topology. Another example is the dynamics of accretion disks where magnetic reconnection may be important (Verbunt, 1982). In this section, three examples of astrophysical phenomena which are strongly tied to magnetic reconnection, interstellar media, accretion disks, and magnetospheres of compact objects, are described.

1. Magnetic reconnection in interstellar medium

Because of the high conductivity of interstellar gas and the large size of its structures, Ohmic diffusion times are extremely long. As suggested in Table II, reconnection in interstellar medium occurs in the MHD region because the Sweet-Parker width is much larger than the ion skin depth and the Sweet-Parker model suggests that magnetic reconnection is extremely slow. Many interstellar problems such as dynamos and star formation appear to require rapid reconnection of magnetic field lines. Reconnection could occur in two stages: thin current layers that have relatively short resistive decay times are first formed by MHD processes; then the fields in the layers reconnect. Zweibel and Brandenburg (1997) reported that ambipolar drift can lead to the for-

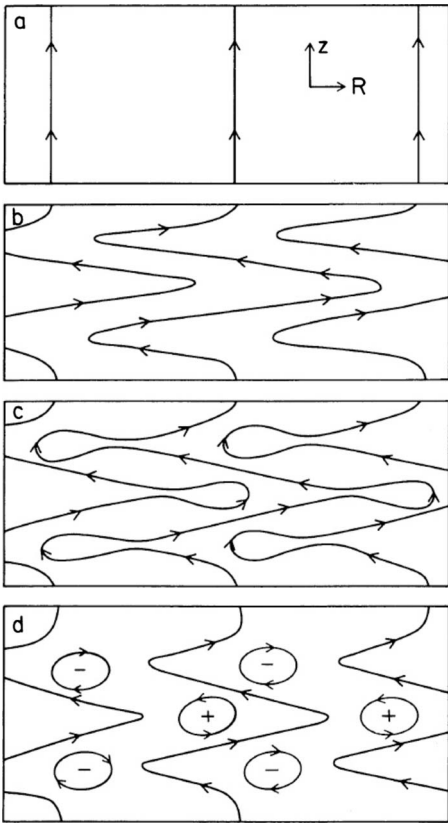


FIG. 57. Schematics of time evolution of MRI in accretion disk with an initial vertical field. Plasmas with excessive angular momentum (+) move out while those with angular momentum deficits (−) move in. Reconnection disconnects these elements from their original fields and thus saturates MRI from its further growth. From Hawley and Balbus, 1992.

mation of thin sheets in weakly ionized interstellar gas, resulting in faster reconnection rates.

2. Magnetic reconnection in accretion disks

Accretion disks are an important class of astrophysical objects where gas, dust, and plasmas rotate around and slowly fall onto a central pointlike object during (i) the formation of stars and planets in protostar systems, (ii) mass transfer and energetic activity in binary stars, and (iii) the release of energy in quasars and active galactic nuclei. The magnetic field plays an important role in generating the turbulence required to explain the rapid angular momentum transport associated with the observed accretion rates. The magnetorotational instability (MRI) can be destabilized when a weak magnetic field is introduced into Keplerian flows of sufficiently conductive plasmas (Balbus and Hawley, 1998). The nonlinear evolution of the MRI leads to radial flows associated with highly bent field lines (Goodman and Xu, 1994) which may subsequently reconnect. The saturation of the MRI and the resulting angular momentum transport crucially depend on the efficiency of magnetic reconnection. An example of an axisymmetric simulation of the MRI is shown in Fig. 57 (Hawley and Balbus, 1992). Figure 57 shows that reconnection inhibits radial flows

transporting angular momentum. This process has been confirmed in 3D simulations by Fleming *et al.* (2000). Magnetic reconnection can saturate the MRI and limit the efficiency of angular momentum transport. This has been demonstrated in simulations with explicit resistivity and viscosity; large resistivity leads to efficient reconnection but inefficient angular momentum transport (Fromang *et al.*, 2007; Lesur and Longaretti, 2007).

Efficient reconnection may take place in protostellar disks where the explicit resistivity is large due to extremely low ionization. In addition, the effective ion mass is increased by collisions with neutral ions. The ion skin depth can be larger than the classic Sweet-Parker width $c/\omega_{pi} \gg \delta_{SP}$ leading to non-MHD conditions where electrons and ions respond differently to the external fields. Hall effects may be important and further accelerate the reconnection process in these environments. Efficient reconnection due to large resistivity and/or two-fluid effects may saturate the MRI at low levels, reducing the effectiveness of the MRI in these disks. It has been pointed out that coronal plasmas above the disk surface may be similar to the solar corona plasma, and the reconnection process can cause field lines to open (Romanova *et al.*, 1998). The reconnection rate determines the local dissipation efficiency and the resulting angular momentum transport (van Ballegooijen, 1994; Uzdensky and Goodman, 2008).

When accretion disks are directly linked to the central stars by an initial dipolelike magnetic field, field lines are twisted on the rotational time scale. The resulting toroidal field pressure pushes field lines away from the star forming a singular current sheet extending at an angle on the order of 60° from the axis. The evolution of field topology depends critically on the reconnection efficiency. With no reconnection allowed, field lines stay open indefinitely (Lovelace *et al.*, 1995). With reconnection, field lines close back, forming a new current sheet. The reconnection efficiency determines the period and amplitude of these oscillations (van Ballegooijen, 1994; Uzdensky *et al.*, 2002).

Accretion disk plasmas vary significantly from disk to disk, from interior to corona, and even for the same disk. In some instances the plasma is hot and often relativistic, and thus is collisionless around galactic centers and black holes or neutron stars. In other cases, the plasma is cold, weakly ionized, and thus collisional—such as in star-forming disks. This large parameter space is beyond the scope of the space, solar, and laboratory plasmas covered by this review. Nonetheless, progress in our physical understanding can provide useful guidance to research into the physics of MRI-driven turbulence and its influences on accretion disk dynamics.

3. Magnetic reconnection in magnetospheres of compact objects

The last area deals with magnetic reconnection in magnetospheric plasmas near black holes and neutron stars. These plasmas are likely to be pair plasmas consisting of electrons and positrons created by strong mag-

netic and electric fields. The plasmas are relativistic and collisionless due to their energetic environments. Pioneering work has been done on acceleration of relativistic particles during reconnection (Zenitani and Hoshino, 2001). Reconnection in pair plasmas has been used to study the dependence of fast reconnection on the Hall effects which are absent in such plasmas due to equal mass of species. Using PIC simulations, Bessho and Bhattacharjee (2005) showed that magnetic reconnection proceeds very quickly in collisionless pair plasmas. Localization of plasma dissipation due to nongyrotropic pressure and inertial effects may be more essential than the Hall effects for determining the properties of fast reconnection. Comparative studies of electron-positron plasmas and electron-ion plasmas may provide new insights into the mechanisms governing fast reconnection.

Magnetic reconnection is invoked as a possible explanation (Lyutikov, 2006) for the observed soft- γ -ray repeaters (Woods and Thompson, 2006). These are magnetars, or neutron stars with an extremely strong magnetic fields ($>10^{15}$ G). Magnetic reconnection is applied to magnetized winds from pulsars which are rapidly rotating magnetized neutron stars. When the magnetic axis is aligned with the rotational axis, the radial outflow opens the dipole field to form a current sheet in the equatorial plane. When the magnetic axis is oblique to the rotation axis, the current sheet oscillates with the pulsar period around the equatorial plane, forming a wind with stripes of a toroidal field of alternating polarity propagating away radially (Michel, 1971). These features are found in recent numerical force-free solutions at an arbitrary angle (Spitkovsky, 2006). Magnetic reconnection near the current sheet may convert electromagnetic energy to particle energy at ultrarelativistic values, resulting in the observed radiation (Arons, 2009). Reconnection in such plasmas is unconventional. The particles are generally relativistic, and the magnetic field energy can exceed the plasma thermal energy and the rest mass energy. The usual reconnection models must be modified (Lyutikov and Uzdensky, 2003), leading to possible new solutions for reconnection. The reconnecting electric field may be strong enough to generate pair plasmas in the current sheet. These plasmas may be further accelerated to relativistic speeds and efficiently radiate their energy to affect the reconnection rate.

IX. SUMMARY, DISCUSSIONS, AND MAJOR OUTSTANDING ISSUES

We have reviewed the fundamental physics of magnetic reconnection discussing recent important advances and discoveries from theory and numerical simulations, from space satellite observations, and especially new findings from laboratory plasma experiments during the past decade. Theory and numerical simulations have contributed valuable insights into two-fluid effects and important clues to the dynamics accounting for collisionless reconnection. Laboratory experiments dedicated to the study of fundamental reconnection physics have

verified the existence of Hall effects and other significant processes relevant to collisionless reconnection. Satellite observations of the Earth's magnetosphere have provided evidence of Hall effects playing a key role in speeding up the reconnection rate in space plasmas. The dynamics of global magnetic reconnection through self-organization of the configurations have been exhibited in magnetic fusion experiments.

The fundamental physics of magnetic reconnection appears in a large variety of disparate situations in which it plays an important and sometimes crucial role. Perhaps, its most exciting and vital role occurs in space, solar, and astrophysical problems. Reconnection was first realized to be important in an attempt to understand solar flare phenomena. Reconnection is fundamental to the formation and behavior of our magnetosphere. Proceeding from a single reconnection event on the subsolar side, Dungey developed a theory of the dynamics of the entire magnetosphere including its magnetic tail. In terrestrial experiments such as tokamaks, it is at the heart of the disruption events, in the formation and relaxation processes of the field reversed pinch and spheromak, and of course in experiments dedicated to the understanding of the magnetic reconnection process.

The possibility of rapid conversion of magnetic energy into other forms, in spite of the constraint of flux freezing, provides astrophysicists and space physicists with a mechanism to understand many of their more exciting discoveries. It provides a tool to develop theories of stellar formation, dynamo generation of cosmic magnetic fields, the origin and evolution of magnetic fields in gamma-ray burst, the role of the magnetorotational instability in the operation of accretion disks, and the mysterious source of energy in magnetar outbursts.

This review has surveyed the evidence for magnetic reconnection phenomena on the Earth and in the Universe. The different areas in which reconnection is important were separately considered. The research has been divided into early and recent phases. In each of these areas we distinguish two separate aspects of reconnection: local and global reconnection.

The global picture alone does not give the reconnection rate, which is generally determined by the physics inside the current layer or multiple current layers. However, the global picture does determine the boundary conditions for the current layer(s): the magnetic field and pressure just outside the layer and the length.

The local reconnection in turn affects the global picture at any given time by the amount of magnetic flux that has passed through the current layer and been reconnected. A main question is how fast the flux passes through the reconnection layer, or in other words, how much reconnection has happened. As the reconnection proceeds, the topology of the lines of force changes with the amount of unconnected flux decreasing and the amount of connected flux increasing. If the local reconnection is not too fast, the global regions outside of the layer change slowly compared to any dynamical rate and are in quasistatic equilibrium. The topology is characterized by the reconnected and unconnected lines.

The rate of change of each is the reconnection rate. Sections III.B and VIII showed that each global MHD equilibrium has a certain energy and if the energy is lowered by the reconnection it proceeds. Reconnection will stop if it no longer lowers the total energy.

Most present day theories and experiments have concentrated on local reconnection and, in general, have not addressed the question of how the local reconnection connects to global reconnection. This is understandable since local reconnection is generic and presumably adaptable to global situation. But for a correct application of reconnection this connection must be established. For a working hypothesis it is generally assumed that the field outside the layer is of the same size as the global field that reverses across the layer. There is often an additional field perpendicular to the reconnection plane which is given by the global picture. In local theory it is arbitrarily included as a *guide field*. The current length is usually assumed to be of the global size. The latter assumption is not always valid.

A. Local physics issues for the reconnection layer

In benchmark studies of the two-fluid physics of the local reconnection layer, important progress has been made in understanding fast collisionless reconnection. Hall effects are now believed to facilitate the fast reconnection observed in the neutral sheets in the magnetosphere and laboratory plasmas.

Major findings are the following:

- (1) Many numerical simulations have demonstrated the importance of Hall effects in the neutral sheet for collisionless reconnection. In laboratory experiments and space satellite data, observations of an out-of-reconnection plane quadrupolar structure in the reconnecting magnetic field provides experimental evidence for the presence of collisionless two-fluid processes that speed up the reconnection rate.
- (2) It has been observed in a laboratory experiment and also in numerical simulations that the shape of the reconnection layer changes dramatically as the collisionality of plasma is varied. In a highly collisional plasma, a rectangularly shaped Sweet-Parker reconnection layer is identified. In the collisionless regime, the shape of the reconnection layer changes to a Petschek-like double wedge with a much faster reconnection rate.
- (3) In the laboratory experiment, the reconnection rate is found to increase rapidly as the ratio of the electron mean free path to the scale length increases. This result is attributed to the large Hall electric field in the reconnection layer except inside the electron diffusion layer near the X point where a strong dissipation mechanism takes place.
- (4) The electron diffusion region has been identified in the laboratory and magnetospheric plasmas. The thickness of the observed diffusion region is notably

larger than the value ($\sim 1.5c/\omega_{pe}$) predicted by recent 2D numerical calculations.

- (5) Electrostatic and electromagnetic fluctuations are observed in the neutral sheets of laboratory and space plasmas with notable similarities in their characteristics. Although a correlation was found between the reconnection rate and the amplitude of electromagnetic waves in laboratory experiments, a causal relationship is yet to be found.

The Sweet-Parker model, which was formulated to address the localized physics of the reconnection layer, has been reevaluated by numerical simulations and laboratory experiments. As discussed in Sec. III, this model predicts a reconnection rate that is too slow to explain the observed rates in the Sun and in space. This is due to the assumption that plasma and magnetic flux are constrained to pass through a narrow neutral sheet with a thickness of $\delta_{SP}=L/\sqrt{S}$, where L is the system size. To resolve this issue, Petscheck introduced a slow shock model which succeeded in predicting fast enough reconnection speeds. However, after a number of investigations of this model, it was concluded that this model could not be justified because the steady-state shocks could not be self-consistently formed.

One of the most important long-standing questions in this area of research dealing with why reconnection occurs so fast in collisionless plasmas has been addressed in the light of two-fluid physics. It is found that the conditions for which the original Sweet-Parker model is applicable are rather stringent. This model was experimentally verified when the mean free path of electrons is shorter than the width of the neutral sheet. As the collisionality is reduced to satisfy the relationship between the ion skin depth c/ω_{pi} and the Sweet-Parker width δ_{SP} , as $c/\omega_{pi} > \delta_{SP}$, a much faster reconnection rate was observed in the MRX, and the results were verified by numerical simulations. This ratio $(c/\omega_{pi})/\delta_{SP}$ is equal to $5(\lambda_{mfp}/L)^{1/2}$, where λ_{mfp}/L is another collisionality parameter. It is important to note that the two-fluid effects become important even when the electron mean free path is in order of magnitude less than the system size.

Even with the recent notable advances in two-fluid analysis of the reconnection layer, many important questions remain unsolved. In particular, what really determines the reconnection rate and the rate of conversion from magnetic to kinetic energy? How does the latter depend on the former? Except in the vicinity of the X point, the reconnection electric field appears to be supported by the Hall field, $\mathbf{j} \times \mathbf{B}/ne$. The consensus of the GEM challenge project was that the reconnection rate is governed by the Hall term in the generalized Ohm's law. However, this term does not provide energy dissipation or break field lines. The other terms in the generalized Ohm's law, the inertia term, $\nabla \cdot \mathbf{P}$ term, and fluctuations, must be responsible for line breaking and the energy conversion. Recent studies of local reconnecting layer dynamics by PIC codes have learned that energy dissipation in the neutral sheet occurs in a small region, leading to a much smaller rate of energy conversion from

magnetic to particle kinetic energy. This rate is too small to explain the observed particle heating during reconnection observed in RFP plasma relaxation events, in spheromak merging experiments, or in solar flare evolution. It is necessary to develop models which would lead to the formation of a large number of reconnection layers. Another concern is whether or how the global boundary conditions, either periodic or open, affect the reconnection rate.

At the moment, there is no clear theory dealing with macrofluctuation and microfluctuation, concerning which ones are most relevant, how they are excited, and how they determine the reconnection rate by influencing the energy conversion processes. In order to understand how magnetic energy is converted to particle energy, we need to investigate the relationship between the anomalous particle acceleration and heating and reconnection rates. It is expected that analytic theory together with numerical calculations will aid progress in understanding how fluctuations are excited and how they dissipate energy in the reconnection layer.

B. Global physics issues for reconnection

In the area of global reconnection research described in Sec. VIII, major progress has been made in documenting key features of magnetic self-organization or relaxation phenomena of plasmas. The magnetic self-organization is influenced and determined by both local plasma dynamics in the reconnection region and global boundary conditions in 3D global topology. It has been found in laboratory plasmas that a large MHD instability caused by external conditions can often produce a current layer which undergoes magnetic reconnection and can determine its rate. The major findings are the following:

- (1) In solar flares, reconnection sites were identified with hard-x-ray emissions near the top of solar flare arcades during CME and coronal eruptions. Reconnection speed was measured to be much faster than the Sweet-Parker rate.
- (2) In tokamaks, it is found that magnetic reconnection is often driven by an ideal kink instability generated by a gradual change of tokamak equilibrium and the reconnection time is much shorter than the classical (Sweet-Parker) value.
- (3) In RFP experiments, reconnection occurs in the plasma core and, under some conditions, at the edge. It is observed that two unstable tearing modes in the core region can nonlinearly couple to produce a driven reconnection at a third location in the plasma edge region. It is conjectured that a similar phenomenon occurs in active solar arcade flares where a spontaneous reconnection at one location can drive reconnection at other locations, leading to eruptions.

It has been recognized that global reconnection phenomena almost always occur impulsively. A fast local

reconnection generally leads to an impulsive global topology change or global magnetic self-organization phenomena. In the RFP, spheromak, tokamak, magnetospheric substorms, and solar flares, reconnection often occurs suddenly with a very fast speed. Although in each case theoretical models have been proposed to describe the impulsive behavior, there is no basic theory at hand which can be generally applied to all cases. Section VIII include descriptions of many impulsive phenomena related to magnetic self-organization of plasmas. This impulsiveness is one of the most distinctive properties that allows the explosive burst of magnetic energy release and the sudden onset of a fast change in magnetic field topology. It is desirable to have a theory which universally explains impulsive reconnection phenomena for laboratory and astrophysical plasmas. The theory should address the following general questions. Is there any general criterion or reason why magnetic energy is stored for a long period and then suddenly released, globally driving the plasma to a relaxed state? Is the relationship between the local reconnection rate and the buildup of global stored energy a key? What is the physical trigger that initiates the reconnection? Is the presence of multiple reconnection important? How do two-fluid effects cause impulsive reconnection? As described in Sec. VI, for magnetospheric and laboratory plasmas, two-fluid effects are considered to facilitate impulsive reconnection in some cases. These questions should be answered by collaborated efforts of theorists and experimentalists.

One of the major questions still remaining is as follows: How do global systems generate local reconnection structures through formation of one or multiple current sheets either spontaneously or forced by boundary conditions? Concomitant occurrence of multiple reconnection layers may provide a key to resolving fast magnetic self-organization or global reconnection phenomena. Another unresolved key issue is the energy transport between the local reconnection layer and the global plasma and its boundaries during the evolution of the global plasma configuration. Can the magnetic self-organization of a plasma be affected by the energy or particle transport between the local region and the global plasma? Examples for addressing this issue are found in tokamak sawtooth and RFP relaxation phenomena. Another related unresolved issue is the effect of line tying of the magnetic field at the boundary, which is expected to affect the stability of plasmas and the reconnection rate.

We could hypothesize that global magnetic self-organization phenomena in both tokamak sawtooth crashes and solar flares share a common process. When reconnection occurs in a certain region of the globally connected plasma, a topology change results. A sudden change of magnetic flux over a short time (large $d\Psi/dt$) is induced in a singly connected part of the global

plasma. This leads to a large electric field along the magnetic field lines and acceleration of electrons to superthermal energy. Indeed in reconnection events in both solar flares and tokamak sawteeth, we observe a significant amount of high energy tail (runaway) electrons. A careful comparative study of tokamak sawteeth and RFP relaxation events may illuminate this important energy flow channel.

In addressing these global issues, we note that all classical models fail when particularly long global lengths are assumed for the current layers. Only a small amount of research has actually focused on the formation process of current layers—with most studies directed toward a symmetric equilibrium where the current layer is assumed to be the global length. In this respect, it is important to consider a highly asymmetrical equilibrium in which there could exist multiple current layers whose lengths are closer to the shorter scale on which the equilibrium varies. This point was also made by Lu who considered a simple automaton model for solar flares and demonstrated that if multiple reconnection layers were dynamically related (such that one reconnection would trigger another), then one could explain the singular result that the distribution function for the number of flares of a given energy is a nearly perfect power law. As suggested by Parker, it would be of great value to develop and elucidate a general theory of current layer formation in a highly nonsymmetric magnetic equilibrium such as is observed on the Sun.

There may be mechanisms to generate multiple small-scale current sheets in which field-line reconnection takes place. These structures can often be small enough to decouple the motion of electrons from that of ions in collisionless plasmas. These smaller scale sheets can fluctuate leading to faster reconnection, and a large number of these layers should lead to a large energy release—as seen, for example, in the magnetosphere and RFPs. In RFP plasmas, reconnection in multiple layers is observed to generate a significant magnetic self-organization of the global plasma producing strong ion heating, which is currently under intensive investigation. A theory from a first principles may lead us to a breakthrough for solving this problem.

C. Final remark

Significant progress has been made in the past decades in research of magnetic reconnection, resulting from the extensive cross-discipline studies by experimentalists, space physicists, numerical researchers, and theorists. However, many important questions are not yet resolved including the most essential question regarding the conversion of magnetic energy, particularly with respect to in what channel the energy flow takes place, i.e., through electrons or ions. With the recent strong upsurge of research through satellite observations, experiments, and theoretical studies, a much improved understanding of this important process should emerge.

ACKNOWLEDGMENTS

We greatly benefited from many stimulating and productive discussions with Amitava Bhattacharjee, William Daughton, James Drake, Forrest Mozer, Stewart Prager, William Tang, Dmitri Uzdensky, and Ellen Zweibel. We express our sincere thanks to David Meyerhofer for his very helpful editorial effort.

APPENDIX: THE NATURE OF RECONNECTION

The basic idea of magnetic reconnection involves the concept of the topology of a set of magnetic lines of force. A crucial concept underlying plasma equilibria states is that given certain boundary conditions and several other relations involving the plasma pressure, there is a unique magnetostatic equilibrium for each such topology (Kruskal and Kulsrud, 1958).

This is most easily understood by the example of the solar atmosphere where the plasma pressure is negligible. In this example, we introduce the idea of a footpoint mapping. Assume that all field lines in the solar atmosphere are attached to the solar surface and consider a point P where a line of force leaves the solar surface and enters the atmosphere. Now, by our assumption, all lines that leave the solar surface re-enter it at some other place. Let the line that left it at P re-enter it at P' . For any magnetic configuration the point P' is determined by P . These are called its footpoints and the function that relates P' to P is called the footpoint mapping. The topology of the magnetic line configuration is defined by this footpoint mapping. If the lines in the atmosphere are moved continuously preserving their identity, but there is no motion of their footpoints in the solar surface, then the footpoint mapping is preserved and so is its topology. Conversely, any magnetic line configuration can be moved continuously into another with the same topology. (This disregards a complication due to magnetic line braiding.) Now, only one configuration is actually a static equilibrium state, and we show below that this *force-free* state is the one that minimizes the energy of the magnetic field while preserving its topology.

Any change in topology of the lines involves a change in the corresponding equilibrium and, in general, a change in the energy of this equilibrium. An abrupt change in the topology to a new topology, say by breaking magnetic field lines at some place, puts the plasma into a nonequilibrium state with generally no change in its energy. After this change the plasma will evolve with ideal plasma motions that will conserve this new topology but will lower its energy, say by viscous processes, until it reaches the new equilibrium corresponding to its new topology.

This discussion is based on the result that ideal plasma motions do not break lines or change their topology. In this manner, one sees that a sudden change in topology by a nonideal motion leads to a rapid conversion of magnetic energy into kinetic energy and then a subsequent conversion of this kinetic energy into heat, radia-

tion, or particle acceleration by some viscous process. This abrupt change of topology is a nonideal change which magnetic reconnection can trigger. It is of considerable importance just because it can lead to a rapid conversion of magnetic energy to other forms.

A prime example is the solar flare in which a large amount of energy is released as the magnetic field is relaxed to a lower energy state. The flare is generally preceded by twisting of field lines by a slow motion of the footpoints in the solar surface leading to a slow change in the magnetic field in the solar atmosphere. During this change the magnetic field evolves through a sequence of force-free equilibria. Even though the motions in the atmosphere are ideal, this footpoint motion still leads to a gradual change in the magnetic topology. This twisting gradually increases the stored magnetic energy. After the energy has increased enough, a magnetic reconnection can be triggered. While this reconnection occurs, footpoints in the solar surface hardly change but the footpoint mapping and the topology changes throwing the magnetic field out of equilibrium. The plasma then relaxes by ideal motions to a new equilibrium of lower energy releasing its increased energy (that had been produced by the motion in the solar surface). This release manifests itself as the solar flare.

Thus, to understand the basics of magnetic reconnection one has to appreciate two important properties of a plasma. The first property is *flux freezing*. Flux freezing implies that magnetic field lines maintain their physical reality and any given set of field lines (that represents the magnetic field in strength and direction) continues to represent the magnetic field at later times. Indeed, this is achieved by the field lines being bodily carried with the plasma. As a consequence, if two plasma fluid elements A and B lie on the same magnetic line of force at time t they will continue to lie on a common line of force at any later time t' . Further, if a given line of force passes through a fluid element A at a particular time, the line passes through the identical fluid element at a later time and is regarded as the same line of force.

Flux freezing generally holds in a highly conducting plasma unless magnetic reconnection occurs. The condition for flux freezing to hold is (Newcomb, 1958)

$$\mathbf{E} + \mathbf{v} \times \mathbf{B}/c = 0. \quad (\text{A1})$$

Combining this equation with the induction equation we have the equation of motion for the field

$$\partial\mathbf{B}/\partial t = \nabla \times (\mathbf{v} \times \mathbf{B}). \quad (\text{A2})$$

This equation is called the magnetic differential equation or the magnetic induction equation.

This manner of realization of a line of force over time by keeping track of a plasma particle on it is independent of which particle is chosen to identify the field line. This geometrical characterization of flux freezing can also be carried out more mathematically by making use of Clebsch coordinates to describe the magnetic field. It is known that an arbitrary divergence-free vector field, such as a magnetic field \mathbf{B} , can be expressed in terms of two scalar functions of positions α and β as

$$\mathbf{B} = \nabla\alpha \times \nabla\beta. \quad (\text{A3})$$

[It is clear that this representation is automatically divergence-free so the theorem is rather that two such scalar functions can be found to satisfy Eq. (A3).]

Now, if we assume that α and β are functions of time and space such that

$$\begin{aligned} d\alpha/dt &= \partial\alpha/\partial t + \mathbf{v} \cdot \nabla\alpha = 0, \\ d\beta/dt &= \partial\beta/\partial t + \mathbf{v} \cdot \nabla\beta = 0, \end{aligned} \quad (\text{A4})$$

then \mathbf{B} as given by Eq. (A3) satisfies Eq. (A2).

Now, a line of force is given by $\alpha=\text{const}$, and $\beta=\text{const}$ and by Eq. (A4), these are constant following a plasma element. This shows that any line is thus bodily transmitted by the plasma motion. This is a mathematical way to represent flux freezing. For the solar magnetic field we have that if the velocity in the solar surface is zero, then α and β are fixed at the solar surface, the field line is frozen at the surface, and the footpoint mapping and the topology are preserved during any motions in the atmosphere.

The second point is that any static plasma equilibrium is largely determined by the topology of the magnetic field. In fact, consider the solar magnetic field, neglect its plasma pressure, and consider a particular magnetic topology, as given by the footpoint mapping. Then, of all the magnetic fields \mathbf{B} that are divergence-free and have this topology, the magnetic field that minimizes the total magnetic energy is a force-free equilibrium and is the unique force-free equilibrium associated with this topology.

To see why this theorem holds for the solar magnetic field, consider minimizing the magnetic energy

$$\mathcal{E} = \frac{1}{8\pi} \int \mathbf{B}^2 d^3x = \frac{1}{8\pi} \int (\nabla\alpha \times \nabla\beta)^2 d^3x \quad (\text{A5})$$

over all possible functions α and β with the restriction that α and β are fixed on the solar surface. This is the same condition as the footpoints being held fixed. Now, vary \mathcal{E} by changing α by $\delta\alpha$ integrate by parts and use Gauss's theorem to get rid of the integrated term which vanishes on the boundary by $\delta\alpha=0$ there. Then

$$\delta\mathcal{E} = \frac{2}{8\pi} \int \delta\alpha [\nabla\beta \cdot \nabla \times \mathbf{B}] d^3x = 0, \quad (\text{A6})$$

so $\mathbf{j} \cdot \nabla\beta = 0$ everywhere since $\delta\alpha$ is essentially arbitrary. Similarly, from varying β we get $\mathbf{j} \cdot \nabla\alpha = 0$. Thus, expanding the triple product

$$\mathbf{j} \times (\nabla\alpha \times \nabla\beta) = \nabla\alpha(\mathbf{j} \cdot \nabla\beta) - \nabla\beta(\mathbf{j} \cdot \nabla\alpha) = 0 \quad (\text{A7})$$

or $\mathbf{j} \times \mathbf{B} = 0$ which is the condition for force-free equilibrium.

For the case of nonzero pressure p the energy is also a minimum when p is properly constrained, but the argument is more sophisticated (Kruskal and Kulsrud, 1958). This unique relationship between topology and equilibrium shows that any change in topology by reconnection has a significant impact on the entire equilibrium.

In this way all equilibria are characterized by their topology. Any change in the topology implies a different equilibrium with a different energy. The tendency of plasmas to lower their energy then gives rise to a tendency for a plasma to carry out a magnetic reconnection if the new equilibrium, to which it would evolve after reconnection, has a lower energy. The main question is how fast this can happen and this is perhaps the most important question concerning magnetic reconnection. Of course, magnetic reconnection cannot happen if Eq. (A1) is exactly satisfied. The more exact magnetic differential equation for the evolution of \mathbf{B} that allows reconnection must include the resistivity term and is

$$\partial\mathbf{B}/\partial t = \nabla \times (\mathbf{v} \times \mathbf{B}) + \eta \nabla^2 \mathbf{B}, \quad (\text{A8})$$

where η is the plasma resistivity. The last term gives a diffusion of the magnetic field changing it over a scale $\sqrt{(\eta c^2/4\pi)t}$ in a time t . Equation (A8) shows that the field lines are not exactly tied to the plasma but can slip this distance. If this distance is small compared to the scale of the magnetic field then one can consider the field as frozen even if the resistivity is not exactly zero. Now it is the case that the resistivity in the Sun is not so different from the resistivity in the laboratory. In the Sun the time scales are longer but the length scales are also longer and since the time occurs under the square root the breakdown of flux freezing is much less severe in the Sun.

REFERENCES

- al Karkhy, A., P. Browning, G. Cunningham, S. Gee, and M. Rusbridge, 1993, Phys. Rev. Lett. **70**, 1814.
 Anderson, J. K., C. B. Forest, T. M. Biewer, J. S. Sarff, and J. C. Wright, 2004, Nucl. Fusion **44**, 162.
 Antiochos, S. K., J. T. Karpen, and C. R. DeVore, 2002, Astrophys. J. **575**, 578.
 Arons, J., 2009, in *Neutron Stars and Pulsars*, edited by W. Becker (Springer, New York), Vol. 357, p. 373.
 Asano, Y., T. Mukai, M. Hoshino, Y. Saito, H. Hayakawa, and T. Nagai, 2004, J. Geophys. Res. **109**, A02212.
 Balbus, S., and J. Hawley, 1998, Rev. Mod. Phys. **70**, 1.
 Bale, S., F. Mozer, and T. Phan, 2002, Geophys. Res. Lett. **29**, 2180.
 Baum, P., and A. Bratenahl, 1974, Phys. Fluid **17**, 1232.
 Becker, U., T. Neukirch, and K. Schindler, 2001, J. Geophys. Res. **106**, 3811.
 Bellan, P., 2000, *Spheromaks* (Imperial College Press, London).
 Bergerson, W., C. Forest, G. Fiksel, D. Hannum, R. Kendrick, J. Sarff, and S. Stambler, 2006, Phys. Rev. Lett. **96**, 015004.
 Bessho, N., and A. Bhattacharjee, 2005, Phys. Rev. Lett. **95**, 245001.
 Bhattacharjee, A., K. Germaschewski, and C. S. Ng, 2005, Phys. Plasmas **12**, 042305.
 Bhattacharjee, A., and E. Hameiri, 1986, Phys. Rev. Lett. **57**, 206.
 Bhattacharjee, A., Z. W. Ma, and X. Wang, 2001, Phys. Plasmas **8**, 1829.
 Birdsall, C., and A. Langdon, 1985, *Plasma Physics via Computer Simulation* (McGraw-Hill, New York).
 Birn, J., J. Drake, M. Shay, B. Rogers, R. Denton, M. Hesse, M. Kuznetsova, Z. Ma, A. Bhattacharjee, A. Otto, and P. Pritchett, 2001, J. Geophys. Res. **106**, 3715.
 Birn, J., and E. R. Priest, 2007, in *Reconnection of Magnetic Fields: Magnetohydrodynamics and Collisionless Theory and Observations*, edited by J. Birn and E. R. Priest (Cambridge University Press, Cambridge), p. 3.
 Biskamp, D., 1986, Phys. Fluids **29**, 1520.
 Biskamp, D., 2000, *Magnetic Reconnection in Plasmas* (Cambridge University Press, Cambridge).
 Biskamp, D., and K. Schindler, 1971, Plasma Phys. **13**, 1013.
 Biskamp, D., E. Schwarz, and J. F. Drake, 1997, Phys. Plasmas **4**, 1002.
 Bodin, H. A. B., 1990, Nucl. Fusion **30**, 1717.
 Bratenahl, A., and C. M. Yeates, 1970, Phys. Fluids **13**, 2696.
 Breslau, J. A., and S. Jardin, 2003, Phys. Plasmas **10**, 1291.
 Brittnacher, M., and E. C. Whipple, 2002, J. Geophys. Res. **107**, 1022.
 Brown, D. S., and E. R. Priest, 2001, Astron. Astrophys. **367**, 339.
 Brown, M., 1999, Phys. Plasmas **6**, 1717.
 Brown, M., C. Cothran, M. Landreman, D. Schlossberg, and W. Matthaeus, 2002, Astrophys. J. **577**, L63.
 Brown, M. R., C. D. Cothran, and J. Fung, 2006, Phys. Plasmas **13**, 056503.
 Cai, H. J., D. Q. Ding, and L. C. Lee, 1994, J. Geophys. Res. **99**, 35.
 Cai, H. J., and L. C. Lee, 1997, Phys. Plasmas **4**, 509.
 Carmichael, H., 1964, in *The Physics of Solar Flares, Proceedings of the AAS-NASA Symposium*, edited by W. N. Hess (NASA, Washington, D.C.), p. 451.
 Carter, T., H. Ji, F. Trintchouk, M. Yamada, and R. Kulsrud, 2001, Phys. Rev. Lett. **88**, 015001.
 Carter, T., M. Yamada, H. Ji, R. Kulsrud, and F. Trintchouk, 2002, Phys. Plasmas **9**, 3272.
 Cassak, P. A., M. A. Shay, and J. F. Drake, 2005, Phys. Rev. Lett. **95**, 235002.
 Cattell, C., J. Dombeck, J. Wygant, J. Drake, M. Swisdak, M. Goldstein, W. Keith, A. Fazakerley, M. Andre, E. Lucek, and A. Balogh, 2005, J. Geophys. Res. **110**, A01211.
 Chen, L. J., et al., 2008, Nat. Phys. **4**, 19.
 Close, R. M., C. E. Parnell, D. W. Longcope, and E. R. Priest, 2004, Astrophys. J. Lett. **612**, L81.
 Cothran, C. D., J. Fung, M. R. Brown, and M. J. Schaffer, 2006, Rev. Sci. Instrum. **77**, 063504.
 Cothran, C. D., M. Landreman, M. R. Brown, and W. H. Matthaeus, 2003, Geophys. Res. Lett. **30**, 1213.
 Cowley, S. W. H., 1978, Planet. Space Sci. **26**, 1037.
 Daughton, W., 1999, J. Geophys. Res. **104**, 28701.
 Daughton, W., 2003, Phys. Plasmas **10**, 3103.
 Daughton, W., G. Lapenta, and P. Ricci, 2004, Phys. Rev. Lett. **93**, 105004.
 Daughton, W., J. Scudder, and H. Karimabadi, 2006, Phys. Plasmas **13**, 072101.
 Deng, X. H., and H. Matsumoto, 2001, Nature (London) **410**, 557.
 Den Hartog, D. J., et al., 2007, Nucl. Fusion **47**, L17.
 De Pontieu, B., et al., 2007, Science **318**, 1574.
 Ding, W. X., D. L. Brower, D. Craig, B. H. Deng, G. Fiksel, V. Mirnov, S. C. Prager, J. S. Sarff, and V. Svidzinski, 2004, Phys. Rev. Lett. **93**, 045002.
 Ding, W. X., D. L. Brower, D. Craig, B. H. Deng, S. C. Prager, J. S. Sarff, and V. Svidzinski, 2007, Phys. Rev. Lett. **99**, 055004.

- Sugiyama, T., and K. Kusano, 2007, *J. Comp. Physiol.* **227**, 1340.
- Sullivan, B. P., B. N. Rogers, and M. A. Shay, 2005, *Phys. Plasmas* **12**, 122312.
- Svidzinski, V. A., G. Fiksel, V. V. Mirnov, and S. C. Prager, 2008, *Phys. Plasmas* **15**, 062511.
- Sweet, P., 1958, in *Electromagnetic Phenomena in Cosmical Physics*, edited by B. Lehnert (Cambridge University Press, New York), p. 123.
- Swisdak, M., J. F. Drake, M. A. Shay, and J. G. McIlhargey, 2005, *J. Geophys. Res.* **110**, A05210.
- Syrovatskii, S., 1971, *Sov. Phys. JETP* **33**, 933.
- Syrovatskii, S., 1981, *Annu. Rev. Astron. Astrophys.* **19**, 163.
- Syrovatskii, S. I., A. G. Frank, and A. Z. Khodzhaev, 1973, *Sov. Phys. Tech. Phys.* **18**, 580.
- Taylor, J. B., 1974, *Phys. Rev. Lett.* **33**, 1139.
- Taylor, J. B., 1986, *Rev. Mod. Phys.* **58**, 741.
- Terasawa, T., 1983, *Geophys. Res. Lett.* **10**, 475.
- Trintchouk, F., M. Yamada, H. Ji, R. Kulsrud, and T. Carter, 2003, *Phys. Plasmas* **10**, 319.
- Tsuneta, S., 1996, *Astrophys. J.* **456**, 840.
- Ugai, M., and T. Tsuda, 1977, *J. Plasma Phys.* **17**, 337.
- Uzdensky, D., and J. Goodman, 2008, *Astrophys. J.* **682**, 608.
- Uzdensky, D., and R. Kulsrud, 2000, *Phys. Plasmas* **7**, 4018.
- Uzdensky, D., and R. Kulsrud, 2006, *Phys. Plasmas* **13**, 062305.
- Uzdensky, D. A., 2003, *Astrophys. J.* **587**, 450.
- Uzdensky, D. A., 2007, *Phys. Rev. Lett.* **99**, 261101.
- Uzdensky, D. A., A. Königl, and C. Litwin, 2002, *Astrophys. J.* **565**, 1205.
- van Ballegooijen, A. A., 1994, *Space Sci. Rev.* **68**, 299.
- Vasyliunas, V., 1975, *Rev. Geophys. Space Phys.* **13**, 303.
- Verbunt, F., 1982, *Space Sci. Rev.* **32**, 379.
- von Goeler, S., W. Stodiek, and N. Sauthoff, 1974, *Phys. Rev. Lett.* **33**, 1201.
- Waelbroeck, F. L., 1989, *Phys. Fluids B* **1**, 2372.
- Wang, X., A. Bhattacharjee, and Z. W. Ma, 2000, *J. Geophys. Res.* **105**, 27633.
- Wang, X., A. Bhattacharjee, and Z. W. Ma, 2001, *Phys. Rev. Lett.* **87**, 265003.
- Wang, Y., R. Kulsrud, and H. Ji, 2008, *Phys. Plasmas* **15**, 122105.
- Wesson, J., 1987, *Tokamaks* (Clarendon, Oxford).
- Woltjer, L., 1958, *Proc. Natl. Acad. Sci. U.S.A.* **44**, 489.
- Woods, P. M., and C. Thompson, 2006, *Compact Stellar X-Ray Sources* (Cambridge University Press, Cambridge), p. 547.
- Wygant, J. et al., 2005, *J. Geophys. Res.* **110**, A09206.
- Xiao, C. J., et al., 2006, *Nat. Phys.* **2**, 478.
- Xiao, C. J., et al., 2007, *Nat. Phys.* **3**, 609.
- Yagi, Y., and N. Kawashima, 1985, *Jpn. J. Appl. Phys., Part 2* **24**, L259.
- Yamada, M., 1999a, in *Magnetic Helicity in Space and Laboratory Plasmas*, edited by M. Brown, R. Canfield, and A. Pevtsov, AGU Monograph Vol. 111 (AGU, Washington, D.C.), p. 129.
- Yamada, M., 1999b, *J. Geophys. Res., [Space Phys.]* **104**, 14529.
- Yamada, M., 2001, *Earth, Planets Space* **53**, 509.
- Yamada, M., 2007, *Phys. Plasmas* **14**, 058102.
- Yamada, M., H. Furth, W. Hsu, A. Janos, S. Jardin, M. Okabayashi, J. Sinnis, T. Stix, and K. Yamazaki, 1981, *Phys. Rev. Lett.* **46**, 188.
- Yamada, M., H. Ji, S. Hsu, T. Carter, R. Kulsrud, N. Bretz, F. Jobes, Y. Ono, and F. Perkins, 1997a, *Phys. Plasmas* **4**, 1936.
- Yamada, M., H. Ji, S. Hsu, T. Carter, R. Kulsrud, Y. Ono, and F. Perkins, 1997b, *Phys. Rev. Lett.* **78**, 3117.
- Yamada, M., H. Ji, S. Hsu, T. Carter, R. Kulsrud, and F. Trintchouk, 2000, *Phys. Plasmas* **7**, 1781.
- Yamada, M., F. Levinton, N. Pomphrey, R. Budny, J. Manickam, and Y. Nagayama, 1994, *Phys. Plasmas* **1**, 3269.
- Yamada, M., Y. Nagayama, W. Davis, E. Fredrickson, A. Janos, and F. Levinton, 1992, *Rev. Sci. Instrum.* **63**, 4623.
- Yamada, M., Y. Ono, A. Hayakawa, M. Katsurai, and F. Perkins, 1990, *Phys. Rev. Lett.* **65**, 721.
- Yamada, M., F. Perkins, A. MacAulay, Y. Ono, and M. Katsurai, 1991, *Phys. Fluids B* **3**, 2379.
- Yamada, M., Y. Ren, H. Ji, J. Breslau, S. Gerhardt, R. Kulsrud, and A. Kuritsyn, 2006, *Phys. Plasmas* **13**, 052119.
- Yin, L., and D. Winske, 2003, *Phys. Plasmas* **10**, 1595.
- Yokoyama, T., K. Akita, T. Morimoto, K. Inoue, and J. Newmark, 2001, *Astrophys. J. Lett.* **546**, L69.
- Yoon, P., and A. Lui, 2004, *J. Geophys. Res.* **109**, A02210.
- Yoon, P., A. Lui, and M. Sitnov, 2002, *Phys. Plasmas* **9**, 1526.
- Yoon, P. H., and A. T. Y. Lui, 2005, *J. Geophys. Res.* **110**, A01202.
- Zenitani, S., and M. Hoshino, 2001, *Astrophys. J. Lett.* **562**, L63.
- Zweibel, E. G., and A. Brandenburg, 1997, *Astrophys. J.* **478**, 563.